UC Berkeley
UC Berkeley Electronic Theses and Dissertations

Title
Identifying Determinants of Epigenetic States and Epigenetic Memory

Permalink
https://escholarship.org/uc/item/2wx6q0c1

Author
Saxton, Daniel Strome

Publication Date
2021

Peer reviewed|Thesis/dissertation

eScholarship.org Powered by the California Digital Library
University of California

Identifying Determinants of Epigenetic States and Epigenetic Memory

By

Daniel Strome Saxton

A dissertation submitted in partial satisfaction of the

requirements for the degree of

Doctor of Philosophy

in

Molecular and Cell Biology

in the

Graduate Division

of the

University of California, Berkeley

Committee in charge:
Professor Jasper Rine, Chair
Professor Kathleen Collins
Professor Barbara Meyer
Professor Oskar Hallatschek

Fall 2021

Abstract

Identifying Determinants of Epigenetic States and Epigenetic Memory

by

Daniel Strome Saxton

Doctor of Philosophy in Molecular and Cell Biology

University of California, Berkeley

Professor Jasper Rine, Chair

Many cells possess a remarkable ability to pass on non-genetic information to daughter cells. In some cases, the transmission of epigenetic information is clearly linked to processes such as DNA methylation, RNAi, or transcription factor feedback loops. In other cases, a mechanism for epigenetic memory clearly exists but has evaded discovery. One such example is the inheritance of heterochromatin. Heterochromatic gene silencing often requires silencing machinery that can both deposit and bind to specific histone modifications, sometimes referred to as writers and readers of epigenetic information, coupled with inheritance of histones during DNA replication. Therefore, a feedback loop between silencing factors and modified histones could allow a silenced state to be "remembered" through DNA replication. However, multiple studies argue that this intuitive model is either incorrect or incomplete, as discussed in Chapter 1 of this manuscript. During my thesis work, I investigated the histone-based memory model by studying epigenetic states in *S. cerevisiae.*

In Chapter 2, I tested two predictions of the histone-based memory model. One prediction builds on the observation that histone H3-H4 tetramers are randomly distributed between daughter chromatids during DNA replication. This phenomenon suggests that rare events of asymmetric H3-H4 tetramer inheritance could cause one daughter chromatid to receive an insufficient number of modified parental tetramers, and thereby lose the silenced state. In this case, reductions in heterochromatin domain size would be predicted to increase the frequency of asymmetric inheritance and silencing loss. However, I found that severe reductions in heterochromatin domain size had no effects on the rate of silencing inheritance. Additionally, two mutations that led to severe reductions in H3-H4 tetramer inheritance had minimal effects on the inheritance of silencing. Finally, combining these tetramer-inheritance defects with reductions in heterochromatin domain size still permitted robust inheritance of the silenced state. Therefore, reducing the number of inherited H3-H4 tetramers and reducing the number of H3-H4 tetramers available for inheritance had surprisingly minor effects on the inheritance of silencing. These findings argue that the histone-based memory model cannot explain epigenetic memory.

In Chapter 3, I asked whether robust nucleosome positioning can contribute to the efficiency of silencing. To test this, I made a series of deletions between two nucleosome-depleted regions (NDRs) in a silenced domain, which would be predicted to affect nucleosome

packing. These deletions revealed a striking oscillatory relationship between inter-NDR distance and silencing stability. I found that instances of robust silencing corresponded to efficient nucleosome packing, and weak silencing corresponded to poorly positioned nucleosomes. Additionally, organized nucleosome packing correlated with an enhanced ability to both establish and inherit a silenced epigenetic state. These findings argue that proper NDR placement in heterochromatin is important for silencing and suggest that well-organized nucleosome arrays provide a better substrate to produce a silenced structure.

Under normal conditions, mating-type loci in *S. cerevisiae* are constitutively silenced. In Chapter 4, I worked with a talented undergraduate/research technician, Delaney Farris, to perform a screen for mutations that cause constitutive silencing to become metastable. This screen uncovered many mutations, as expected, in *SIR1*. Surprisingly, this screen also identified a point mutation, *sir2-G436D*, that caused cells to exhibit bistable silencing at the single-cell level. Interestingly, whereas bistable silencing normally manifests as a mix of cells that are either fully silenced or fully expressed, *sir2-G436D* exhibited a mix of cells that were either fully silenced or partially silenced. This is the first time that a heritable intermediate silenced state has been documented, to our knowledge. Additionally, given that Sir2 is a histone deacetylase, this finding suggests that histone modifiers are important for silencing to mature from an intermediate silenced state to a fully silenced state. This idea is consistent with previous studies, and the *sir2-G436D* mutant provides an exciting avenue to examine the structure of chromatin that can achieve intermediate levels of repression and how that structure might be inherited through DNA replication.

Table of Contents

List of Figures iii
List of Tables v
Acknowledgements vi

Chapter 1: Introduction 1
1.1 The Question 1
1.2 Defining *cis* memory 1
1.3 The histone-based memory model 2
1.4 The Paradox 2
1.5 References 3

Chapter 2: Epigenetic Memory Independent of Symmetric Histone Inheritance 6
2.1 Abstract 6
2.2 Introduction 6
2.3 Results 8
2.3.1 Nucleosome number did not determine the rate of silencing loss 8
2.3.2 Nucleosome number did not affect transmission of epigenetic states in *sir1*Δ. 15
2.3.3 Replisome defects affected epigenetic inheritance 19
2.3.4 Variations in nucleosome number in replisome mutant backgrounds 25
2.4 Discussion 28
2.4.1 Evidence that H3-H4 Tetramers Did Not Carry Epigenetic Memory 28
2.4.2 Addressing the Possibility that Tetramer Inheritance is Not Random 28
2.4.3 Epigenetic Inheritance of the Expressed State 29
2.5 Materials and Methods 31
2.6 References 36

Chapter 3: Nucleosome Positioning Regulates the Establishment, Stability, and Inheritance of Heterochromatin in *Saccharomyces cerevisiae* 39
3.1 Abstract 39
3.2 Introduction 39
3.3 Results 40
3.3.1 Inter-NDR Distance Affected Silencing Stability 40
3.3.2 Inter-NDR Distance Affected Nucleosome Positioning 45
3.3.3 NDR-R was Required for Oscillatory Silencing Effects 47
3.3.4 Replacement of NDR-R with Heterologous NDRs 48
3.3.5 Contributions of Inter-NDR DNA Content 52
3.3.6 Inter-NDR Distance Affected Silencing Stability at *HMRα* 54
3.3.7 Inter-NDR Distance Influenced Epigenetic Inheritance 55
3.4 Discussion 57
3.4.1 Effects of Inter-NDR Distance on Nucleosome Positioning 57
3.4.2 Contributions of Nucleosome Positioning to Heterochromatin Stability 57
3.4.3 Effects of Nucleosome Positioning on Epigenetic States 58

3.4.4 Potential Effects of Inter-NDR Distance in Disease Contexts 58
3.5 Materials and Methods 59
3.6 References 62

Chapter 4: A novel allele of *SIR2* reveals a heritable intermediate state of gene silencing **66**
4.1 Abstract 66
4.2 Introduction 66
4.3 Results 67
4.3.1 Identification of metastable mutants. 67
4.3.2 Genetic analysis identified eight unique *sir1* alleles 68
4.3.3 A metastable phenotype from a mutation in *SIR2* 71
4.3.4 A unique silencing defect in *sir2-G436D* 71
4.3.5 *sir2-G436D* produced intermediate, heritable expression 74
4.3.6 *sir2-G436D* silencing defects were partially due to reduced levels of Sir2 77
4.3.7 rDNA recombination accounted for variegated silencing in *sir2-G436D* colonies 80
4.3.8 *sir2-G436D* affects rDNA recombination rates 82
4.4 Discussion 83
4.4.1 Sir1 was the main factor preventing metastable silencing of *HML* and *HMR* 84
4.4.2 The unique phenotype of *sir2-G436D* 84
4.4.3 rDNA copy number contributed to variegated expression in *sir2-G436D* 84
4.4.4 The impact of *sir2-G436D* on rDNA recombination 85
4.4.5 The existence of an intermediate silenced state 86
4.5 Materials and Methods 87
4.6 References 91

List of Figures

2.1	Chromatin Domain Size Did Not Affect Silencing-Loss Rates	10
2.2	Nucleosome set deletions did not affect positions of remaining nucleosomes	11
2.3	Chromatin domain-size of *HMRα::cre* had minimal effects on silencing	12
2.4	*HMLα::cre* contained 22 nucleosomes	12
2.5	Chromatin domain size of *HMLα::cre* had minimal effects on silencing-loss rates	13
2.6	Chromatin domain size of *HMLα::cre* had minimal effects on silencing-loss rates measured by flow cytometry	14
2.7	Chromatin Domain Size Did Not Affect Silencing-Loss Rates in *sir1*Δ	16
2.8	*sir1*Δ cells exhibited metastability at *HMRα::GFP*	17
2.9	*sir1*Δ cells exhibited metastability at *HMLα::RFP* and *HMRα::GFP*	17
2.10	*HMLα::GFP* contained 12 nucleosomes	18
2.11	Chromatin domain size of *HMRα::GFP* in *sir1*Δ did not affect the frequencies of different epigenetic states but did affect GFP expression levels	18
2.12	Replisome mutants exhibited higher silencing-loss rates in the CRASH assay	20
2.13	Replisome mutants exhibited defects in epigenetic inheritance in the FLAME assay	22
2.14	Replisome mutants exhibited different frequencies of silenced and expressed cells in *sir1*Δ	23
2.15	Flow cytometry profiles of *sir1*Δ *dpb3*Δ *mcm2-3A HMRα::GFP* after FACS sorting	23
2.16	*dpb3*Δ exhibits a higher expression level of *HMRα::GFP* in expressed cells	24
2.17	Chromatin domain size did not strongly affect epigenetic switching rates in replisome mutant backgrounds	26
2.18	Chromatin domain size of *HMRα::GFP* did not strongly affect the frequencies of different epigenetic states in replisome mutant backgrounds	27
3.1	Inter-NDR distance affected silencing stability	42
3.2	Nucleosome positions and serial deletions in *HML*	43
3.3	Representative CRASH colonies for strains with large inter-NDR distances at *HML*	44
3.4	Quantification of apparent silencing-loss rates by flow cytometry	44
3.5	Strains with different inter-NDR distances had similar expression levels of *cre* in unsilenced cells	45
3.6	Inter-NDR distance affected nucleosome positioning.	46
3.7	NDR-R was necessary for oscillatory silencing effects	47
3.8	Representative CRASH colonies for strains with different inter-NDR distances and deletion of NDR-R	48
3.9	Oscillatory silencing effects were observed with heterologous NDRs	49
3.10	A trio of Reb1 binding sites depleted nucleosomes and did not generate oscillations of *cre* transcription in unsilenced cells	50
3.11	Representative CRASH colonies for strains with different distances between NDR-L and either NDR-RΔ::3xReb1	51
3.12	The *α1* initiation site was not necessary for oscillatory silencing effects	53
3.13	Effects of inter-NDR DNA content on oscillatory silencing effects	53

3.14	Inter-NDR distance affected silencing stability at *HMRα*	54
3.15	Inter-NDR distance influenced transmission of epigenetic states in *sir1*Δ	56
4.1	A screen for metastable silencing mutants revealed eight unique alleles of *sir1*	69
4.2	Additional FLAME phenotypes and characterization of the *sir1* mutants identified	70
4.3	Characterization of mutant *sir2-G436D*	72
4.4	Genetic analysis of the mutant isolated from the second mutagenesis screen	73
4.5	Overlap in GFP and RFP channels in *sir2-G436D* was not due to spectral bleedthrough	73
4.6	Live-cell imaging revealed the intermediate and heritable *sir2-G436D* expression state	75
4.7	Live-cell imaging of *hmlα2*Δ*::RFP* in *sir2-G436D*	76
4.8	Sir2-G436D levels were partially responsible for variegated silencing	78
4.9	Sir2-G436D was present at lower levels than Sir2	78
4.10	Effects of *SIR2* and *sir2-G436D* overexpression	79
4.11	Changes in rDNA copy number were partially responsible for silencing variegation in *sir2-G436D*	81
4.12	Effects of rDNA recombination on *sir2-G436D*	82
4.13	*sir2-G436D* lacks the ability to repress rDNA recombination	83

List of Tables

2.1 Comparison of epigenetic switching rates and proportion of silenced cells at equilibrium. 24

Acknowledgments

The academic journey is one of eternal surprises. In hindsight, one of the finest surprises I've experienced was my introduction to Jasper Rine. Little did I know, at the time, that my mother (who happens to know Jasper personally, well before I did) requested that he keep an eye on her son as he started a graduate career at UC Berkeley. If there was any theme to Jasper's role as my sentinel, it was one of stealth and nonchalance. I didn't know of him upon arriving at Berkeley, and had my sights firmly set upon other labs. But then, in a twist of fate that would come to define the next six years of my life, I sat down in an old auditorium to witness a group of professors present the questions they were pursuing, and perhaps capture the curiosity of individuals within my cohort.

Anyone that has seen Jasper tell a tale, scientific or otherwise, knows that he is riveting. It was a joy to see him wax poetic about the dogmatic relationship between genotype and phenotype, and present a modern subversion of this dogma: epigenetics. Indeed, I was so captivated by his performance that I can't remember much of what he said, just the thought that I had to work with him. The subsequent events were something of a domino effect in my memory; I met Jasper (which solidified my interest), rotated in his lab (pleasantly discovering that it was full of fun and ridiculous people), and discovered that I truly enjoyed this first jaunt into the world of genetics. Somehow, after biting on the line of Jasper's enthusiasm, I found myself in an intellectual wonderland. Here was a phenomenon, Sir-based silencing, that involved a truly simple phenotypic readout (is this gene transcribed?) and could be dissected with a powerful array of genetic and molecular tools. To boot, Jasper dangled a fascinating question in front of me: how can a cell transmit the memory of a silenced state?

What followed remains a haze of fond memories that evokes nostalgia as I write. Everyone in the lab was beautifully unique, and the lab thus represented a melting pot of personalities that loved spending so much time as a group, often not actually working, that a neighboring lab prudishly informed us that our scientific pursuits were probably suffering. Alas, they turned out to be completely wrong, and probably watched in horror as we continued to fill the break room with raucous laughter while simultaneously publishing many elegant papers. Lucky for them, we did move our lab to a different building eventually, thus allowing the third floor of Stanley Hall to return to the more quiet, dignified state that many of its members had previously enjoyed.

Rather than list the impressive attributes of each Rine lab member I got to work with, which would likely double the length of this thesis, it would be more entertaining for myself (and any readers) to write some stories of how some particular people influenced me (if you disagree, I apologize; I'm doing it anyway). In the beginning, I shared a bay with Anne Dodson, which she had named the Arctic Bay – indeed, when our feet were resting on the floor for more than a couple hours, they would slowly go numb. Anne worked very hard but was also very humble. This led to an interesting phenomenon in which she would quietly perform experiments at an alarming rate, and each of her lab meetings would provide a deluge of beautifully organized data complimented by a narration so relaxed that it could have been mistaken for nonchalance. Then, leaving the audience awe-struck, she would quietly return to her bench and the rest of us would slowly forget what she was capable of until her next lab meeting came about. Even after Anne had moved on to start a postdoc, lab meetings that had a lot of data were sometimes referred to as "Anne lab meetings". As such, Anne has been and continues to be a wonderful scientist that I try to emulate.

As if one inspiring coworker was not enough, I had the great fortune of both rotating and joining the Rine lab alongside my fellow graduate student, Davis Goodnight. One struggles to think of someone that better exemplifies miscellaneous fun and razor-sharp intellect. For the former quality, one must simply look to the time that our lab attended a GSA conference in Florida. While I bumbled around playing Pokemon Go, Davis persistently demanded that the group go to something called Disney Springs; things came to a fore one evening when everyone was trying to convince him otherwise, and he defiantly stated that he would be going with or without us. Whether a bluff or not, the plan worked, and we all ended up visiting what turned out to be a glorified Disney shopping mall. Indeed, if you are the type of person that dislikes those pesky rides at Disney World, Disney Springs is the place for you.

Intellectually speaking, Davis has a superpower. If an experiment has a flaw, no matter how obscure, he can quickly uncover and describe it with a wit that balances healthy criticism, a large chance to invoke laughter, and a small chance to offend (importantly, he is also quite able to calibrate it to different individuals). In contrast, I tend to jump at the opportunity to do any experiment and think about the ornamental flaws after the results are in. This led to a trend in which Davis and I, often later in the evening when the lab was empty, managed to engage in comical battles about the flaws or general importance of experiments (mostly mine), and pepper the discussion with self-deprecating comments about our respective tendencies to be pedantic (Davis) and stubbornly optimistic (me). Indeed, I have never had someone more frequently ask me *why* I was doing something and listen politely as I respond with wild gesticulations. These were truly some of my favorite memories of graduate school, and in some future scientific endeavors, I will probably ask myself, "What would Davis say?", and then promptly continue what I was doing anyway.

Part way through graduate school, Jasper accepted his final graduate student, Molly Brothers. It was probably some divine act that put her, a fiercely intelligent and annoying well-organized individual, as the scientific finale of Jasper's long and storied lab history. In 2020, when the pandemic hit, Molly sent me some pictures of her cat and I decided to return them as scientific cat memes. At this point, any reasonable person would have labeled me as a buffoon and demoted our friendship to "acquaintance" level, but I guess Molly likes buffoons, and we subsequently became something close to siblings. Many coffees, small trips, and scientific discussions later, I have learned two life lessons from Molly: it is important to be yourself, and color-code all of your notes. I will cherish and maintain many things that I've learned from Molly as I move on to future endeavors.

As people have come and gone from the Rine lab, Jasper has always been the enthusiastic and inspiring center. Numerous were the times that I would spontaneously enter his office and ask for advice or ask to show him some data, and he would respond, "Are you kidding?! I would like nothing more!" This was typically accompanied by a pronounced display of turning away from his computer, which always had multiple hundreds of files in disarray on the desktop. Indeed, anyone that may wonder how life arose in an entropic universe could also ponder how Jasper is able to extract a particular file out of such profound digital chaos. Anyway, you will never see Jasper be more gleeful than when he turns away from bureaucratic chores to talk about science, and he has stated many times that these conversations are the favorite part of his job. Of Jasper's numerous good qualities, a potent enthusiasm for science is the one that I will always remember most, as it has helped me find my own joy within this profession.

Over the course of graduate school, my thesis committee (consisting of Dr. Barbara Meyer, Dr. Kathy Collins, Dr. Oskar Hallatshek, and, of course, Dr. Jasper Rine) has provided

expert guidance and a valuable sense of continuity. Though, it must be said that we had a rocky start, as the first time that most of them convened in a room was to witness me fumble my way through a disastrous qualifying exam. Lest one interprets that has hyperbole, the review of my exam stated that my understanding of histones (which are, perhaps, the most important proteins of my thesis work) was “woefully lacking, even in response to leading questions.” Crestfallen, I spent that evening eating a tub of ice cream and watching the comfort movie, “Mean Girls”. However, since then I have learned a lot about histones, and even added a few things to the massive ledger of histone findings. I will always appreciate the patience and wisdom of my thesis committee through the arc of my graduate career.

Finally, the family. First, I must thank my parents for giving me both a nice mix of funtional alleles and a nurturing environment to grow as a person. I will also take this opportunity to publicly document that, even though they are both scientists, neither of them ever pushed for me to pursue science myself. However, Dad did pull a sneaky trick in 6th grade where he lightly suggested that I could map a *Drosophila* transgene for my science fair project. This had the dual result of sparking my interest in science and eliminating any possibility of visitors to my science fair poster. I must also thank my sister, Sarah, for being an endearing gremlin that never left my side until we went to college. Funny enough, I seem to have chased her to Berkeley and soon to Boston, which must suggest that I miss having her around. However, in all seriousness, I owe everything to my family. They are all givers in the deepest sense of the word, and if I could choose any family in the world, I would always choose them, without hestiation.

Chapter 1:

Introduction

1.1 The Question

A central tenant of cell biology is that cells transmit phenotypic traits to their offspring. While the heritability of traits is largely driven by inheritance of specific sequence variants in DNA, it can also be influenced by transmission of other non-genetic information. Therefore, it is possible for two genetically identical cells to exhibit different, heritable phenotypes. This phenomenon is a defining feature of the epigenetics field, which largely seeks to identify different types of non-genetic information and understand how such information can be inherited. Though many types of epigenetic memory exist, an especially mysterious example is the inheritance of heterochromatin. Specifically, it remains unclear how silencing factors create a heterochromatic state and how silencing can be faithfully inherited through multiple generations. Thus, the purpose of my thesis work was to address the last big conceptual question in heterochromatin biology, what defines an epigenetic state and what carries epigenetic memory?

1.2 Defining *cis* memory

When transcription in bistable, meaning that a gene can be "on" or "off" in different members of a genetically identical population of cells, this implies the existence of a feedback loop. For example, in the case of heterochromatin, the production of a silencing factor could be driven by a feedback loop, such that some cells are able to initiate the feedback loop and establish silencing while others are not. In this case, the feedback loop would exist in *trans*, meaning that the feedback loop is separate from the silenced domain but influences silencing by modulating the presence or absence of a diffusible silencing factor. Alternatively, the feedback loop could exist at or within the silenced domain itself, which would constitute a *cis*-acting feedback loop. An example of a cis-acting feedback loop could be the ability of silencing factors to modify local histones in some cells but not others. Thus, distinguishing between *cis*- and *trans*-acting feedback loops can support or exclude possible models of epigenetic inheritance.

One way to test *cis* versus *trans* effects is to have two different alleles of a bistable heterochromatic locus in a single cell. If the expression states of each allele are dependent (i.e. they are either both expressed or both silenced), then the memory component resides in *trans* and affects both loci equally. Conversely, if the expression states are independent (i.e. they can both be expressed, both be silenced, or one can be silenced while the other is expressed), then the memory component resides in *cis*. This test has been performed for bistable states of *HML* in *S. cerevisiae* (Xu et al., 2006) and bistable states of *FLC* in *Arabidopsis* (Berry et al., 2015); both studies found that the relevant memory components are *cis*-based. In a related experiment that involved bistable states of *mat2/3* in *pombe*, silenced cells were mated to expressed cells, and the resulting diploids were sporulated to generate haploids. Approximately half of the resulting haploids were silenced, and linkage analysis demonstrated that these cells inherited *mat2/3* from the parent that had been silenced at *mat2/3* (Grewal and Klar, 1996). Therefore, epigenetic states of *mat2/3* are also inherited in *cis*.

These observations of *cis*-based memory demonstrate that epigenetic inheritance occurs locally at heterochromatin for the cases studied. In this view, the identity of a heritable silencing

factor is limited to something that physically associates with heterochromatin and can be transmitted to each daughter chromatid during DNA replication.

1.3 The histone-based memory model

To establish a silenced state, silencing factors bind to silencers, spread across adjacent nucleosomes, and modify histones. This process requires read-write mechanisms of histone modifying complexes. For example, Sir2 deacetylates specific positions on the tails of histones H3 and H4 in *S. cerevisiae,* and Sir3 binds robustly to deacetylated histones. In principle, this pair of activities could allow the Sir complex to iteratively spread across nucleosomes (Carmen et al., 2002; Imai et al., 2000; Landry et al., 2000; Onishi et al., 2007). Consistent with this idea, catalytically-inactive alleles of Sir2 and a version of Sir3 that lacks nucleosome-binding activity are individually spreading-deficient (Hoppe et al., 2002; Rusché et al., 2002). In *S. pombe*, Clr4 methylates H3K9 and Swi6 binds efficiently to H3K9me3, and mutations in these factors also disrupt spread from nucleation sites (Hall et al., 2002). Therefore, a remarkable property of many silencing factors is that they can both modify histones and bind to the modifications that they generate. This property is important for silencing factors to coat nucleosomes within a silenced domain.

During DNA replication, daughter chromatids locally inherit modified histone H3-H4 tetramers from the parental chromatid and receive newly synthesized histones from the nucleoplasm (Gaydos et al., 2014; Prior et al., 1980; Schlissel and Rine, 2019). The combination of histone inheritance and the read-write mechanism of silencing machinery forms the basis of the histone-based memory model. Specifically, this model allows silencing factors to be evicted from chromatin during DNA replication, re-bind to modified histones on daughter chromatids, and modify adjacent, naïve histones to maintain the silenced state. Therefore, epigenetic memory could be driven by the inheritance of modified histones and a positive feedback loop between histone modifications and silencing factors.

1.4 The paradox

The histone-based memory model makes a simple prediction. If histones are sufficient to carry epigenetic memory, then silencer elements should be dispensible for memory once the silenced state is established. However, multiple studies have found that silencers are necessary for either silencing maintenance and/or inheritance, depending on the context. In one example, the induced removal of silencers from *HML* permitted the maintenance of silencing in arrested cells but led to loss of silencing in ~95% of cells upon one passage through the cell cycle (Holmes and Broach, 1996). This result suggests that heterochromatin can be maintained in the absence of silencers but is subsequently lost during a cell cycle event, which is likely DNA replication. In partial contrast, another study excised of *HMR* from the *S. cerevisiae* genome to generate a plasmid that was silenced but lacked the *HMR* silencers (Cheng and Gartenberg, 2000). This plasmid lost silencing rapidly even though it was non-replicating, arguing that silencers are required for silencing maintenance. One explanation for this discrepancy is that silencing on a plasmid is inherently unstable, and more likely to fail when subjected to insults such as silencer removal.

To provide a different test of silencer activity, two different studies in *S. pombe* made fusion proteins with the silencing factor Clr4, such that it could be inducibly recruited to a euchromatic site (Audergon et al., 2015; Ragunathan et al., 2015). These studies found that targeted recruitment of Clr4 was able to silence a nearby reporter gene, but that this silencing

gradually disappeared upon removal of Clr4 recruitment. Importantly, this process occurred in a strain containing wild-type Clr4, which can both methylate H3K9 and bind to H3K9me3. Thus, even though a histone-based feedback loop existed in these strains, silencing was not durably heritable in the absence of a nucleation mechanism. Interestingly, silencing did become heritable upon removal of Epe1, the H3K9 demethylase that antagonizes silencing. Therefore, modified histones and/or factors associated with modified histones are sufficient to carry a memory of silencing when a silencing antagonist is removed but are not sufficient to carry memory under normal conditions.

In an extension of these *S. pombe* studies, additional studies searched for mutations other than *epe1*Δ that could facilitate silencing memory in the absence of nucleation. One study found that removal of the chromatin remodeler Fft3 reduced the rate of nucleosome turnover and facilitated silencing memory (Taneja et al., 2017). Additionally, the transient silencing generated by transient Clr4 recruitment becomes heritable when combined with a weak silencer element termed *REIII* (Wang et al., 2021; Wang and Moazed, 2017). Interestingly, this silencer is not sufficient to silence alone, yet is able to support previously established silencing. When multiple *REIII* elements are positioned together, they exhibit *de novo* silencing activity. Therefore, silencers are not only necessary for silencing inheritance in some contexts but can also directly contribute to silencing memory.

These findings provide a paradox. The definition of an epigenetic phenomenon is that genetically identical cells can exhibit different, heritable traits. How could a silencer, which is a specific DNA sequence, perpetuate an DNA-sequence-independent state in some cells but not others? Silencers are generally regarded merely as sites bound by DNA binding proteins and their associated silencing factors. One possibility is that post-translational modifications vary at silencers, allowing some silencer structures to promote a silenced state while others do not. Alternatively, some researchers propose that histones carry epigenetic memory, but silencers are permissive to silencing and therefore are required to observe the silenced state *per se* (Wang and Moazed, 2017). Regardless, biology textbooks often state that the histone-based memory model could explain epigenetic memory, yet also caution that this model remains contentious. Within this thesis work, I aimed to address this paradox with studies in *S. cerevisiae.*

1.5 References:

Audergon PNCB, Catania S, Kagansky A, Tong P, Shukla M, Pidoux AL, Allshire RC. 2015. Epigenetics. Restricted epigenetic inheritance of H3K9 methylation. *Science* 348:132–135. doi:10.1126/science.1260638

Berry S, Hartley M, Olsson T, Dean C, Howard M. 2015. Local chromatin environment of a Polycomb target gene instructs its own epigenetic inheritance. *eLife*. doi:10.7554/elife.07205.001

Carmen AA, Milne L, Grunstein M. 2002. Acetylation of the Yeast Histone H4 N Terminus Regulates Its Binding to Heterochromatin Protein SIR3. *Journal of Biological Chemistry* 277:4778–4781. doi:10.1074/jbc.m110532200

Cheng TH, Gartenberg MR. 2000. Yeast heterochromatin is a dynamic structure that requires silencers continuously. *Genes & development* 14:452–463.

Gaydos LJ, Wang W, Strome S. 2014. Gene repression. H3K27me and PRC2 transmit a memory of repression across generations and during development. *Science* 345:1515–1518. doi:10.1126/science.1255023

Grewal S, Klar A. 1996. Chromosomal inheritance of epigenetic states in fission yeast during mitosis and meiosis. *Cell*.

Hall IM, Shankaranarayana GD, Noma K-I, Ayoub N, Cohen A, Grewal SIS. 2002. Establishment and maintenance of a heterochromatin domain. *Science* 297:2232–2237. doi:10.1126/science.1076466

Holmes SG, Broach JR. 1996. Silencers are required for inheritance of the repressed state in yeast. *Gene Dev* 10:1021–1032. doi:10.1101/gad.10.8.1021

Hoppe GJ, Tanny JC, Rudner AD, Gerber SA, Danaie S, Gygi SP, Moazed D. 2002. Steps in Assembly of Silent Chromatin in Yeast: Sir3-Independent Binding of a Sir2/Sir4 Complex to Silencers and Role for Sir2-Dependent Deacetylation. *Molecular and Cellular Biology* 22:4167–4180. doi:10.1128/mcb.22.12.4167-4180.2002

Imai S, Armstrong CM, Kaeberlein M, Guarente L. 2000. Transcriptional silencing and longevity protein Sir2 is an NAD-dependent histone deacetylase. *Nature* 403:795–800. doi:10.1038/35001622

Landry J, Sutton A, Tafrov ST, Heller RC, Stebbins J, Pillus L, Sternglanz R. 2000. The silencing protein SIR2 and its homologs are NAD-dependent protein deacetylases. *Proc National Acad Sci* 97:5807–5811. doi:10.1073/pnas.110148297

Onishi M, Liou G-G, Buchberger JR, Walz T, Moazed D. 2007. Role of the Conserved Sir3-BAH Domain in Nucleosome Binding and Silent Chromatin Assembly. *Mol Cell* 28:1015–1028. doi:10.1016/j.molcel.2007.12.004

Prior CP, Cantor CR, Johnson EM, Allfrey VG. 1980. Incorporation of exogenous pyrene-labeled histone into Physarum chromatin: a system for studying changes in nucleosomes assembled in vivo. *Cell* 20:597–608.

Ragunathan K, Jih G, Moazed D. 2015. Epigenetics. Epigenetic inheritance uncoupled from sequence-specific recruitment. *Science* 348:1258699. doi:10.1126/science.1258699

Rusché LN, Kirchmaier AL, Rine J. 2002. Ordered nucleation and spreading of silenced chromatin in Saccharomyces cerevisiae. *Molecular biology of the cell* 13:2207–2222. doi:10.1091/mbc.e02-03-0175

Schlissel G, Rine J. 2019. The nucleosome core particle remembers its position through DNA replication and RNA transcription. *Proceedings of the National Academy of Sciences of the United States of America* 12:201911943–7. doi:10.1073/pnas.1911943116

Taneja N, Zofall M, Balachandran V, Thillainadesan G, Sugiyama T, Wheeler D, Zhou M, Grewal SIS. 2017. SNF2 Family Protein Fft3 Suppresses Nucleosome Turnover to Promote Epigenetic Inheritance and Proper Replication. *Molecular cell* 66:50-62.e6. doi:10.1016/j.molcel.2017.02.006

Wang X, Moazed D. 2017. DNA sequence-dependent epigenetic inheritance of gene silencing and histone H3K9 methylation. *Science* eaaj2114-8. doi:10.1126/science.aaj2114

Wang X, Paulo JA, Li X, Zhou H, Yu J, Gygi SP, Moazed D. 2021. A composite DNA element that functions as a maintainer required for epigenetic inheritance of heterochromatin. *Mol Cell* 81:3979-3991.e4. doi:10.1016/j.molcel.2021.07.017

Xu EY, Zawadzki KA, Broach JR. 2006. Single-Cell Observations Reveal Intermediate Transcriptional Silencing States. *Molecular cell* 23:219–229. doi:10.1016/j.molcel.2006.05.035

Chapter 2:

Epigenetic Memory Independent of Symmetric Histone Inheritance

2.1 Abstract

Heterochromatic gene silencing is an important form of gene regulation that usually requires specific histone modifications. A popular model posits that inheritance of modified histones, especially in the form of H3-H4 tetramers, underlies inheritance of heterochromatin. Because H3-H4 tetramers are randomly distributed between daughter chromatids during DNA replication, rare occurrences of asymmetric tetramer inheritance within a heterochromatic domain would have the potential to destabilize heterochromatin. This model makes a prediction that shorter heterochromatic domains would experience unbalanced tetramer inheritance more frequently, and thereby be less stable. In contrast to this prediction, we found that shortening a heterochromatic domain in *Saccharomyces* had no impact on the strength of silencing nor its heritability. Additionally, we found that replisome mutations that disrupt inheritance of H3-H4 tetramers had only minor effects on heterochromatin stability. These findings suggest that histones carry little or no memory of the heterochromatin state through DNA replication.

2.2 Introduction

A central question in biology is how cells with identical genotypes can exhibit different, heritable phenotypes. By definition, these phenotypes are determined by information that is epigenetic, or "above the genome." Just as genetic inheritance requires faithful replication of DNA, epigenetic inheritance requires replication of information that is transmitted to both daughter cells during division. Faithful transmission of epigenetic information is crucial for multiple heterochromatin-based processes such as X-chromosome inactivation in mammals and cold-induced gene silencing in *Arabidopsis*. In these cases and others, the epigenetic inheritance of heterochromatin indicates that some components of heterochromatin must behave as heritable units. Surprisingly, the identity of this epigenetic information remains unclear and heavily debated.

The histone subunits of nucleosomes, especially histones H3 and H4, are modified by a variety of covalent modifications that are integral to heterochromatin function. During DNA replication, nucleosomes are partially disrupted and marked parental H3-H4 tetramers are locally inherited to daughter chromatids. As these tetramers are inherited, they are reassembled into nucleosomes that are interspersed with nucleosomes containing newly synthesized H3-H4 tetramers (Prior et al. 1980; Jackson 1988; Schlissel & Rine 2019). One model for epigenetic inheritance posits that marked parental histones inherited through DNA replication recruit histone modifiers to deposit similar marks on new adjacent nucleosomes, thereby reestablishing the previous local landscape of histone modifications (Hecht et al. 1995; Hoppe et al. 2002; Gaydos et al. 2014). In support of this model, the H3K27 methyltransferase PRC2 binds preferentially to H3K27me3 *in vitro* (Hansen et al. 2008) and some other modifying enzymes show a similar ability to bind their histone modifications (Zhang et al. 2008; Hecht et al. 1995; Imai et al. 2000). If this model is correct, modified H3-H4 tetramers would constitute heritable units that drive epigenetic memory of chromatin states.

Studies have come to different conclusions regarding whether histones can carry epigenetic memory. In *S. pombe,* localized methylation of H3K9 can silence a reporter gene, and this silenced state is heritable in the presence of the H3K9 methyltransferase Clr4p as long as the demethylase

Epe1p is absent (Audergon et al. 2015; Ragunathan et al. 2015). These studies suggest that histone modifications can facilitate epigenetic inheritance, and caution that such a mechanism is normally obscured by H3K9 demethylation activity. Conversely, induced removal of silencer elements from silenced chromatin in *S. cerevisiae* causes almost all cells to lose silencing of adjacent genes after just one round of DNA replication (Holmes & Broach 1996). Similar results are found when silencers are removed from *Drosophila* chromatin silenced by the Polycomb complex (Laprell et al. 2017). These silencer-removal experiments suggest that modified histones are not sufficient to propagate the silenced chromatin state through DNA replication.

The model in which histones carry epigenetic memory makes a testable prediction: since parental H3-H4 tetramers have long been thought to be randomly partitioned between daughter chromatids (Sogo et al. 1986; Cusick et al. 1984), rare events could occur in which most or all marked parental H3-H4 tetramers within a domain segregate asymmetrically to one daughter chromatid, causing the other to inherit primarily newly synthesized histones. A chromatin domain with an insufficient number of marked parental tetramers would be expected to experience a loss-of-chromatin-state event. In this view, a smaller chromatin domain would correspond to fewer marked nucleosomes and yield more frequent events in which parental H3-H4 tetramers segregate asymmetrically and the chromatin state is lost. This potential use of domain size for protection against epimutation is widely conjectured (Dodd et al. 2007; Kaufman & Rando 2010; Moazed 2011; Ramachandran & Henikoff 2015), and may explain why chromatin domains subject to stable epigenetic inheritance are often many kilobases long. For example, chromatin domains silenced by Polycomb Responsive Elements (PREs) in *Drosophila* usually extend beyond 10kb (Schwartz et al. 2006). In contrast, one study in *A. thaliana* found that a chromatin domain containing only three H3K27me3-marked nucleosomes is inherited more frequently than would be predicted if random segregation of tetramers caused loss events (Yang et al. 2017). However, no study to our knowledge has systematically tested this prediction.

To test directly whether inheritance of a chromatin state is affected by chromatin-domain size, we focused on the heterochromatin domains at the *HMR* and *HML* loci in *S. cerevisiae*. These loci contain copies of mating-type genes that are silenced by the activity of Sir proteins. Specifically, the *E* and *I* silencers flanking *HMR* and *HML* are occupied by the DNA-binding proteins Rap1, Abf1, and ORC, that collectively recruit Sir proteins; Sir1 is present only at silencers, whereas Sir2/3/4 complexes bind to silencers and spread across the locus in a process that requires deacetylation of H4K16 (Rusché et al. 2002; Thurtle & Rine 2014). Notably, DNA methylation and RNA interference do not exist in *S. cerevisiae*.

Under normal conditions, *HMR* and *HML* are constitutively silenced. Rare and transient loss-of-silencing events can be measured by a sensitive assay that uses the *cre* recombinase under control of the *HMLα2* promoter to convert transient transcriptional events into permanent, heritable changes in fluorescence phenotypes (Dodson & Rine 2015). In contrast, deletion of *SIR1* causes genetically identical cells to be in either of two states at *HMR* and *HML*: either fully silenced or fully expressed (Pillus & Rine 1989; E. Y. Xu et al. 2006; Dodson & Rine 2015). These different transcriptional states are mitotically heritable and cells switch between states at a low frequency. This study addresses three questions regarding the inheritance of heterochromatin in *Saccharomyces*: 1) Does the size of a silenced domain determine the fidelity of inheritance? 2) Does removal of Sir1, a protein that facilitates recruitment of silencing machinery to silencers, uncover an effect of chromatin domain size on heritability of transcriptional states? 3) Do replisome components that facilitate symmetric inheritance of parental H3-H4 tetramers also promote inheritance of transcriptional states?

2.3 Results

Local inheritance of nucleosomes and their locus-specific modifications are thought to facilitate inheritance of chromatin states. According to this view, if parental H3-H4 tetramers were randomly partitioned between the two daughter chromatids during replication, one would expect a chromatin state to be lost if, by chance, one of the daughter chromatids failed to receive enough parental H3-H4 tetramers to support the propagation of that state. By this model, the number of nucleosomes in the chromatin domain would influence the fidelity of chromatin-state inheritance.

2.3.1 Nucleosome number did not determine the rate of silencing loss

To test if nucleosome number affected the stable inheritance of a chromatin state, we used the Cre-Reported Altered States of Heterochromatin (CRASH) assay (Dodson & Rine 2015) (**Figure 2.1A**). In this assay, *cre* replaces the *α2* coding sequence in *HMRα*, and a *lox* cassette containing fluorescent reporters separated by *loxP* sites is located on a separate chromosome. Though *HMRα* is transcriptionally repressed, rare loss-of-silencing events cause transient expression of *cre*. These events lead to excision of *RFP* from the lox cassette, and a switch from RFP to GFP expression. Because this change is heritable, loss-of-silencing events during colony growth lead to formation of sectors of cells expressing GFP, appearing green on an otherwise red background. The number of sectors in a colony reflects the frequency at which *HMRα* transiently loses silencing: more sectors indicate less stable silencing.

HMRα::cre contained fourteen well-positioned nucleosomes between the *E* and *I* silencers (**Figure 2.2**). To change nucleosome number within the locus, we deleted DNA corresponding to different sets of nucleosomes (**Figure 2.1B**). Notably, removing DNA corresponding to different combinations of nucleosomes allowed us to discern whether any effects on silencing stability were due to nucleosome number or to removal of specific DNA sequences. These deletions did not affect the local positions of the remaining nucleosomes as measured by MNase-Seq (**Figure 2.2**).

At the limit of models by which nucleosomes transmit memory of transcriptional states, inheritance of a single parental H3-H4 tetramer to a daughter chromatid would be sufficient to template the silenced state. The expected loss-of-silencing rate would thereby reflect the frequency at which a chromatid inherits no marked parental H3-H4 tetramers due to random segregation of these tetramers during replication. For example, considering a hypothetical chromatin domain that has three nucleosomes, one would expect that a given daughter chromatid would have a one-in-eight chance of inheriting no parental tetramers during replication. Therefore, one in eight daughter cells would be expected to lose silencing. This rate would increase exponentially with shorter chromatin domains as the probability of inheriting at least one parental tetramer decreases (**Figure 2.1C**). Additionally, if inheritance of two or more parental H3-H4 tetramers were necessary to template the silenced state, the expected loss-of-silencing rate would be even higher.

The silencing-loss rate predicted by random segregation of H3-H4 tetramers would be approximately 0.006% of cell divisions for full-length *HMRα::cre* (Strain N14) (**Figure 2.1D**). Previous studies demonstrate that this strain loses silencing in approximately 0.1% of cell divisions (Dodson & Rine 2015). This difference between expected and observed values could be explained by the existence of other processes besides histone inheritance that potentially destabilize silencing and thereby contribute to the overall silencing-loss rate. In contrast to the

full size *HMRα::cre*, the smallest version of *HMRα::cre* (Strain N7) would be expected to lose silencing in approximately 1% of cell divisions. Therefore, if this model were correct, we would expect to see increased sectoring rates in strains with shorter versions of *HMRα::cre*. Surprisingly, decreasing nucleosome number at *HMRα::cre* led to a slight decrease in silencing loss as measured by sector frequency (**Figure 2.1E**).

To provide an independent measurement of the silencing-loss rate, we also measured fluorescence profiles of single cells. Cells that have recently lost silencing of *cre* at *HMRα* contain both RFP and GFP due to GFP expression and the persistence of RFP prior to its degradation and dilution. Using flow cytometry to measure the frequency of cells that contain both RFP and GFP, we confirmed that nucleosome number did not strongly affect silencing-loss rates, and that reduction of nucleosomes might have a slight stabilizing effect on silencing (**Figure 2.1F**, **Figure 2.3**). Thus, the size of *HMRα::cre* did not dramatically influence inheritance of the silenced state, in contrast to the expectation from models in which H3-H4 tetramers carry memory of chromatin states through cell divisions. Additionally, we found that changing nucleosome number at *HMLα::cre* led to a small increase in silencing loss, and that these effects were not due strictly to domain size (**Figures 2.4-2.6**). Since studies at *HMLα* are potentially complicated by its proximity to a telomere, which is also bound by Sir proteins, further studies were performed only at *HMRα.*

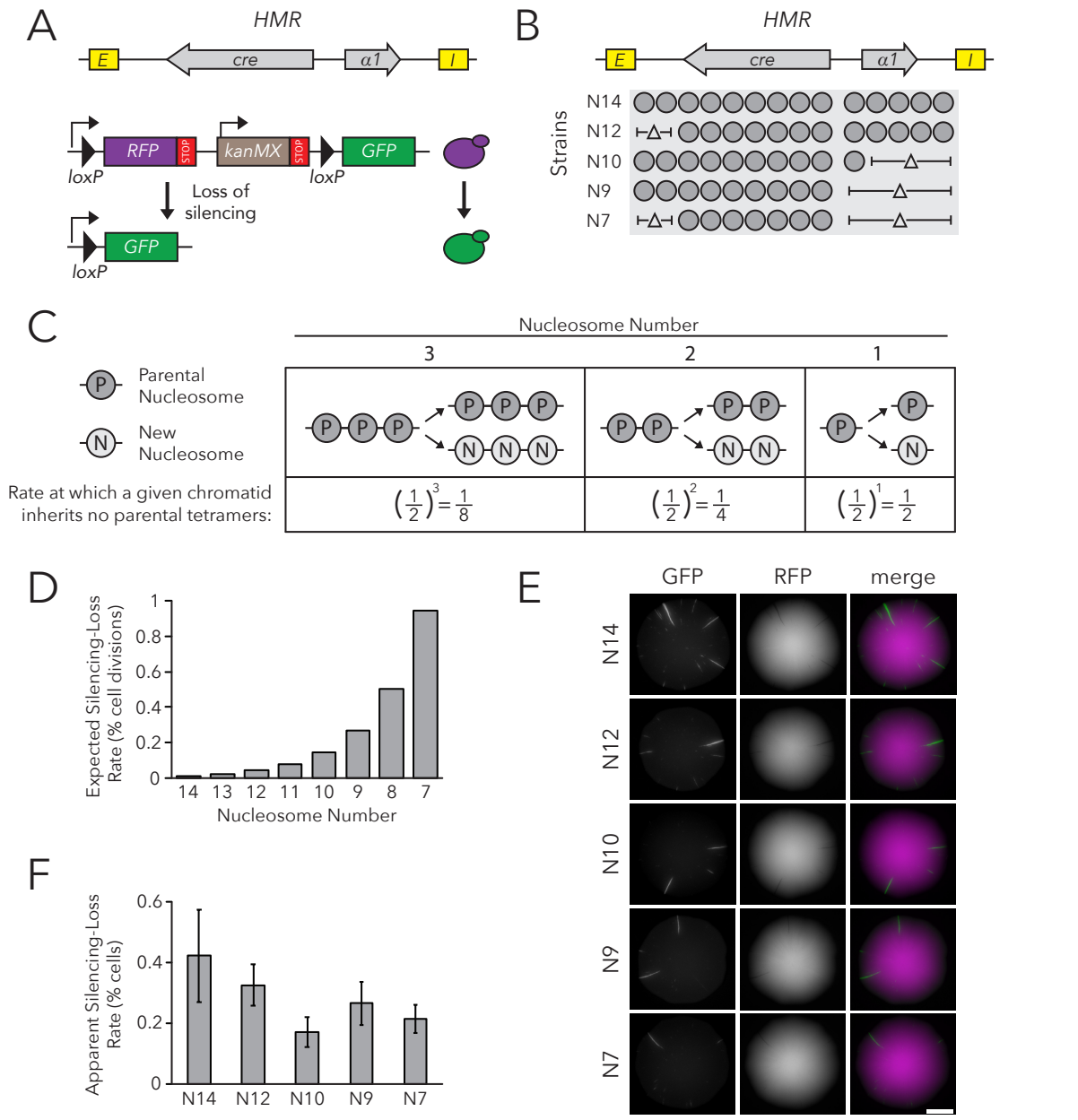

Figure 2.1: Chromatin Domain Size Did Not Affect Silencing-Loss Rates. (A) Schematic of the Cre-Reported Altered States of Heterochromatin (CRASH) assay (Dodson & Rine 2015). *HMRα::cre* contains the *E* and *I* silencers, the *α1* gene, and a *cre* transgene. Transient loss of silencing at *HMRα::cre* causes Cre-mediated recombination of *loxP* sites in a *RFP-GFP* cassette. This process creates a permanent, heritable switch from RFP to GFP expression. (B) Diagram of nucleosomes in *HMRα::cre*. Fourteen nucleosomes were present in full-length *HMRα::cre*, which we term Strain N14 (JRY11471). Combinations of nucleosomal DNA were deleted to change the size of *HMRα::cre*; the smallest size was seven nucleosomes (Strain N7) (JRY11540). Nucleosome positions were determined by MNase-seq as shown in **Figure 2.2**. (C) Schematic of how random segregation of parental H3-H4 tetramers to daughter chromatids could cause silencing loss. Under the model that inheritance of a single marked H3-H4 tetramer to a daughter chromatid would be sufficient to propagate the silenced state, the chance that a daughter chromatid inherits no parental tetramers and loses the silenced state would be 0.5^(the number of nucleosomes in *HMRα::cre*). Parental nucleosomes contain inherited H3-H4 tetramers, whereas new nucleosomes contain newly synthesized H3-H4 tetramers. Hypothetical chromatin domains of different sizes are provided for comparison. (D) Expected loss-of-silencing rates for different sizes of *HMRα::cre.* (E) Representative CRASH

colonies for Strains N14 through N7. Because loss of silencing leads to a heritable switch from RFP to GFP expression, progeny of a cell that loses silencing will form a GFP sector; the frequency of sectors in a colony represents the frequency at which that strain loses silencing. Scale bar, 2 mm. (F) Quantification of apparent silencing-loss rates, as described in *Materials and Methods*. Data are means ± SD (n = 6 independent cultures). ANOVA and Tukey tests were used to test statistical significance. Only strains N10 and N7 were significantly different ($p < 0.05$) than N14. Data are presented as a scatter plot in **Figure 2.3**.

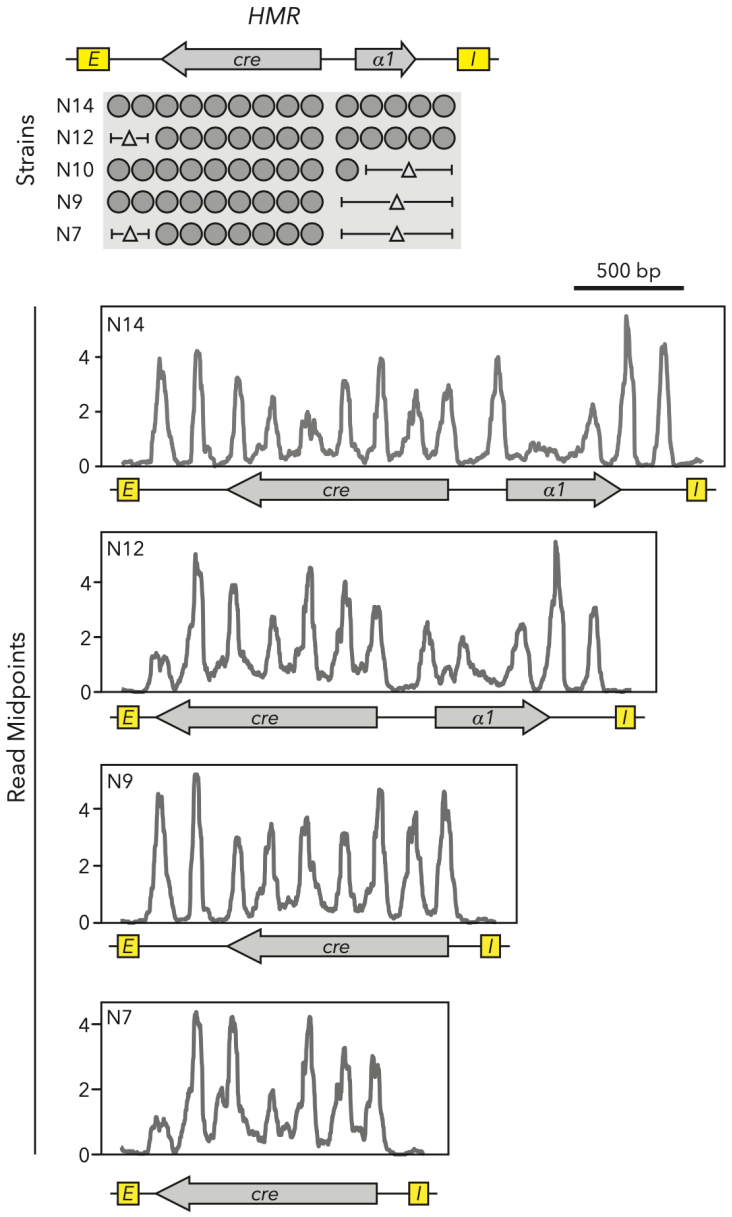

Figure 2.2: Nucleosome set deletions did not affect positions of remaining nucleosomes. MNase-seq was performed on strains with different sizes of *HMRα::cre*. Midpoints of nucleosome-sized fragments were calculated, plotted, and smoothed.

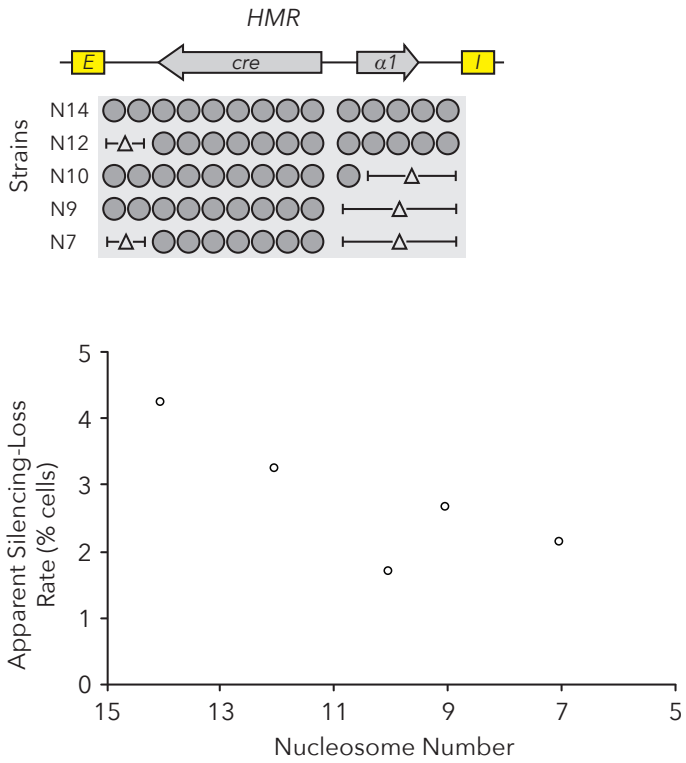

Figure 2.3: Chromatin domain-size of *HMRα::cre* had minimal effects on silencing. Data represent means of apparent silencing-loss rates (n = 6 independent cultures) from **Figure 2.1F**, presented as a scatter plot.

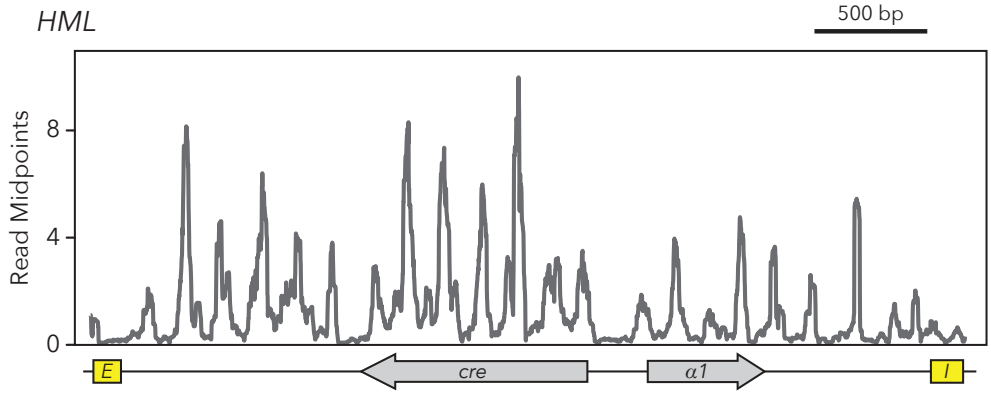

Figure 2.4: *HMLα::cre* contained 22 nucleosomes. MNase-seq was performed on the strain with full-length *HMLα::cre* (JRY11259). Midpoints of nucleosome-sized fragments were calculated, plotted, and smoothed.

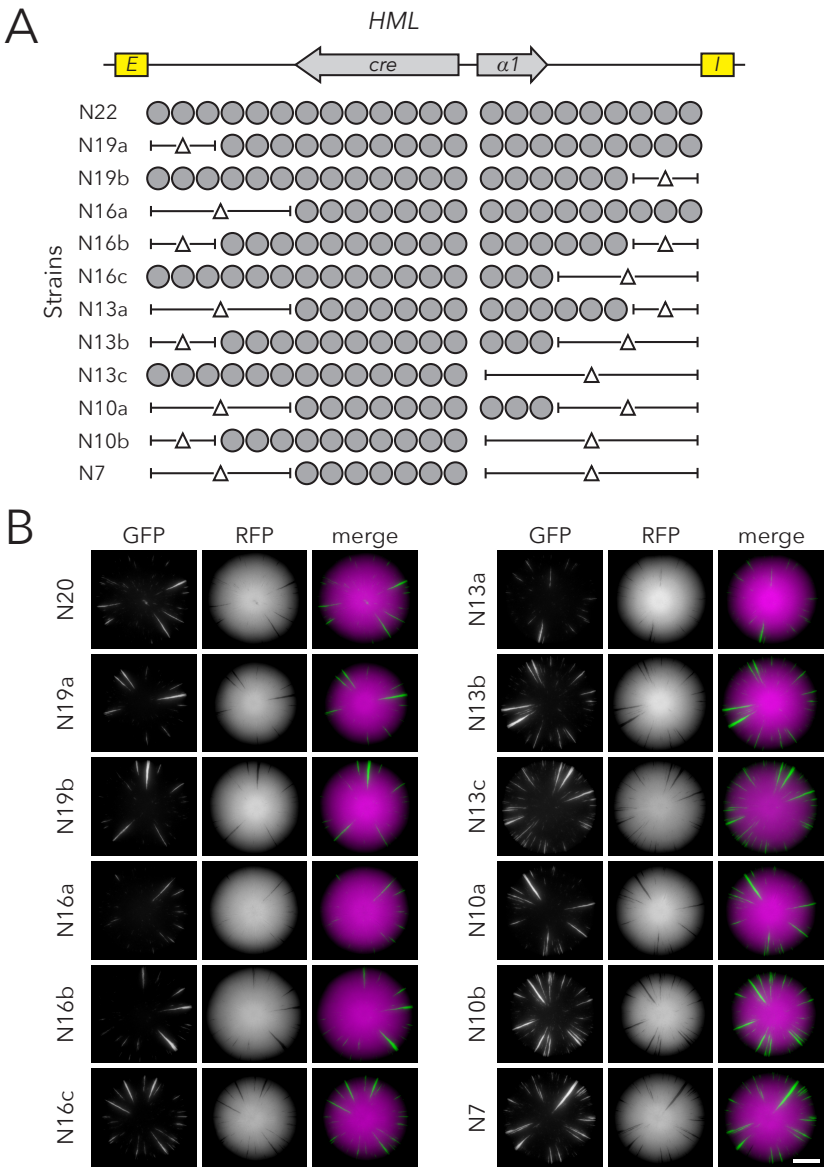

Figure 2.5: Chromatin domain size of *HMLα::cre* had minimal effects on silencing-loss rates. (A) Diagram of nucleosomes in full-length *HMLα::cre* (N22) (JRY11259) and strains with deletions of nucleosomal DNA. The smallest version of *HMLα::cre* had seven nucleosomes (N7) (JRY11292). (B) Representative CRASH colonies for Strains N22 (JRY11259) through N7 (JRY11292). Scale bar, 2 mm.

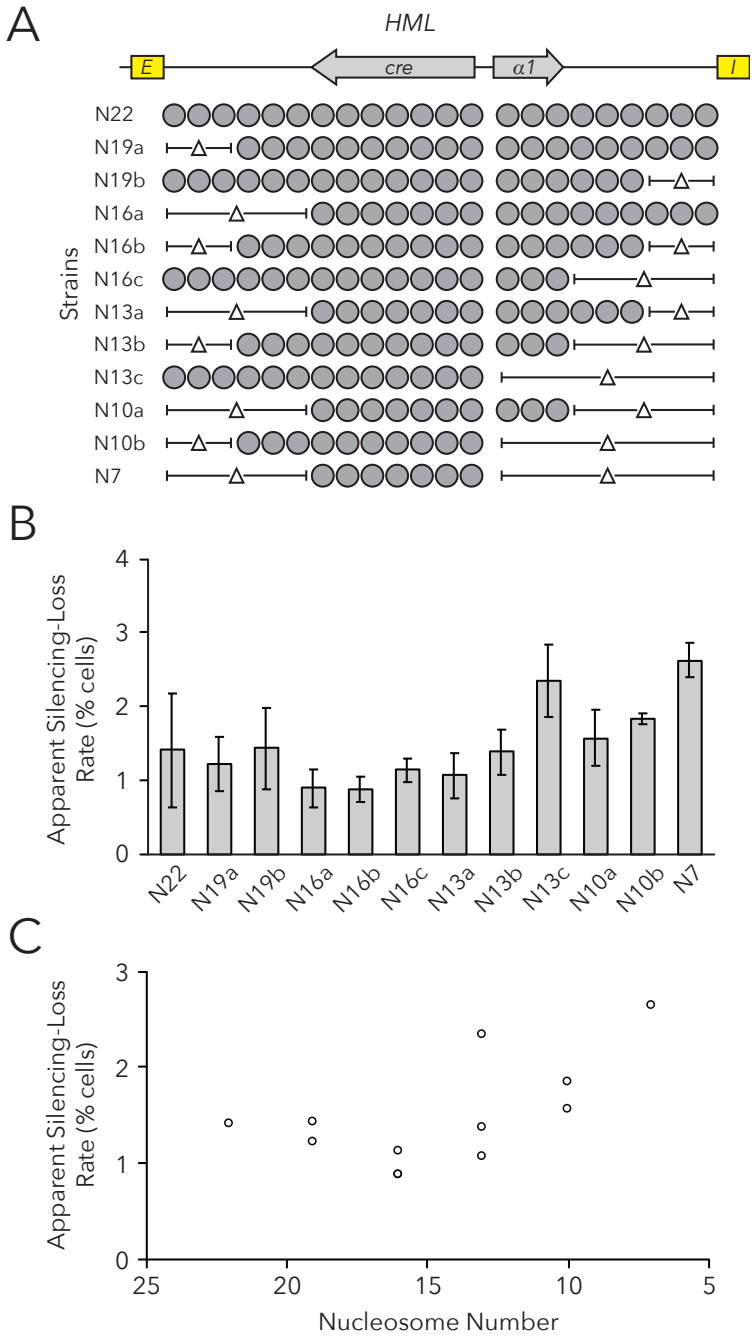

Figure 2.6: Chromatin domain size of *HMLα::cre* had minimal effects on silencing-loss rates measured by flow cytometry. (A) Diagram of nucleosomes in *HMLα::cre*, as shown in **Figure 2.4**. (B) Quantification of apparent silencing-loss rates, as described in *Materials and Methods*. Data are means ± SD (n = 6 independent cultures). ANOVA and Tukey tests were used to test for statistical significance. Only strains N13c and N7 were significantly different ($p < 0.05$) than N22. (C) Data from (B), with means of apparent silencing-loss rates presented on a scatter plot.

2.3.2 Nucleosome number did not affect transmission of epigenetic states in *sir1*Δ.

The silencers flanking *HMRα* are bound by three different proteins that collaborate to recruit Sir proteins (Rusché et al. 2003). One possibility for the apparent insensitivity of silencing inheritance to nucleosome number was that the constant recruitment of Sir proteins to these sites was efficient enough to mask a contribution of histone inheritance to inheritance of chromatin states. In this scenario, silencers would be capable of recruiting enough Sir proteins to keep the locus silenced during DNA replication, regardless of histone segregation patterns. Sir1 binds to silencers, and deletion of *SIR1* partially disrupts silencer activity, as measured by defects in silencing establishment and silencing heritability (Pillus & Rine 1989; Dodson & Rine 2015). We therefore tested if parental H3-H4 tetramer inheritance contributed to transmission of the silenced state when silencer-based recruitment of Sir proteins was impaired by the *sir1*Δ mutation.

Within individual cells in a population of *sir1*Δ cells, *HMR* is either transcriptionally silenced or fully expressed. These different states are mitotically heritable: a cell in one state usually gives rise to more cells of that state. To observe this epigenetic phenomenon, we placed the *GFP* coding sequence into *HMRα*, such that it was expressed under control of the *α2* promoter. Silencing was monitored by GFP expression at the single-cell level using fluorescence microscopy and flow cytometry. In comparison to control strains in which *HMRα* was fully silenced (*SIR+)* or expressed (*sir4*Δ), *HMRα* was silenced in roughly 99% of *sir1*Δ cells and was expressed in the remaining cells (**Figure 2.8**, **Figure 2.9**). We also observed different epigenetic states for *HMLα::RFP*. We used live-cell imaging to monitor divisions of *sir1*Δ cells to identify cells in which silencing of *HMR* was lost, and other cases in which it was gained (**Figure 2.7A**). Thus *HMRα::GFP* could be used to measure the efficiency of epigenetic inheritance in *sir1*Δ, similarly to previous studies (E. Y. Xu et al. 2006). For simplicity, we named measurements of epigenetic inheritance in *sir1*Δ as the FLuorescent Analysis of Metastable Expression (FLAME) assay.

To test the prediction that chromatin domain size affects silencing heritability with the FLAME assay, we removed DNA corresponding to sets of nucleosomes in the *HMRα::GFP* locus (**Figure 2.7B**, **Figure 2.10**, **Figure 2.11**). As before, models in which nucleosomes were carriers of epigenetic memory predicted that shorter chromatin domains would have a higher rate of silencing loss (**Figure 2.7C**). Using time-lapse fluorescence microscopy to monitor transcriptional states in individual cells and their descendants as they divided, we found that nucleosome number did not affect the frequency of silencing loss (**Figure 2.7D**). Because the expressed state is also heritable, with occasional switches to the silenced state, we also asked if the heritability of the expressed state was influenced by the number of nucleosomes in the locus. The frequency of silencing establishment was similar between strains with different numbers of nucleosomes at *HMRα::GFP* (**Figure 2.7E**). Therefore, even in a background with defective silencer activity, chromatin-domain size did not strongly influence silencing dynamics. These findings argued against models in which parental H3-H4 tetramers and their modifications are required for the epigenetic inheritance of gene expression states in *Saccharomyces*.

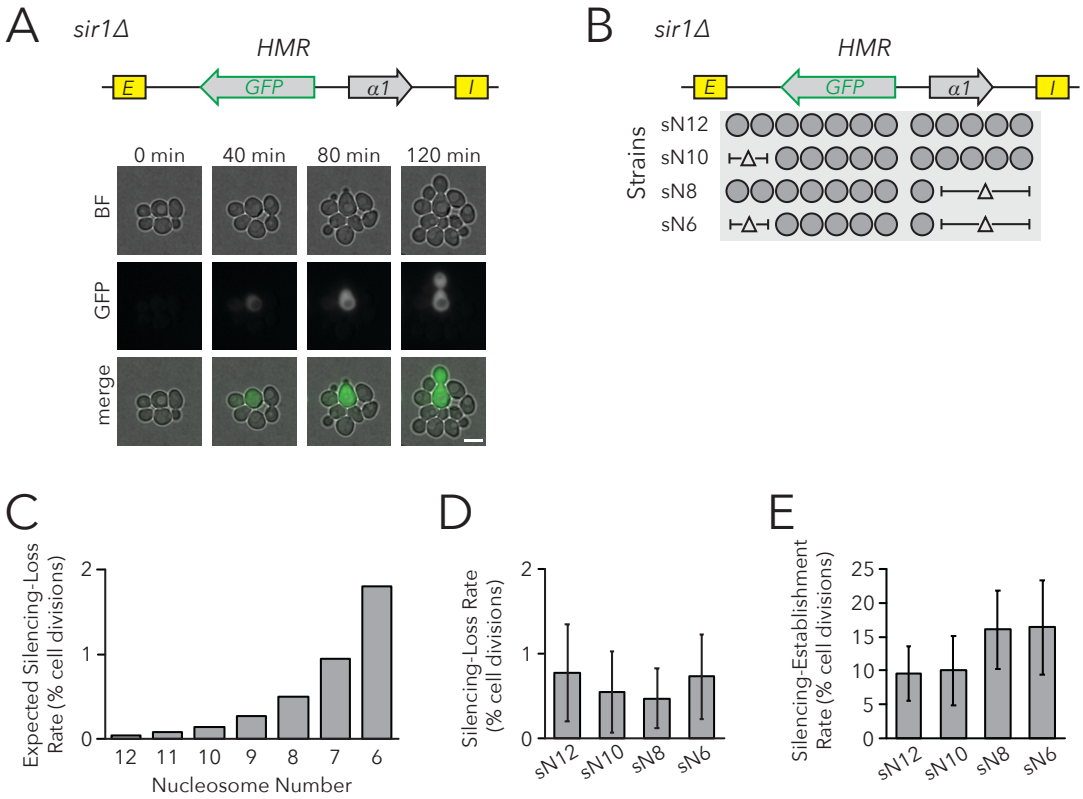

Figure 2.7: Chromatin Domain Size Did Not Affect Silencing-Loss Rates in *sir1*Δ. (A) Diagram of the FLuorescent Analysis of Metastable Expression (FLAME) assay. In a *sir1*Δ background, *GFP* replaced the *α2* gene so that transcriptional activity of *HMRα::GFP* could be monitored at the single-cell level (JRY11478). Loss-of-silencing events were observed in dividing cells by using time-lapse microscopy. Scale bar, 5 μm. Establishment-of-silencing events were also observed. Silencing defects in different *sir* mutants are shown by microscopy in **Figure 2.8** and by flow cytometry in **Figure 2.9**. (B) Diagram of nucleosomes in *HMRα::GFP*. Twelve nucleosomes were present in full-length *HMRα::GFP* (Strain sN12) (JRY11478) (**Figure 2.10**). Combinations of nucleosomal DNA were deleted to change the size of the *HMRα::GFP* locus; the smallest version of the locus contained six nucleosomes (Strain sN6) (JRY11547). (C) Expected loss-of-silencing rate from random segregation of H3-H4 tetramers to daughter chromatids. See the legend of **Figure 2.1** for a description of how these expected rates were calculated. (D) Observed loss-of-silencing rates using the FLAME assay. Cell divisions were monitored by time-lapse microscopy (n > 900 cell divisions per genotype). Silencing-loss rates were not significantly different (Yates chi-square test, $p > 0.05$ for all pairwise comparisons). (E) Observed establishment-of-silencing rates using the FLAME assay (n > 110 cell divisions per genotype). Silencing establishment rates were not significantly different (Yates chi-square test, $p > 0.05$ for all pairwise comparisons). These strains showed similar frequencies of silenced and expressed cells as measured by flow cytometry in **Figure 2.11**. Error bars represent 95% confidence intervals.

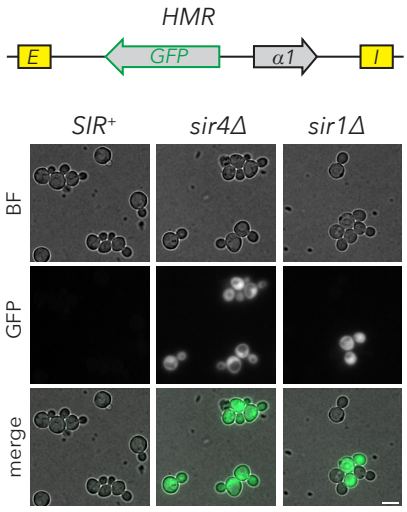

Figure 2.8: *sir1*Δ cells exhibited metastability at *HMRα::GFP*. Fluorescence images of *HMRα::GFP* strains that were *SIR*$^+$ (JRY11474), *sir4*Δ (JRY11496), or *sir1*Δ (JRY11478). Cells were grown to log-phase before imaging. Scale bar, 5 μm.

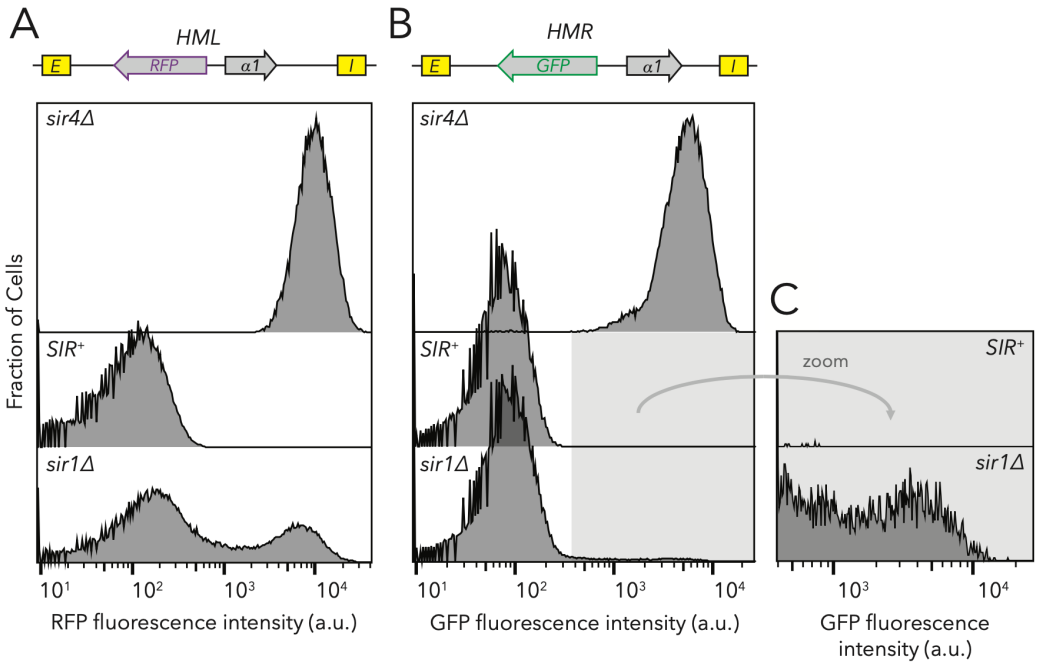

Figure 2.9: *sir1*Δ cells exhibited metastability at *HMLα::RFP* and *HMRα::GFP*. Distribution of fluorescence intensity per cell as measured by flow cytometry after 24 hours of log-phase growth. (A) *HMLα::RFP* expression was measured in *SIR*$^+$ (JRY11472), *sir4*Δ (JRY11494), or *sir1*Δ (JRY11476). (B) *HMRα::GFP* expression was measured in *SIR*$^+$ (JRY11474), *sir4*Δ (JRY11496), or *sir1*Δ (JRY11478). Because very few cells expressed *HMRα::GFP* in *sir1*Δ, zoomed profiles are provided in (C). At least 50,000 cells were analyzed for each strain.

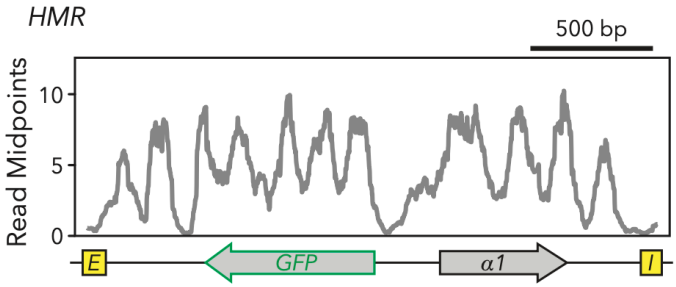

Figure 2.10: *HMLα::GFP* contained 12 nucleosomes. MNase-seq was performed on the strain with full-length *HMLα::GFP* in *sir1*Δ (JRY11478). Midpoints of nucleosome-sized fragments were calculated, plotted, and smoothed.

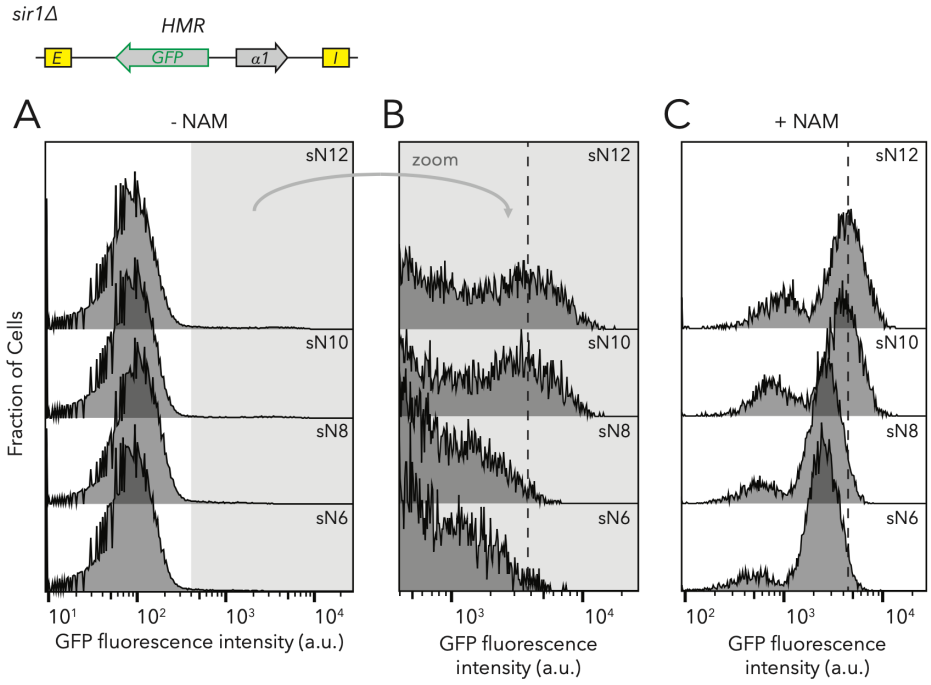

Figure 2.11: Chromatin domain size of *HMRα::GFP* in *sir1*Δ did not affect the frequencies of different epigenetic states but did affect GFP expression levels. Distribution of fluorescence intensity per cell as measured by flow cytometry after 24 hours of log-phase growth. (A) *HMRα::GFP* expression was measured in Strains sN12 (JRY11478) through sN6 (JRY11547). (B) Zoomed profiles of flow cytometry profiles in (A). The dashed line indicates the mean fluorescence intensity of expressed cells in sN12, for comparison to the mean-fluorescence-intensity values of other strains. (C) Distribution of fluorescence intensity per cell for cells grown at log for 12 hours in 5 mM Nicotinamide (NAM). NAM inhibits Sir2p activity and causes cells to be fully expressed at *HMR*. Strains sN12 through sN6 were analyzed. The dashed line indicates the mean fluorescence intensity of expressed cells in sN12, for comparison to other strains. Because the smaller peaks at lower fluorescence intensities were not visible in *sir4*Δ (**Figure 2.9**), we considered them an artifact of NAM treatment. At least 50,000 cells were analyzed for each strain.

2.3.3 Replisome defects affected epigenetic inheritance

An orthogonal approach to test the role of histones in carrying epigenetic memory would be to consistently bias parental H3-H4 tetramer inheritance to one daughter chromatid, leaving the other daughter chromatid with fewer parental H3-H4 tetramers. Recent reports demonstrate conserved roles of two replisome components, Dpb3 and Mcm2, in producing a more symmetric distribution of parental H3-H4 tetramers between the leading and lagging strands. Specifically, *dpb3*Δ causes biased parental H3-H4 tetramer inheritance to the lagging strand (Yu et al. 2018) and a set of point mutations in *MCM2* (*mcm2-3A*) causes biased parental H3-H4 tetramer inheritance to the leading strand (Petryk et al. 2018; Gan et al. 2018). A complementary study that was able to observe local inheritance of histone H4 in a small chromatin domain, though was unable to distinguish leading versus lagging strand biases, found that local histone H4 inheritance was moderately reduced in both the *dpb3*Δ and *mcm2-3A* single mutants, and severely reduced in the *dpb3*Δ *mcm2-3A* double mutant (Schlissel & Rine 2019). Together, these studies demonstrate that Dpb3 and Mcm2 are necessary for efficient inheritance of parental H3-H4 tetramers to both daughter chromatids during DNA replication.

If parental H3-H4 tetramer inheritance contributes to transmission of chromatin states, we would predict more loss-of-silencing events in strains with defects in tetramer inheritance. To test this idea, we measured silencing loss in replisome mutants using the CRASH assay (**Figure 2.12A**). The *dpb3*Δ and *mcm2-3A* single mutants exhibited higher silencing-loss rates, consistent with previous studies done at *HML* (Yu et al. 2018; Gan et al. 2018), and the *dpb3*Δ *mcm2-3A* double mutant lost silencing more frequently than either single mutant. Similar results were obtained by using flow cytometry to measure silencing-loss rates (**Figure 2.12B**). These data were consistent with a model in which inheritance of parental H3-H4 tetramers could contribute to inheritance of the silenced state at *HMR*. However, the data were also compatible with the possibility that heterochromatin assembled in such mutants was simply unstable for reasons independent of defects in its inheritance. Additionally, since previous studies did not specifically test the effects of Dpb3 and Mcm2 on histone inheritance within heterochromatin, any interpretations of silencing defects operated under the assumption that these replisome components act similarly between heterochromatin and euchromatin.

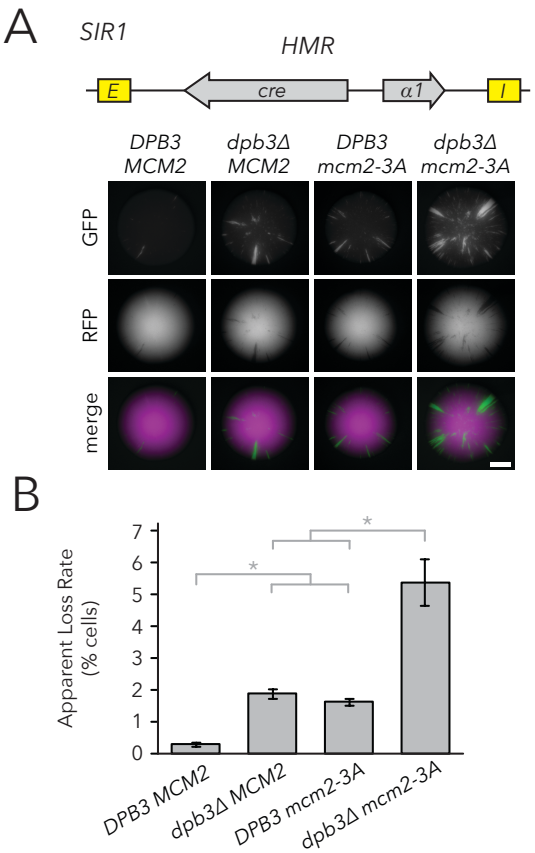

Figure 2.12: Replisome mutants exhibited higher silencing-loss rates in the CRASH assay. (A) Representative CRASH colonies for *DPB3 MCM2* (JRY11471), *dpb3*Δ *MCM2* (JRY11562), *DPB3 mcm2-3A* (JRY11591), and *dpb3*Δ *mcm2-3A* (JRY11592). Scale bar, 1 mm. (B) Quantification of apparent silencing-loss rates of strains in (A), as described in *Materials and Methods*. Data are means ± SD (n = 6 independent cultures). ANOVA and Tukey tests were used to test statistical significance. *DPB3 MCM2* was significantly different than *dpb3*Δ *MCM2* and *DPB3 mcm2-3A* ($p < 0.05$ each), and *dpb3*Δ *mcm2-3A* was significantly different than *dpb3*Δ *MCM2* and *DPB3 mcm2-3A* ($p < 0.05$ each).

It is possible that parental H3-H4 tetramer inheritance affects both transient loss-of-silencing events, as detected by the CRASH assay, and heritability of epigenetic states. Testing this possibility was important because the currently unidentified epigenetic information that determines expression states in *sir1*Δ is transmitted locally at *HML* and *HMR*, respectively, rather than being transmitted in *trans* from processes elsewhere in the cell (E. Y. Xu et al. 2006). If parental H3-H4 tetramers were the crucial local factors that transmitted this information, we would predict that disrupted tetramer inheritance would cause more loss-of-silencing events in *sir1*Δ. To test this, we generated replisome mutant strains in combination with *sir1*Δ and evaluated the inheritance of transcriptional states using two different FLAME assay measurements: Fluorescence-Activated Cell Sorting (FACS) and live-cell microscopy.

Populations of *dpb3*Δ, *mcm2-3A*, and *dpb3*Δ *mcm2-3A* mutants all showed a mix of cells that were silenced or expressed at *HMRα::GFP*; all three mutant strains also showed a higher frequency of expressed cells than wildtype (**Figure 2.14, Table 2.1**). Because silencing-loss rates and silencing-establishment rates both affect the frequency of cells in which *HMR* is silenced or expressed, one or both of these rates were presumably different in replisome mutants. To measure these rates, we used FACS to sort cells from each strain into two separate populations of *HMR*-silenced and *HMR*-expressed cells, and used flow cytometry to monitor the rates at which these initial sorted populations relaxed back to a mixed population of silenced and expressed cells (**Figure 2.13A**). These relaxation rates, and the frequency of silenced cells at equilibrium, were a product of competing silencing-loss and silencing-establishment rates. By using these relaxation rates to calculate silencing-loss rates (**Figure 2.13B**, **Figure 2.15**), we observed that *dpb3*Δ and *mcm2-3A* had a higher loss-of-silencing rate than wildtype (**Figure 2.13C**). The *dpb3*Δ *mcm2-3A* double mutant had a higher loss rate than the single mutants. Similar loss trends were observed using time-lapse fluorescence microscopy (**Figure 2.13D**), albeit with overall higher loss rates than those seen with FACS sorting. Together, these data suggested that faithful inheritance of parental H3-H4 tetramers helped transmit the silenced state of *HMR*. However, we also noted that the vast majority of silenced cells still faithfully transmitted the silenced state in the replisome mutant backgrounds.

We also asked if replisome mutants had differences in the frequency of silencing-establishment events. Curiously, any strain containing *dpb3*Δ had an increased establishment rate, whereas *mcm2-3A* had minimal, if any, effects on establishment rate (**Figure 2.13E-G**). Additionally, any strain containing *dpb3*Δ showed elevated levels of *HMRα::GFP* expression in unsilenced cells, as measured by flow cytometry (**Figure 2.16**). Because *dpb3*Δ cells more readily established silencing, we inferred that the expressed state was less efficiently inherited. Therefore, Dpb3 contributed to the inheritance of the expressed state of *HMR* as well as to the silenced state.

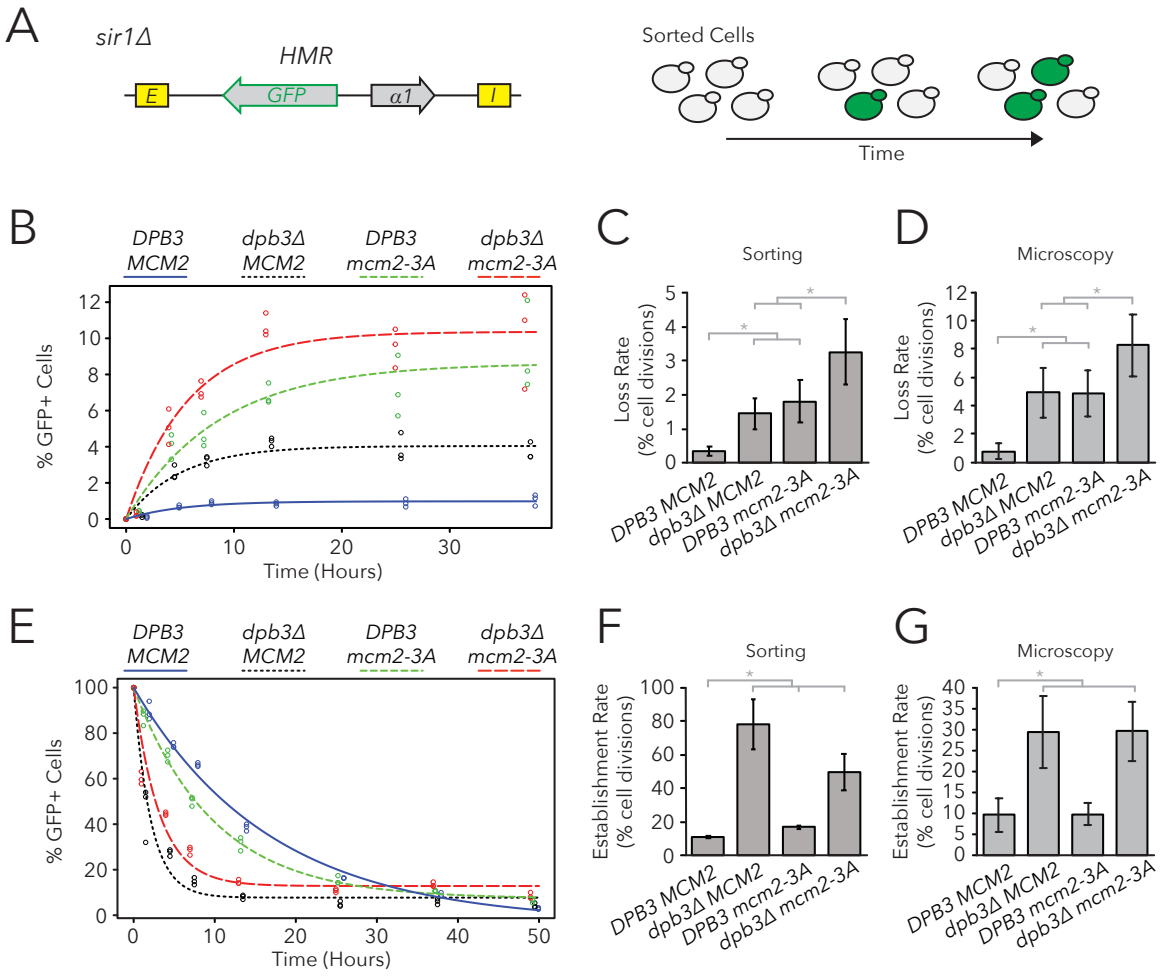

Figure 2.13: Replisome mutants exhibited defects in epigenetic inheritance in the FLAME assay. (A) FACS-based approach to measure switching rates of *HMRα::GFP* in the FLAME assay. Populations of silenced cells were isolated and allowed to divide; as silencing loss occurred, the percentage of expressed cells in the population increased. The frequencies of fluorescence intensity per cell at equilibrium are shown in **Figure 2.14**. (B) For *DPB3 MCM2* (blue) (JRY11471), *dpb3*Δ *MCM2* (black) (JRY11550), *DPB3 mcm2-3A* (green) (JRY11589), and *dpb3*Δ *mcm2-3A* (red) (JRY11590), silenced cells were isolated at t = 0 hrs, allocated into three separate populations each, and monitored over time. At each time-point, the percentage of expressed cells in each population was determined by flow cytometry (for an example, see **Figure 2.15**). (C) Silencing-loss rates calculated from (B), as explained in *Materials and Methods*. (D) Silencing-loss rates calculated by monitoring dividing cells with time-lapse microscopy (n > 550 cell divisions per genotype). (E) Similar to (B), except expressed cells were sorted and monitored over time. (F) Silencing-establishment rates calculated from (E), as explained in *Materials and Methods*. (G) Silencing-establishment rates calculated by monitoring dividing cells with time-lapse microscopy (n > 100 cell divisions per genotype). GFP expression levels in expressed cells were calculated by flow cytometry. Error bars represent 95% confidence intervals. Two-tailed t-tests were used in statistical analysis of switching rates by sorting, and Yates chi-square tests were used for microscopy (*$p < 0.05$).

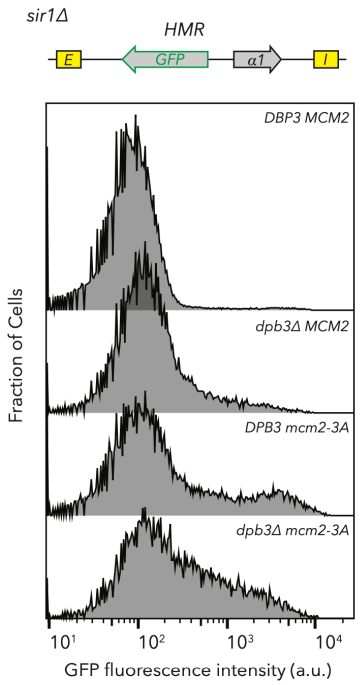

Figure 2.14: Replisome mutants exhibited different frequencies of silenced and expressed cells in *sir1*Δ. Distribution of fluorescence intensity per cell as measured by flow cytometry after 24 hours of log-phase growth. *HMRα::GFP* expression was measured in *DPB3 MCM2* (JRY11471), *dpb3*Δ *MCM2* (JRY11550), *DPB3 mcm2-3A* (JRY11589), and *dpb3*Δ *mcm2-3A* (JRY11590). At least 50,000 cells were analyzed for each strain.

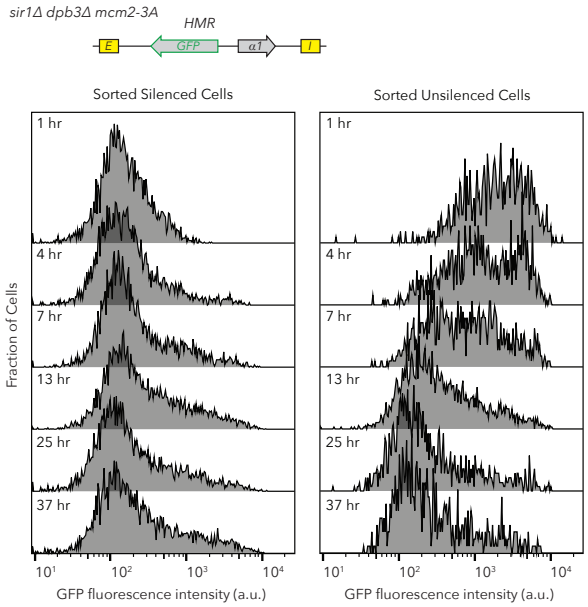

Figure 2.15: Flow cytometry profiles of *sir1*Δ *dpb3*Δ *mcm2-3A HMRα::GFP* after FACS sorting. Silenced and expressed cells were sorted at t = 0 hrs and allowed to divide at log-phase. Samples were taken at different time-points and analyzed by flow cytometry. These data correspond to experiments shown in **Figure 2.13**B and **Figure 2.13E**. At least 700 cells were analyzed for each time-point.

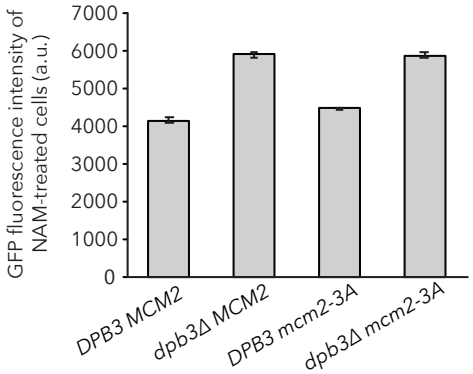

Figure 2.16: *dpb3*Δ exhibits a higher expression level of *HMRα::GFP* in expressed cells. *DPB3 MCM2* (JRY11478), *dpb3*Δ *MCM2* (JRY11550), *DPB3 mcm2-3A* (JRY11589), and *dpb3*Δ *mcm2-3A* (JRY11590) were grown at log phase for 12 hours in 5 mM Nicotinamide (NAM) and *HMRα::GFP* expression was measured with flow cytometry. The geometric mean intensity of GFP for each strain was calculated using FlowJo software. Data are means ± SD (n = 3 independent cultures). ANOVA and Tukey tests showed GFP expression levels in *DPB3 MCM2* were significantly different than those seen in *dpb3*Δ *MCM2*, *DPB3 mcm2-3A*, and *dpb3*Δ *mcm2-3A* ($p < 0.05$ each). GFP expression in *dpb3*Δ *MCM2* was not significantly different than *dpb3*Δ *mcm2-3A* ($p > 0.05$).

Genotype	Silenced (S)	Expressed (E)	S→E (k_{on}, gen^{-1})	E→S (k_{off}, gen^{-1})	$K_D(E/S)$	$K_D(k_{on}/k_{off})$
DPB3 MCM2	99	1	0.003	0.11	0.01	0.031
dpb3Δ MCM2	96	4	0.014	0.78	0.042	0.019
DPB3 mcm2-3A	91	9	0.018	0.17	0.094	0.107
dpb3Δ mcm2-3A	90	10	0.033	0.5	0.115	0.066

Table 2.1: Comparison of epigenetic switching rates and proportion of silenced cells at equilibrium. Data for *DPB3 MCM2* (JRY11471), *dpb3*Δ *MCM2* (JRY11550), *DPB3 mcm2-3A* (JRY11589), and *dpb3*Δ *mcm2-3A* (JRY11590) in the FLAME assay was extracted from **Figure 2.13**. The percentages of Silenced (S) and Expressed (E) cells at equilibrium were determined from **Figure 2.13B**. Silencing-loss rates (k_{on}, gen^{-1}) correspond to data from **Figure 2.13C** and silencing-establishment rates (k_{off}, gen^{-1}) correspond to data from **Figure 2.13F**.

2.3.4 Variations in nucleosome number in replisome mutant backgrounds

Though the rate of silencing loss increased in replisome mutant backgrounds, the large majority of silenced cells still faithfully transmitted the silenced state through cell divisions. Indeed, though *dpb3*Δ and *mcm2-3A* single mutants exhibit asymmetric parental H3-H4 tetramer inheritance (Yu et al. 2018; Petryk et al. 2018), it is likely that this asymmetry is not complete and some parental H3-H4 tetramers are still stochastically transmitted to each daughter chromatid during DNA replication. Similarly, the *dpb3*Δ *mcm2-3A* double mutant exhibits residual local inheritance of histone H4 (Schlissel & Rine 2019). We reasoned that, if a daughter chromatid consistently inherits fewer parental H3-H4 tetramers and thereby loses the silenced state more frequently, an additional reduction in the size of a chromatin domain would cause that daughter chromatid to inherit even fewer marked parental H3-H4 tetramers and experience loss-of-silencing events even more frequently. Therefore, if parental H3-H4 tetramers carry epigenetic memory, we would expect loci with fewer nucleosomes to exhibit more loss-of-silencing events in replisome mutant backgrounds. To test his idea, we used the FLAME assay on nucleosome-number mutants in *dpb3*Δ and *dpb3*Δ *mcm2-3A* strains (**Figure 2.17**, **Figure 2.17**). There was no clear correlation between silencing-loss rates and nucleosome number in these sensitized backgrounds (**Figure 2.17B**). Establishment-of-silencing rates were also not strongly affected, though there was a slight increase in the establishment rate with fewer nucleosomes in *dpb3*Δ *mcm2-3A* (**Figure 2.17C**). Therefore, even when parental H3-H4 tetramer inheritance was disrupted and the number of parental H3-H4 tetramers available for inheritance at *HMR* was decreased, cells faithfully transmitted epigenetic transcriptional states.

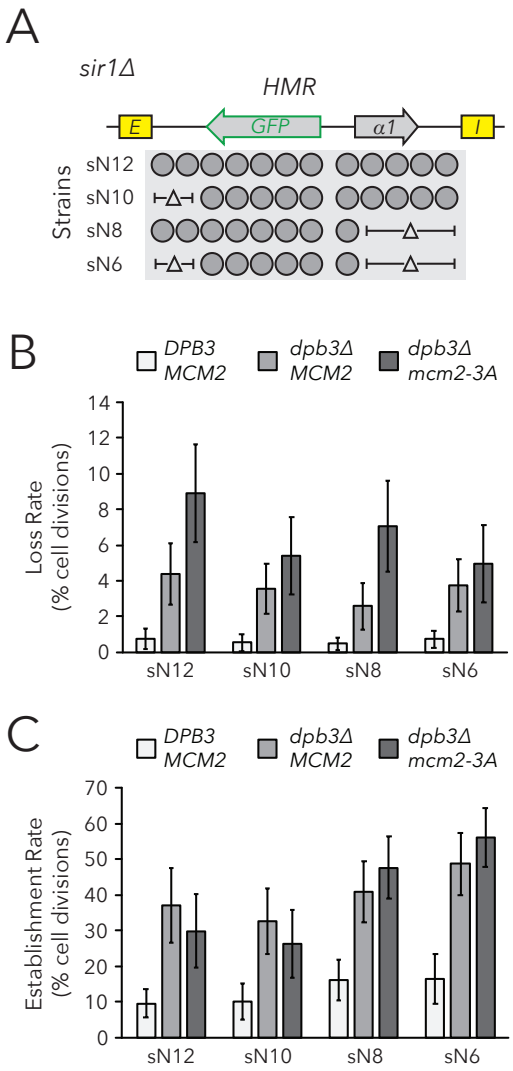

Figure 2.17: Chromatin domain size did not strongly affect epigenetic switching rates in replisome mutant backgrounds. (A) Diagram of nucleosomes in *HMRα::GFP*. As before, combinations of nucleosomal DNA were deleted to change the size of *HMRα::GFP*; the largest size contained thirteen nucleosomes (Strain sN12) (JRY11478) and the smallest size contained six nucleosomes (Strain sN6) (JRY11547). Frequencies of silenced and expressed cells in these strains were measured by flow cytometry and shown in **Figure 2.18**. (B) Loss-of-silencing rates in the FLAME assay. Replisome mutant strains *DPB3 MCM2* (JRY11478) (white), *dpb3*Δ *MCM2* (JRY11550) (grey), and *dpb3*Δ *mcm2-3A* (JRY11590) (dark grey) with different numbers of nucleosomes at *HMRα::GFP* were analyzed by time-lapse microscopy (n > 300 cell divisions for each genotype). (C) Establishment-of-silencing rates for the same strains as in (B), calculated by time-lapse microscopy (n > 80 cell divisions per genotype). Loss and establishment rates of *DPB3 MCM2* (JRY11478) are identical to those in **Figure 2.7D,E** and shown here for convenience. Error bars represent 95% confidence intervals.

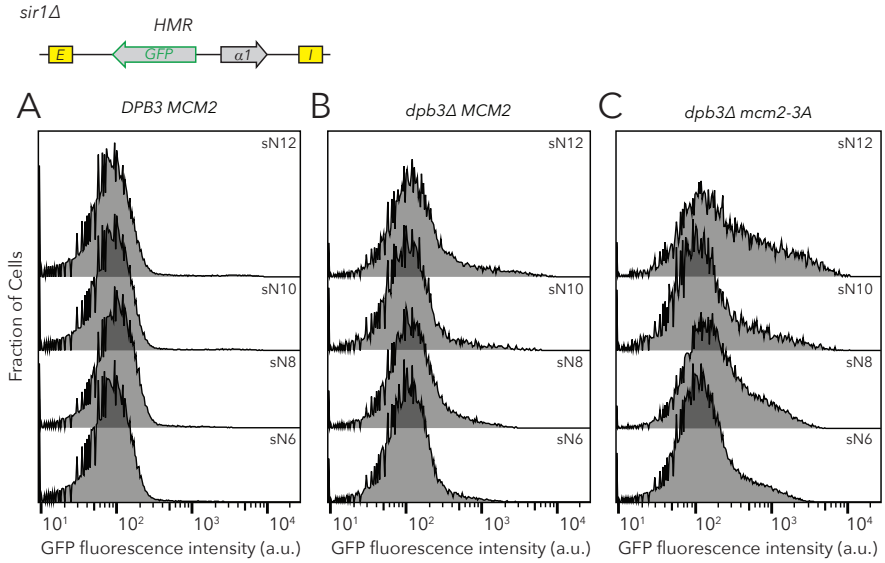

Figure 2.18: Chromatin domain size of *HMRα::GFP* did not strongly affect the frequencies of different epigenetic states in replisome mutant backgrounds. Distribution of fluorescence intensity per cell as measured by flow cytometry after 24 hours of log-phase growth. This analysis was performed on *DPB3 MCM2* (JRY11478) (A), *dpb3*Δ *MCM2* (JRY11550) (B), and *dpb3*Δ *mcm2-3A* (JRY11590) (C) with different numbers of nucleosomes at *HMRα::GFP*. At least 50,000 cells were analyzed for each strain. Data in (A) corresponds to data in **Figure 2.11A**.

2.4 Discussion

Heterochromatin is frequently characterized by specific histone modifications bound by silencing proteins; these components are critical to mechanisms of silencing and have long been considered as mediators of epigenetic inheritance. A popular model is that modified H3-H4 tetramers are heritable units of epigenetic information that are randomly segregated between daughter chromatids during DNA replication (Ramachandran & Henikoff 2015). Models founded on random segregation of parental H3-H4 tetramers predict that shorter chromatin domains would decrease the heritability of chromatin states in those domains. Contrary to the prediction, we found that shortening the silenced chromatin domain at *HMR* had no significant effects on silencing-loss rate as measured by the CRASH and FLAME assays, even in mutants lacking a component of the silencer-binding complex and in mutants with defective versions of two different regulators of parental H3-H4 tetramer segregation.

2.4.1 Evidence that H3-H4 Tetramers Did Not Carry Epigenetic Memory

Removal of silencers from heterochromatin via induced recombination demonstrates that silencers are necessary for maintenance of the silenced state. Specifically, induced silencer excision from *HMR* causes rapid loss of silencing in arrested cells (Cheng & Gartenberg 2000). Studies at other loci in *S. cerevisiae* and *Drosophila* show that removal of silencers permits maintenance of silencing in arrested cells, but causes loss of silencing once the same cells subsequently complete one or two rounds of DNA replication (Holmes & Broach 1996; Laprell et al. 2017). Therefore, the presence of modified histones is not sufficient for silencing maintenance or heritability, depending on the example under consideration. Indeed, given that silencers are constantly recruiting Sir proteins to these loci, any role of H3-H4 tetramers in transmission of epigenetic information might be hard to detect.

We considered the possibility that silencer activity masks an underlying contribution of H3-H4 tetramer inheritance to silencing inheritance. However, the weakened silencer activity in *sir1*Δ mutants did not reveal a sensitivity of silencing inheritance to the size of the silenced domain at *HMR*. Importantly, epigenetic states of *HML* and *HMR* in *sir1*Δ are a property of the locus rather than the cell, demonstrating that factors that determine these epigenetic states are inherited locally at *HML* and *HMR* respectively (E. Y. Xu et al. 2006). Similar studies of an epigenetically-inherited heterochromatin state in *Arabidopsis* also demonstrate that the relevant epigenetic information is carried in *cis* (Berry et al. 2015). Additionally, epigenetic inheritance of transcriptional states in heterochromatin is commonly accompanied by the ability to switch stochastically between states, a feature that implies the existence of imperfectly heritable epigenetic information. Though modified H3-H4 tetramers could theoretically be *cis*-acting, imperfectly heritable units of information, our evidence to the contrary suggests that other *cis*-acting factors determine the epigenetic state of *HMR* in *sir1*Δ. Given the importance of silencers in inheritance of the silenced chromatin state, one possibility is that the silencer complex self-templates by cooperative oligomerization of silencing factors, and that stochastic changes in epigenetic states reflect the formation or dissolution of such a silencer complex.

2.4.2 Addressing the Possibility that Tetramer Inheritance is Not Random

Classic studies of chromatin replication indicate that parental H3-H4 tetramers are randomly segregated between daughter chromatids during DNA replication. For example, chromatin replicated in the presence of cycloheximide, which blocks the synthesis of new histones, produces daughter chromatids with roughly half the number of nucleosomes, and these

nucleosomes appear randomly dispersed along both daughter chromatids (Sogo et al. 1986; Cusick et al. 1984). Though our experiments built on these classic findings, it is also possible that parental H3-H4 tetramers may not be randomly segregated genome wide, or at *HMR* in particular. For example, it was possible that heterochromatin contained factors that facilitated alternating inheritance of tetramers between the leading and lagging strands. In this case, even if H3-H4 tetramers were to act as the sole units of epigenetic information, decreasing chromatin domain size might not affect the rate of silencing loss at *HMR*.

If H3-H4 tetramers carry epigenetic information through DNA replication, mutations that reduce tetramer inheritance would be expected to increase the frequency of silencing loss. Studies describe roles of Dpb3 and Mcm2 in heterochromatic silencing at *HML* (Yu et al. 2018; Gan et al. 2018), and inheritance of epigenetic states at a synthetic telomere (Iida & Araki 2003; Foltman et al. 2013). Using the CRASH and FLAME assays, we found mild but significant increases in *HMR* silencing-loss rates in both *dpb3*Δ and *mcm2-3A* single mutants. Additionally, the *dpb3*Δ *mcm2-3A* double mutant exhibited higher silencing-loss rates than either of the single mutants. Together, these effects suggested that reduced tetramer inheritance caused mild defects in silencing heritability. Though deacetylated H4K16 is crucial for silencing, other modifications such as H3K56 acetylation also affect silencing (Hyland et al. 2005; F. Xu et al. 2007) and reduced inheritance of these modifications may hinder their functions. Considering the variety of histone modifications that parental H3-H4 tetramers can carry through DNA replication, it was striking that cells with moderate or severe reductions in inheritance of parental H3-H4 tetramers still exhibit robust inheritance of the silenced state.

Though replisome mutants exhibit defects in parental H3-H4 tetramer inheritance, some tetramers are still transmitted to both daughter chromatids in replisome mutant backgrounds (Yu et al. 2018; Gan et al. 2018; Schlissel & Rine 2019). Therefore, there are still parental tetramers that are theoretically capable of carrying epigenetic information to both daughter chromatids in the *dpb3*Δ, *mcm2-3A*, and *dpb3*Δ *mcm2-3A* mutants. Given that all replisome mutants tested showed increased silencing-loss rates, further reduction in the number of parental H3-H4 tetramers available for transmission to daughter chromatids should cause even higher rates of silencing loss. However, we saw no significant effects of *HMR* size on the silencing-loss rate in replisome mutant backgrounds. Therefore, cells with both reduced parental H3-H4 tetramer inheritance and a reduction in the number of tetramers available for inheritance at *HMR* exhibited a surprisingly robust ability to transmit the silenced state. These data strongly suggested that inheritance of parental H3-H4 tetramers has little or no impact on epigenetic inheritance of the silenced state of *HMR*.

2.4.3 Epigenetic Inheritance of the Expressed State

The expressed state of *HMR* in *sir1*Δ cells is formally an epigenetic state: it is heritable through cell divisions and can stochastically switch to the silenced state. One possibility is that the expressed state of *HMR* depends on the existence of heritable information, similarly to the silenced state. Histone modifications associated with active transcription can be transmitted through DNA replication (Alabert et al. 2015; Reverón-Gómez et al. 2018) and multiple transcription factors can bind to the histone modifications they generate (Jacobson et al. 2000; Owen et al. 2000). Therefore, histone modifications may form positive feedback loops with both silencing machinery and transcription factors. Indeed, a model that incorporates these positive feedback loops and parental H3-H4 tetramer inheritance generates robust bistable chromatin states (Dodd et al. 2007). This model also predicts that random segregation of parental H3-H4

tetramers would lead to loss-of-chromatin-state events, and that decreasing chromatin domain size would also decrease the heritability of both the expressed and silenced states. However, we found that shorter versions of *HMR* did not strongly affect inheritance of the expressed state of *HMR*.

Alternatively, if parental H3-H4 tetramers carry memory of the expressed state, mutations that disrupt parental H3-H4 tetramer inheritance would be expected to increase the rate of silencing establishment. Curiously, *dpb3*Δ exhibited a ~3-fold increase in the rate of silencing establishment and *mcm2-3A* had no observable effect. These data may suggest that parental tetramer inheritance facilitates heritability of the expressed state, though such an explanation could not account for the *mcm2-3A* phenotype. Alternatively, these data may suggest that inheritance of the expressed state is influenced by a function of Dpb3p that is separate from its role in tetramer inheritance. It is also important to note that *dpb3*Δ but not *mcm2-3A* led to elevated levels of GFP expression when *HMRα::GFP* was fully expressed. This finding is paradoxical, as one would expect elevated transcription to inhibit silencing establishment, rather than facilitate it. However, recruitment of the transcriptional activator Ppr1 to *HMR* causes both increased transcription in expressed cells and an increased establishment rate in *sir1*Δ (E. Y. Xu et al. 2006).

Together, our results suggested that the fidelity of H3-H4 tetramer inheritance has minimal consequences for heritability of the silenced state and may affect heritability of the expressed state in some contexts. These findings raised doubts regarding the model in which histones are significant carriers of epigenetic memory in *S. cerevisiae*. As such, future studies that continue to examine histone-based memory models will be complemented by studies on other possible mechanisms of transcriptional memory.

2.5 Materials and Methods

Yeast strains

The strains and oligonucleotides used in this study are listed in Supplementary Files 1 and 2, accessible from the published manuscript online. All strains were derived from the W303 background. CRASH assay strains, which contained *HMRα, hmrα2*Δ*::cre, ura3*Δ*::loxP::yEmRFP:tCYC1:KanMX:loxP:yEGFP:tADH1* or *hmlα2*Δ*::cre, ura3*Δ*::loxP::yEmRFP:tCYC1:HygMX:loxP:yEGFP:tADH1* were generated as described previously (Dodson & Rine 2015). FLAME assay strains were generated with the following approach. To generate *hmlα2*Δ*::yEmRFP*, a *K. lactis URA3* swap was performed to replace the *α2* coding sequence with *yEmRFP* coding sequence. The *hmlα2*Δ*::yEmRFP* fwd/rev primers were used for integration of *yEmRFP* in the final step. To generate *HMRα, hmrα2*Δ*::yEGFP*, a fragment spanning the X region to the Z1 region of *hmlα2*Δ*::yEGFP* was amplified using *hmlα2*Δ*::yEGFP* fwd/rev primers and swapped into *HMRa*.

To delete DNA corresponding to nucleosomes at *HMRα* and *HMLα*, CRISPR/Cas9 was employed as previously described (Lee et al. 2015). Each deletion or repair fwd/rev primer set contained two partially overlapping primers that were amplified by PCR prior to use. The *HMR-E*-proximal sgRNA was used to induce Cas9 cutting between the *HMR-E* silencer and *cre*, and N14 to N12 deletion fwd/rev was used to delete DNA corresponding to two nucleosomes in this region. This sgRNA and oligo set was also used to convert sN12 to sN10 in the FLAME strain background. The *HMR-I*-proximal sgRNA, which cuts between the *HMR-I* silencer and *cre*, was used with N14 to N10 deletion fwd/rev (to convert N14 to N10, and sN12 to sN8) or with N14 to N9 (to convert N14 to N9). For *HMLα*, the *HML-E*-proximal sgRNA was used to induce Cas9 cutting between the HML-I silencer and *cre*, and used with N22 to N19a deletion fwd/rev (to convert N22 to N19a) or N22 to N16a deletion fwd/rev (to convert N22 to N16a). The *HML-I*-proximal sgRNA was used to induce Cas9 cutting between the *HML-E* silencer and *cre*, and was used with N22 to N19b deletion fwd/rev (to convert N22 to N19b) or N22 to N16c deletion fwd/rev (to convert N22 to N16c) or N22 to N13c deletion fwd/rev (to convert N22 to N13c). Deletions were confirmed by junction primers and sequencing. To generate mutants with combinations of nucleosome set deletions, CRISPR/Cas9 technology was applied (as described above) to strains with one nucleosome set deletion already made.

To generate *dpb3*Δ, the DPB3 sgRNA was used with Cas9 to cut within *DPB3* and *DPB3* deletion fwd/rev was used to delete the coding sequence. To generate *mcm2-3A*, the *MCM2* sgRNA was used with Cas9 to cut 244bp into the *MCM2* coding sequence and *mcm2-3A* repair fwd/rev was used to generate the appropriate point mutations (Y79A Y82A Y91A). Mutations were confirmed by sequencing.

Colony growth and imaging

To generate colonies for analysis by the CRASH assay, RFP-expressing cells were diluted and plated at a density of ~10 cells/plate (CSM-Trp (Sunrise Science Products, San Diego, CA), 1% agar). After 5 days of growth, colonies were imaged using a Leica M205 FA fluorescence stereomicroscope (Leica Camera AG, Wetzlar, Germany) equipped with a Leica DFC3000G CCD camera, a Leica PLANAPO 0.63x objective, ET RFP filter (Leica 10450224), ET GFP filter (Leica 10447408), and Leica Application Suite X (LAS X) imaging software. At least ten colonies were imaged per genotype.

Live-cell imaging

Cells were grown to saturation in CSM (Sunrise Science Products) at 30°C overnight. These cells were then back-diluted in 5 ml CSM and grown to mid-log phase over 6 hours. 500µl was transferred to a microfuge tube and sonicated at 20% for 15 seconds (Branson Ultrasonics Digital Sonifier 100-132-888R with Sonicator Tip 101-135-066R) (Branson Ultrasonics, Fremont, CA) to break up clumps of cells. 5 µl of sonicated cells were spotted onto a CSM plate (1% agar) and allowed to soak into the agar. When dry, a sterile spatula was used to cut a 1 cm × 1 cm agar square surrounding the cell patch. The square was lifted out of the plate, inverted, and placed in a 35 mm glass bottom dish (Thermo Scientific 150682) (Thermo Fisher Scientific, Waltham, MA). Cells were imaged using a Zeiss Z1 inverted fluorescence microscope with a Prime 95B sCMOS camera (Teledyne Photometrics, Tucson, AZ), Plan-Apochromat 63x/1.40 oil immersion objective (Zeiss, Oberkochen, Germany), filters, MS-2000 XYZ automated stage (Applied Scientific Instrumentation, Inc., Eugene, OR), and Micro-Manager imaging software (Open Imaging, San Fransisco, CA). Given that cells were pressed between the agar and glass, the cells were all in the same focal plane and Z-stacks were not used.

For time-lapse microscopy (i.e. **Figure 2.7D**), samples were kept at 30°C and humidified with a P-Set 2000 Heated Incubation Insert (PeCon, Erbach, Germany). Time-lapse experiments involved brightfield and fluorescence imaging of 16 different fields per sample, and images were taken every 10 minutes for 10 hours. Subsequent analysis of cell divisions was done in ImageJ (NIH, Bethesda, MD). To measure epigenetic switching rates in the FLAME assay, cell divisions and switching events were manually counted and the counter was blind to the genotype (single-blind study). This counting was performed only on cells that could be clearly distinguished from each other. If a mother and daughter cell pair switched simultaneously, we counted this as one switching event that probably appeared as two events due to the lag time in yEGFP expression or degradation.

Flow cytometry

To measure fluorescence intensities per cell in the CRASH and FLAME assays, a BD LSR Fortessa cell analyzer (BD Biosciences, San Jose, CA) with a FITC filter (for GFP) and a PE-TexasRed filter (for RFP) was used. Subsequent analysis was performed with FlowJo software.

For quantification of silencing-loss rates in the CRASH assay, cells were first streaked out to form single colonies. Six colonies per genotype were added to CSM-Trp media (Sunrise Science Products) in a 96-well plate (Corning CLS3788) (Corning Inc., Corning, NY) and grown to saturation overnight in an incubating microplate shaker (VWR 12620-930) (VWR International, Radnor, PA) at 30°C. These samples were then back-diluted and grown to mid-log phase over 6 hours. GFP and RFP expression were then analyzed by flow cytometry ($n > 4000$ cells per sample). Distinct populations of RFP+ GFP- (which had not lost silencing), RFP+ GFP+ (which had recently lost silencing), and RFP- GFP+ (which had lost silencing less recently) were observed. The apparent silencing-loss rate was calculated as the number of RFP+ GFP+ cells divided by the number of RFP+ GFP+ cells and RFP+ GFP- cells. Measurements from independent cultures were considered as biological replicates.

For calculating the frequency of silenced and expressed cells at equilibrium in the FLAME assay, cells were first streaked out to generate single colonies. Three colonies per genotype were added to CSM media in a 96-well plate and grown to saturation overnight. These samples were then serially back-diluted in CSM media in 96-well plates and grown at 30°C. After twelve hours, the serial dilutions had a range of cell densities; the dilution that was closest

to ~1 O.D. was again back-diluted in CSM media and grown at 30°C for another 12 hours. At this point, wells close to ~1 O.D. contained cells that had been growing at log-phase for approximately 24 hours. These cells were analyzed by flow cytometry. Because three populations were analyzed per genotype, the most representative profiles of silenced and expressed cells were used for figures. We considered these populations as biological replicates.

To calculate GFP expression levels in expressed cells in the FLAME assay, cells were streaked out for single colonies and three colonies per genotype were grown overnight in CSM + 5 mM Nicotinamide (NAM) (Sigma-Aldrich, St. Louis, MO). These samples were then back-diluted in CSM + 5 mM NAM and grown at 30°C for 12 hours. Samples at ~1 O.D. were analyzed by flow cytometry. For **Figure 2.10**, the most representative profiles of the three profiles generated per strain were shown. For **Figure 2.16**, the geometric mean intensity of GFP per cell (excluding cells that formed a smaller, artifactual peak at a lower GFP intensity) was calculated for each population using FlowJo software. Independent cultures were considered as biological replicates.

FACS was utilized in the FLAME assay to calculate switching rates between epigenetic states in **Figure 2.13**. To perform this experiment, cells from each genotype were serially diluted in CSM media and grown at 30°C. After 12 hours, dilutions closest to ~1 O.D. were sorted into GFP- and GFP+ populations using a BD FACSAria Fusion cell sorter (BD Biosciences) equipped with a FITC filter for GFP. Gates were calibrated from *SIR*$^{+}$ (JRY11474) and *sir4*Δ (JRY11496) cells. For each sample, 150,000 GFP- cells were sorted into one tube and 30,000 GFP+ cells were sorted into another. Each sorted population was divided evenly into three populations and grown in CSM in a 96-well plate at 30°C. Serial back-dilutions were used to maintain constant log-phase growth over two days. Time-points were taken by removing a fraction of cells from each population and fixing them in a 4% paraformaldehyde solution (4% paraformaldehyde, 3.4% Sucrose) for 15 minutes at room temperature. Fixed cells were resuspended in GFP fix buffer (100 mM KPO_4 pH 7.4, 1.2 M Sorbitol) and kept at 4°C. Once the experiment was complete, fixed cells from different time-points were analyzed by flow cytometry (n > 500 cells per sample) and analyzed by FlowJo software. The percent of GFP+ cells for each sample over time is shown in **Figure 2.13B** and **E**. Because the initial sorting event required ~20 minutes per sample, the time of initial sorting (t = 0 hrs) was different between samples; this made the time points between samples slightly staggered as seen in **Figure 2.13B** and **E**. Because cells were divided into subpopulations after the initial sorting, these subpopulations were considered as technical replicates.

Switching rate calculation from cell sorting

The following equations were used to model the dynamics of switching rates between epigenetic states in *sir1*Δ. We considered the balance of GFP+ and GFP- cells over time, and assumed that the birth and death rates of the two populations are similar. Combining the balances and introducing the ratio variable x, we can derive the following equation that describes how a population of GFP+ cells and GFP- cells would move towards equilibrium over time:

$$\left(\frac{1}{k_{ON}+k_{OFF}}\right)\frac{dx_{ON}}{dt}+x_{ON}=\frac{k_{ON}}{k_{ON}+k_{OFF}}$$

k_{ON} is the loss rate per hour, k_{OFF} is the establishment rate per hour, x_{ON} is the fraction of GFP+ cells at a given time, and t is time. Solving the differential equation for x_{ON} yields:

$$x_{ON} = \frac{k_{ON}}{k_{ON} + k_{OFF}}\left(1 - e^{-\frac{t}{k_{ON}+k_{OFF}}}\right) \text{ or } x_{ON} = \frac{k_{ON}}{k_{ON} + k_{OFF}}\left(1 - e^{-\frac{t}{k_{ON}+k_{OFF}}}\right) + e^{-\frac{t}{k_{ON}+k_{OFF}}}$$

if $x_{ON} = 0$ at $t = 0$ if $x_{ON} = 1$ at $t = 0$

Therefore, the following equations were used to model switching rates between epigenetic states from data in **Figure 2.13B** and **E**.

Sorting silenced cells (**Figure 2.13B**):

$$x_{ON} = \frac{k_{ON}}{k_{ON}+k_{OFF}}\left(1 - e^{-\frac{t}{k_{ON}+k_{OFF}}}\right)$$

Sorting expressed cells (**Figure 2.13E**):

$$x_{ON} = \frac{k_{ON}}{k_{ON}+k_{OFF}}\left(1 - e^{-\frac{t}{k_{ON}+k_{OFF}}}\right) + e^{-\frac{t}{k_{ON}+k_{OFF}}}$$

The nls() function in R was used to provide a nonlinear least squares estimate of the unknown variables k_{ON} and k_{OFF} for each genotype, and 95% confidence intervals for estimates. With this approach, each genotype had an estimated k_{ON} and k_{OFF} from sorting silenced cells and an estimated k_{ON} and k_{OFF} from sorting expressed cells. Since sorting silenced cells subsequently allowed for observation of more loss-of-silencing events, the k_{ON} rates from those data were considered more accurate and used in **Figure 2.13C**. Similarly, the k_{OFF} rates calculated from sorting expressed cells were used in **Figure 2.13F**.

Because each population of sorted cells was evenly divided into three subpopulations, each genotype has three calculated values for the percent of GFP+ cells at each given time point after sorting. The nonlinear least squares estimate was made by drawing a best fit line through all data points for a given genotype, effectively combining the values of all subpopulations. The quality of the fit was calculated using the confint2() function and represented as 95% confidence intervals for k_{ON} values in **Figure 2.13C** and k_{OFF} values in **Figure 2.13F**. An alternative approach involved drawing a best fit line for each individual subpopulation to give three k_{ON} values and three k_{OFF} values for each genotype and averaging these values to get a single k_{ON} value and k_{OFF} value for each genotype, with error bars representing a standard deviation. Though we also performed this latter analysis method, we favor the former analysis method because it incorporates how well the data fit the nonlinear least squares estimate. Notably, both analysis methods gave similar k_{ON} and k_{OFF} values.

The generation time of *DPB3 MCM2* (JRY11471) was 1.96 hours in CSM media at 30°C. To convert k_{ON} and k_{OFF} as rates per hour to rates per generation, we multiplied these variables by the generation time. Similar generation times were observed for all replisome mutants.

MNase-seq

Cells were grown to saturation overnight in 5 mL CSM at 30°C. The following day, these cells were back-diluted to ~0.1 O.D. in 50 ml CSM and grown at 30°C for 5 hours. Cells were

then centrifuged and washed twice in 500 µl SKC buffer (1.2 M Sorbitol, 100 mM KH_2PO_4, 0.5 mM $CaCl_2$, 7 mM β-mercaptoethanol) and then resuspended in 100 µl SKC buffer. Cells were incubated at 37°C for 15 minutes, then 30 µl of 1mg/mL Zymolyase-100T (MP Biomedicals, LLC, Solon, OH) was added for a final concentration of 0.23 mg/ml Zymolyase-100T and incubated at 37°C for 15 minutes. All subsequent steps were performed on ice. Once spheroplasting was complete, cells were spun at 3k RPM for 3 minutes at 4°C. Cells were washed twice in 500 µl SPC buffer (1 M Sorbitol, 20 mM PIPES pH 6.3, 0.1 mM $CaCl_2$, with Roche cOmplete protease inhibitors (Sigma)) and spun at 2k RPM for 3 minutes at 4°C between washes. Cells were resuspended in 250 µl SPC buffer, and this solution was gently mixed with 250 µl freshly prepared Ficoll buffer (9% Ficoll, 20 mM PIPES pH 6.3, 0.5 mM $CaCl_2$) to lyse the cell membranes.

Nuclei were then pelleted by centrifugation at 10k RPM for 20 minutes at 4°C. Nuclei were washed twice in 500 µl SPC and spun at 8k RPM for 3 minutes at 4°C between washes. Washed nuclei were subsequently resuspended in 250 µl SPC and $CaCl_2$ was added to a final concentration of 2mM $CaCl_2$. Nuclei were incubated for 5 minutes at 37°C, then 20 units of Worthington MNase was added (Worthington Biochemical Corporation, Lakewood, NJ). Nuclei were incubated for 15 minutes at 37°C. MNase activity was quenched by addition of EDTA to a final concentration of 10 mM EDTA. Nuclei were centrifuged at 3.7k RPM for 5 minutes at 4°C. The nucleosome-containing supernatant was subsequently removed and DNA and RNA were purified using a Qiagen spin column. RNase A (Sigma) was added to a final concentration of 1 mg/ml RNase A and incubated for 2 hours at 37°C. DNA was then purified using a Qiagen spin column. MNase libraries were constructed with NEBnextUltra II library preparation kit (New England Biolabs, Ipswich, MA) and sequenced on an Illumina HiSeq4000 (Illumina, San Diego, CA) as 100 bp paired-end reads.

Reads were mapped to the *Saccharomyces cerevisiae* S288C genome (GenBank accession number GCA_000146045.2) using Bowtie2 (Langmead and Salzberg, 2012). Mapped reads between 140 bp and 180 bp in length were used in all further analysis to ensure mononucleosome resolution. The midpoint for each read was calculated and midpoints were stacked in a histogram. Finally, a 25 bp rolling mean was used to smooth out the resulting nucleosome peaks. All sequences and processed data files have been deposited in the NCBI Gene Expression Omnibus archive under accession number GSE136897.

2.6 References

Alabert, C. et al., 2015. Two distinct modes for propagation of histone PTMs across the cell cycle. *Genes & development*, 29(6), pp.585–590.

Audergon, P.N.C.B. et al., 2015. Epigenetics. Restricted epigenetic inheritance of H3K9 methylation. *Science*, 348(6230), pp.132–135.

Berry, S. et al., 2015. Local chromatin environment of a Polycomb target gene instructs its own epigenetic inheritance. *eLife*.

Cheng, T.H. & Gartenberg, M.R., 2000. Yeast heterochromatin is a dynamic structure that requires silencers continuously. *Genes & development*, 14(4), pp.452–463.

Cusick, M.E., DePamphilis, M.L. & Wassarman, P.M., 1984. Dispersive segregation of nucleosomes during replication of simian virus 40 chromosomes. *Journal of molecular biology*, 178(2), pp.249–271.

Dodd, I.B. et al., 2007. Theoretical Analysis of Epigenetic Cell Memory by Nucleosome Modification. *Cell*, 129(4), pp.813–822.

Dodson, A.E. & Rine, J., 2015. Heritable capture of heterochromatin dynamics in Saccharomyces cerevisiae. *eLife*, 4, p.e05007.

Foltman, M. et al., 2013. Eukaryotic Replisome Components Cooperate to Process Histones During Chromosome Replication. *Cell reports*, 3(3), pp.892–904.

Gan, H. et al., 2018. The Mcm2-Ctf4-Polα Axis Facilitates Parental Histone H3-H4 Transfer to Lagging Strands. *Molecular cell*, pp.1–16.

Gaydos, L.J., Wang, W. & Strome, S., 2014. Gene repression. H3K27me and PRC2 transmit a memory of repression across generations and during development. *Science*, 345(6203), pp.1515–1518.

Hansen, K.H. et al., 2008. A model for transmission of the H3K27me3 epigenetic mark. *Nature Cell Biology*, 10(11), pp.1291–1300.

Hecht, A. et al., 1995. Histone H3 and H4 N-termini interact with SIR3 and SIR4 proteins: a molecular model for the formation of heterochromatin in yeast. *Cell*.

Holmes, S.G. & Broach, J.R., 1996. Silencers are required for inheritance of the repressed state in yeast. *Genes & development*, 10(8), pp.1021–1032.

Hoppe, G.J. et al., 2002. Steps in Assembly of Silent Chromatin in Yeast: Sir3-Independent Binding of a Sir2/Sir4 Complex to Silencers and Role for Sir2-Dependent Deacetylation. *Molecular and Cellular Biology*, 22(12), pp.4167–4180.

Hyland, E.M. et al., 2005. Insights into the Role of Histone H3 and Histone H4 Core Modifiable Residues in Saccharomyces cerevisiae. *Molecular and Cellular Biology*, 25(22), pp.10060–10070.

Iida, T. & Araki, H., 2003. Noncompetitive Counteractions of DNA Polymerase and ISW2/yCHRAC for Epigenetic Inheritance of Telomere Position Effect in Saccharomyces cerevisiae. *Molecular and Cellular Biology*, 24(1), pp.217–227.

Imai, S. et al., 2000. Transcriptional silencing and longevity protein Sir2 is an NAD-dependent histone deacetylase. *Nature*, 403(6771), pp.795–800.

Jackson, V., 1988. Deposition of newly synthesized histones: hybrid nucleosomes are not tandemly arranged on daughter DNA strands. *Biochemistry*, 27(6), pp.2109–2120.

Jacobson, R.H. et al., 2000. Structure and Function of a Human TAFII250 Double Bromodomain Module. *Science*, 288(5470), pp.1422–1425.

Kaufman, P.D. & Rando, O.J., 2010. Chromatin as a potential carrier of heritable information. *Current Opinion in Cell Biology*, 22(3), pp.284–290.

Laprell, F., Finkl, K. & Müller, J., 2017. Propagation of Polycomb-repressed chromatin requires sequence-specific recruitment to DNA. *Science*, pp.eaai8266–7.

Lee, M.E. et al., 2015. A Highly Characterized Yeast Toolkit for Modular, Multipart Assembly. *ACS Synthetic Biology*, 4(9), pp.975–986.

Moazed, D., 2011. Mechanisms for the Inheritance of Chromatin States. *Cell*, 146(4), pp.510–518.

Owen, D.J. et al., 2000. The structural basis for the recognition of acetylated histone H4 by the bromodomain of histone acetyltransferase gcn5p. *The EMBO journal*, 19(22), pp.6141–6149.

Petryk, N. et al., 2018. MCM2 promotes symmetric inheritance of modified histones during DNA replication. *Science*, 3, pp.eaau0294–8.

Pillus, L. & Rine, J., 1989. Epigenetic inheritance of transcriptional states in S. cerevisiae. *Cell*, 59(4), pp.637–647.

Prior, C.P. et al., 1980. Incorporation of exogenous pyrene-labeled histone into Physarum chromatin: a system for studying changes in nucleosomes assembled in vivo. *Cell*, 20(3), pp.597–608.

Ragunathan, K., Jih, G. & Moazed, D., 2015. Epigenetics. Epigenetic inheritance uncoupled from sequence-specific recruitment. *Science*, 348(6230), p.1258699.

Ramachandran, S. & Henikoff, S., 2015. Replicating nucleosomes. *Science Advances*, 1(7), pp.e1500587–e1500587.

Reverón-Gómez, N. et al., 2018. Accurate Recycling of Parental Histones Reproduces the Histone Modification Landscape during DNA Replication. *Molecular cell*, 72(2), pp.239–249.e5.

Rusché, L.N., Kirchmaier, A.L. & Rine, J., 2002. Ordered nucleation and spreading of silenced chromatin in Saccharomyces cerevisiae. *Molecular biology of the cell*, 13(7), pp.2207–2222.

Rusché, L.N., Kirchmaier, A.L. & Rine, J., 2003. The establishment, inheritance, and function of silenced chromatin in Saccharomyces cerevisiae. *Annual review of biochemistry*, 72, pp.481–516.

Schlissel, G. & Rine, J., 2019. The nucleosome core particle remembers its position through DNA replication and RNA transcription. *Proceedings of the National Academy of Sciences of the United States of America*, 12, pp.201911943–7.

Schwartz, Y.B. et al., 2006. Genome-wide analysis of Polycomb targets in Drosophila melanogaster. *Nature genetics*, 38(6), pp.700–705.

Sogo, J.M. et al., 1986. Structure of replicating simian virus 40 minichromosomes. The replication fork, core histone segregation and terminal structures. *Journal of molecular biology*, 189(1), pp.189–204.

Thurtle, D.M. & Rine, J., 2014. The molecular topography of silenced chromatin in Saccharomyces cerevisiae. *Genes & development*, 28(3), pp.245–258.

Xu, E.Y., Zawadzki, K.A. & Broach, J.R., 2006. Single-Cell Observations Reveal Intermediate Transcriptional Silencing States. *Molecular cell*, 23(2), pp.219–229.

Xu, F. et al., 2007. Sir2 deacetylates histone H3 lysine 56 to regulate telomeric heterochromatin structure in yeast. *Molecular cell*, 27(6), pp.890–900.

Yang, H. et al., 2017. Distinct phases of Polycomb silencing to hold epigenetic memory of cold in Arabidopsis. *Science*, 357(6356), pp.1142–1145.

Yu, C. et al., 2018. A mechanism for preventing asymmetric histone segregation onto replicating DNA strands. *Science*, pp.eaat8849–8.

Zhang, K. et al., 2008. Roles of the Clr4 methyltransferase complex in nucleation, spreading and maintenance of heterochromatin. *Nature structural & molecular biology*, 15(4), pp.381–388.

Chapter 3:
Nucleosome Positioning Regulates the Establishment, Stability, and Inheritance of Heterochromatin in *Saccharomyces cerevisiae*

3.1 Abstract

Heterochromatic domains are complex structures composed of nucleosome arrays that are bound by silencing factors. This composition raises the possibility that certain configurations of nucleosome arrays facilitate heterochromatic silencing. We tested this possibility in *S. cerevisiae* by systematically altering the distance between heterochromatic Nucleosome Depleted Regions (NDRs), which is predicted to affect local nucleosome positioning by limiting how nucleosomes can be packed between NDRs. Consistent with this prediction, serial deletions that altered the distance between heterochromatic NDRs revealed a striking oscillatory relationship between inter-NDR distance and defects in nucleosome positioning. Furthermore, conditions that caused poor nucleosome positioning also led to defects in both heterochromatin stability and the ability of cells to generate and inherit epigenetic transcriptional states. These findings strongly suggest that nucleosome positioning can contribute to formation and maintenance of functional heterochromatin, and point to previously unappreciated roles of NDR positioning within heterochromatic domains.

3.2 Introduction

A central challenge to both transcription and transcriptional regulation in eukaryotes is the handling of nucleosomes, the fundamental repeating units of chromatin. Each nucleosome consists of 147 base pairs of DNA wrapped around eight histone subunits, two copies each of histones H2A, H2B, H3, and H4. Nucleosomes can be post-translationally modified at specific amino acid positions, precisely or poorly positioned, and packaged into higher-order chromatin structures to control gene expression. Nucleosome dynamics are especially relevant in heterochromatin, which is composed of covalently modified nucleosome arrays bound by silencing factors. Despite their importance, it remains unclear exactly how nucleosomes are arranged to create functional heterochromatin.

The interplay between silencing factors and nucleosomes is complex. Formation of heterochromatin generally requires recruitment of silencing factors to specific nucleation sites, and subsequent iterative cycles of histone modification and binding of silencing complexes allow these complexes to spread across nucleosome arrays (1–3). Some silencing factors, including HP1, Sir3, and PRC2, can bridge neighboring nucleosomes, allowing the formation of large chromatin structures (4–6). Additionally, some chromatin remodelers are associated with heterochromatin and required for transcriptional silencing (7, 8). These studies indicate that nucleosomes may be positioned in specific ways to permit heterochromatin formation and maintenance.

The organization of nucleosome arrays is driven by multiple factors. First, different DNA sequences have different intrinsic abilities to bend around a histone octamer, which affects their ability to form nucleosomes (9, 10). Second, Nucleosome Depleted Regions (NDRs), which are formed by nucleosome-disfavoring DNA sequences or by tightly bound transcription factors, have the ability to position adjacent nucleosomes into phased arrays (11–13). Additionally, two NDRs in close proximity should constrain the number of nucleosomes that can fit between them (14, 15). For example, if two NDRs are spaced approximately two nucleosome-lengths apart, then two nucleosomes should fit in that space and be relatively well-positioned. Conversely, if

two NDRs are two-and-a-half nucleosome-lengths apart, then two nucleosomes should still fit in that space but may become more poorly positioned by sampling a greater length of DNA. Indeed, a genome-wide study in *S. cerevisiae* found that certain lengths of DNA between NDRs are correlated with, and presumably responsible for, more poorly positioned nucleosomes (16).

If nucleosome positioning affects heterochromatin, then altering inter-NDR distances within heterochromatin could lead to defects in gene silencing. We tested this prediction for two heterochromatic domains in *S. cerevisiae*, *HML* and *HMR*. The *E* and *I* silencers are NDRs that flank each of these domains; each silencer is bound by combinations of the DNA-binding proteins Rap1, Abf1, and ORC (17). These proteins outcompete nucleosomes for binding to silencers (18, 19) and also cooperate to recruit Sir proteins (20, 21). Sir1 is bound only at silencers. In contrast, Sir2/3/4 complexes bind to silencers, spread across the locus, and silence any genes within these domains (1, 2, 22). The bidirectional promoter in *HML* also contains an NDR that is bound by Rap1, and this site likely contributes to both heterochromatic silencing and transcription when *HML* is unsilenced (23, 24). Here, we tested whether the precise distance between these NDRs affected nucleosome positioning and, if so, whether effects on positioning affected heterochromatin stability.

3.3 Results

3.3.1 Inter-NDR Distance Affected Silencing Stability

In wild-type cells, *HML* and *HMR* are constitutively silenced. Rare, transient loss-of-silencing events can be detected using the Cre-Reported Altered States of Heterochromatin (CRASH) assay (**Figure 3.1A**) (25). In this assay, the coding sequence of the *α2* gene in *HML* is replaced with the coding sequence of *cre*, and a cassette consisting of two fluorescent reporter genes with appropriately placed *lox* sites (hereafter referred to as the *lox* cassette) is located elsewhere in the genome. Transient loss of silencing causes *cre* expression, which leads to recombination of the *lox* cassette and an irreversible switch from expressing only RFP to expressing only GFP. In a colony, the descendants of cells that lost silencing continue expressing GFP and form radial GFP+ sectors during colony growth. Therefore, the apex of each sector represents a single cell that lost silencing, and the number of GFP+ sectors in a colony represents the frequency of loss-of-silencing events.

Consistent with previous studies that utilized MNase and histone H3 ChIP, MNase-Seq of *HMLα::cre* revealed the existence of NDRs at the *HML-E* and *HML-I* silencers, as well as at the bidirectional promoter (**Figure 3.2**) (18). Nucleosomes between these NDRs appeared well-positioned. To alter inter-NDR distance in *HML*, we generated a series of 28 deletions between the Rap1 binding site in the bidirectional promoter, which we term NDR-L, and the Abf1 binding site in the *HML-I* silencer, which we term NDR-R (**Figure 3.1B**, **Figure 3.2**). The largest of these deletions left 24 base pairs between NDR-L and NDR-R, and smaller deletions increased this distance incrementally. The only known DNA elements that were fully or partially deleted in these strains were the *α1* transcription initiation site and the *α1* coding sequence, which are not thought to be involved in expression of *α2* (23).

Strikingly, the frequency of loss-of-silencing events appeared to rise and fall with increasing inter-NDR distances (**Figure 3.1C**, **Figure 3.3**). Additionally, these oscillatory effects diminished with increasing inter-NDR distances. We quantified loss-of-silencing rates by using MORPHE software, which calculates the frequency of sectors and their onset points (**Figure 3.1D**) (26). Additionally, we quantified loss-of-silencing events by measuring fluorescence of single cells. Cells that have recently lost silencing, and thereby recently recombined the *lox*

cassette, contain both RFP and GFP due to a lag time in RFP degradation. By using flow cytometry to measure the frequency of these cells, we also found an oscillatory correlation between inter-NDR distance and silencing-loss rate (**Figure 3.4**). Because these two quantification methods showed similar trends, individual experiments in the rest of this study used one or the other.

Based on the average nucleosome repeat length of 165 base pairs in *S. cerevisiae* (27), we defined one nucleosome "unit" as 165 base pairs. If the distance between NDR-L and NDR-R could be evenly divided into nucleosome units, silencing was more stable than if that distance could not be evenly divided into nucleosome units. For example, an inter-NDR distance of 179 base pairs corresponds to 1.1 nucleosome units, nearly an exact nucleosome unit of 1, and this inter-NDR distance yielded more stable silencing than an inter-NDR distance of 236 base pairs, which corresponds to 1.6 nucleosome units. We estimated the periodicity of changes in silencing-loss rates by calculating the distances between individual peaks, or individual troughs, of silencing-loss rates. These distances averaged to 159 base pairs, similar to the 165 base pairs in a nucleosome unit. This result strongly suggested that the periodicity of silencing-loss rates is correlated with whether or not different inter-NDR distances could be evenly divided into nucleosome units.

In principle, the periodicity of silencing-loss rates was compatible with at least two different mechanisms: one possibility was that inter-NDR distances that were not evenly divisible by nucleosome units resulted in loss of heterochromatin stability. Alternatively, variation in the lengths of the deletions might impact transcription from the bidirectional promoter, which could affect transcription of *cre* in both silenced and unsilenced cells. To test these possibilities, we blocked silencing in a subset of strains with different inter-NDR distances by exposing them to nicotinamide (NAM), a chemical inhibitor of Sir2, and quantified *cre* expression with RT-qPCR. Interestingly, strains which showed large differences in silencing-loss rates with the CRASH assay did not exhibit significant differences in *cre* expression when *HML* was unsilenced (**Figure 3.5**). These results suggested that different lengths between NDR-L and NDR-R affected heterochromatin stability rather than transcription from the bidirectional promoter.

In this framework, silencing was more stable when the distance between NDR-L and NDR-R was evenly divisible by nucleosome units, and less stable when this distance was not evenly divisible by nucleosome units (**Figure 3.1D**). These findings raised the possibility that altered nucleosome packing between these NDRs could lead to defects in silencing stability.

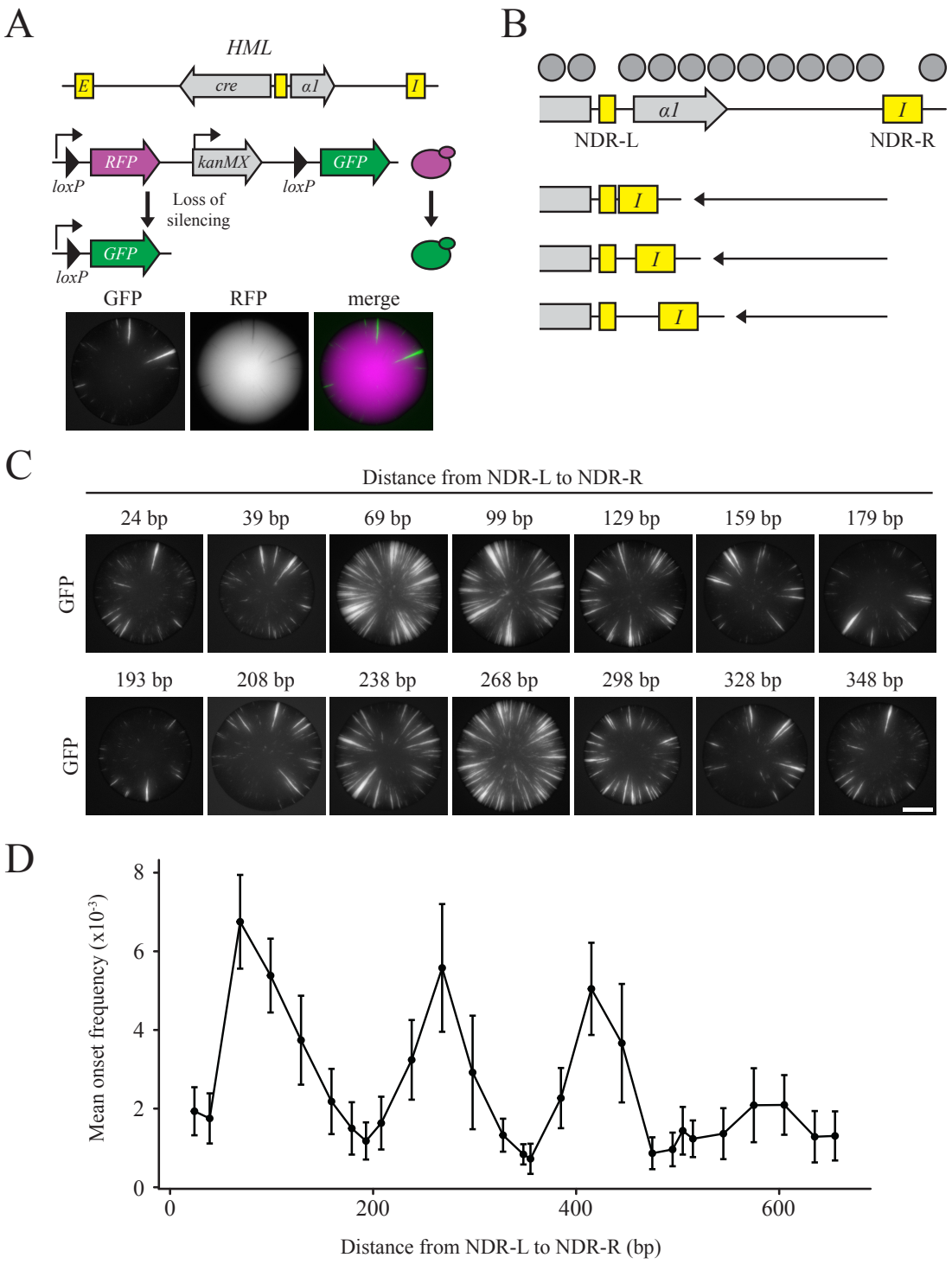

Figure 3.1: Inter-NDR distance affected silencing stability. A. Schematic of the Cre-Reported Altered States of Heterochromatin (CRASH) assay (25). In this assay, *cre* replaces the *α2* coding sequence in *HML*. Nucleosome depleted regions, including the *E* silencer, *I* silencer, and bidirectional promoter, are indicated as yellow boxes. Transient expression of Cre recombines a *lox* cassette elsewhere in the genome, which causes cells to irreversibly switch from expressing RFP to expressing GFP. Therefore, during colony growth, cells that lose silencing lead to formation of GFP+ sectors on an otherwise RFP+ background. B. Schematic of serial deletions used to alter inter-NDR distance. The bidirectional promoter contains a Rap1 binding site and is termed NDR-L. The *HML-I* silencer,

which contains binding sites for Abf1, Rap1, and ORC, is termed NDR-R. Nine well-positioned nucleosomes reside between these NDRs (see **Figure 3.2**) (grey circles). A series of deletions was made to move NDR-R to various distances from NDR-L (JRY11330-11342, JRY11259, JRY11281, JRY11296, JRY11297, JRY11280, JRY11317-11327). C. Representative CRASH colonies from strains with different inter-NDR distances. The distance between NDR-L and NDR-R is indicated for each strain. D. Sectoring rates were quantified with MORPHE software (26). Data are means ± SD (n = 10 colonies per genotype). Scale bar, 2 mm.

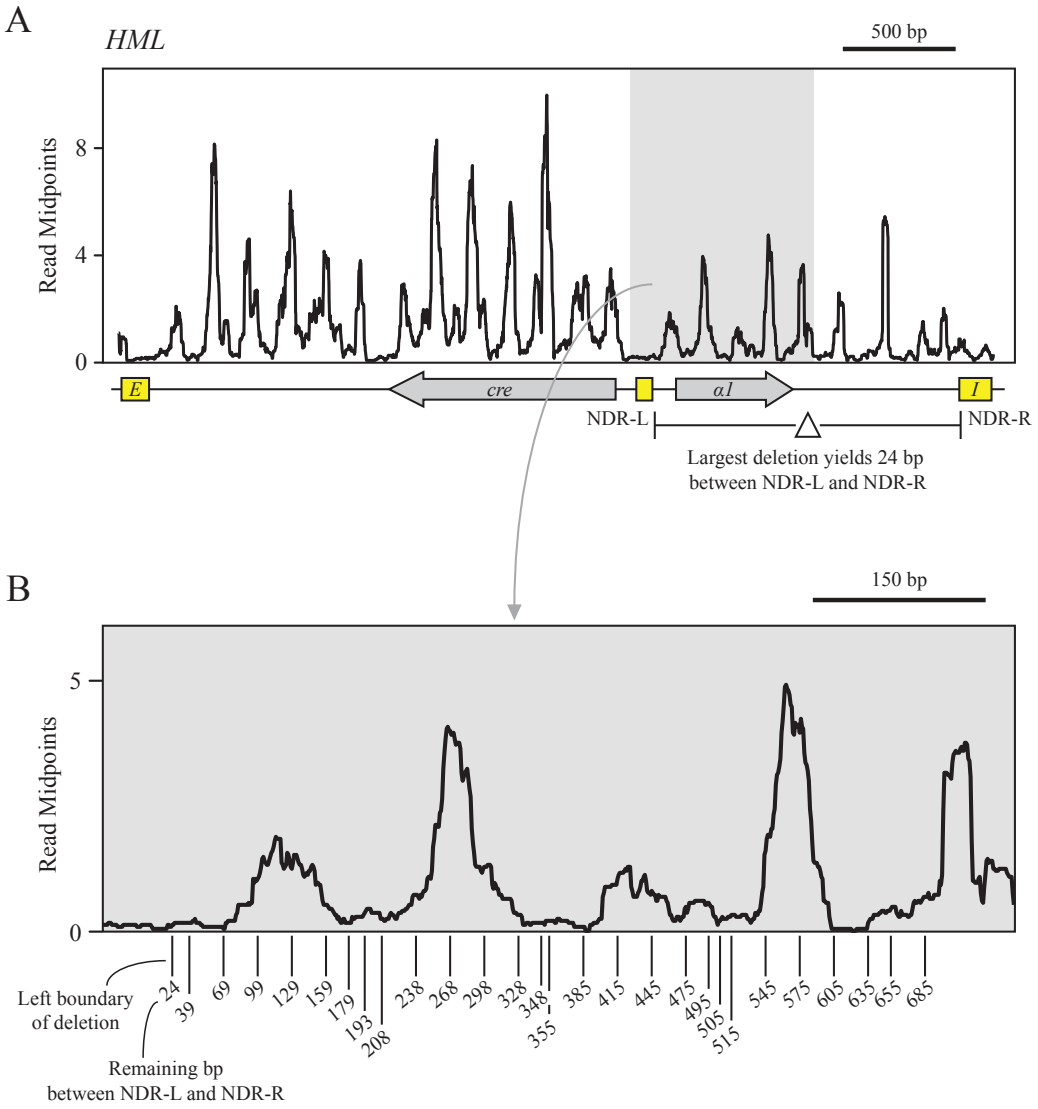

Figure 3.2: Nucleosome positions and serial deletions in *HML*. A. MNase-Seq was used to identify positions of nucleosomes in *HML* (JRY11259). Midpoints of MNase-protected fragments ranging from 140 base pairs to 180 base pairs in length were plotted and smoothed. NDRs, including the bidirectional promoter (NDR-L) and the *I* silencer (NDR-R) are indicated with yellow boxes. The boundaries of the largest inter-NDR deletion are shown; this deletion left 24 base pairs between NDR-L and NDR-R. B. Zoomed profile of smoothed midpoints from a subsection of (A). The left boundaries of deletions used to make different inter-NDR distances are shown, along with the resulting distances between NDR-L and NDR-R.

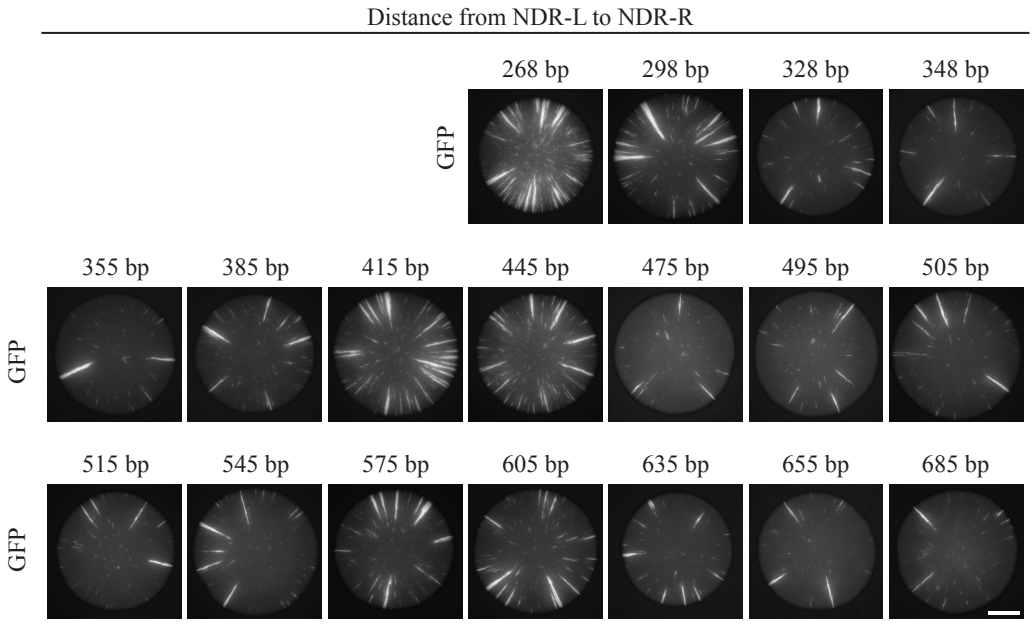

Figure 3.3: Representative CRASH colonies for strains with large inter-NDR distances at *HML* (JRY11280, JRY11324-11327, JRY11330-11342). The distance between NDR-L and NDR-R is indicated for each strain. Scale bar, 2 mm.

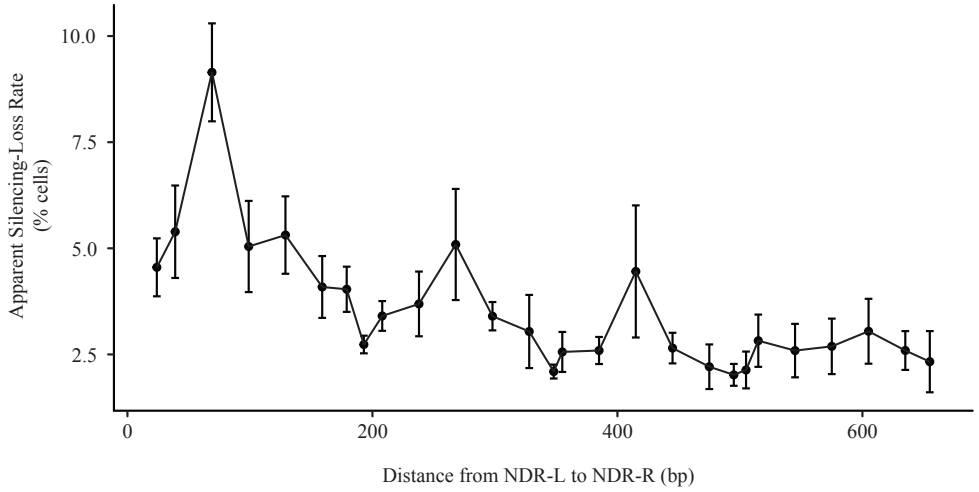

Figure 3.4: Quantification of apparent silencing-loss rates by flow cytometry, as described in Materials and Methods. Strains correspond to those used in **Fig. 3.1D**. Data are means ± SD (n = 3 independent cultures).

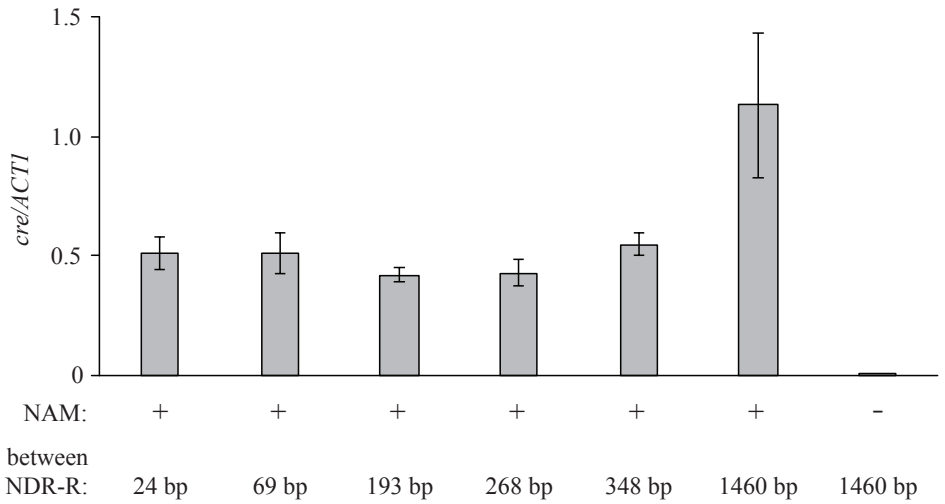

Figure 3.5: Strains with different inter-NDR distances had similar expression levels of *cre* in unsilenced cells (JRY11259, JRY11281, JRY11318, JRY11297, JRY11324, JRY11327). Cells were grown to log phase with or without 5mM NAM and transcript levels were quantified with RT-qPCR. The strain with an inter-NDR distance of 1460 base pairs had no inter-NDR deletions, and is provided as a control. Data are means ± SD (n = 3 independent cultures).

3.3.2 Inter-NDR Distance Affected Nucleosome Positioning

To test the expectation that the distance between NDR-L and NDR-R influences silencing stability through effects on nucleosome positioning, we performed MNase-Seq on strains with different distances between these NDRs (**Figure 3.6**). These data represent smoothed midpoints of protected fragments that were between 140 base pairs and 180 base pairs in length. We inferred that these protected fragments reflected nucleosomes, as they correspond to protected fragments in H3 ChIP-Seq experiments. All strains exhibited nucleosome depletion at NDR-L and NDR-R. Additionally, nucleosomes to the left of NDR-L, and to the right of the NDR-R, appeared regularly positioned in most strains. In contrast, nucleosomes between these NDRs exhibited striking differences in positioning and occupancy at various inter-NDR distances.

There were no strongly protected sequences between NDR-L and NDR-R when the distance between these NDRs was at or below 99 base pairs. When this distance was expanded past 99 base pairs, the appearance of a protected sequence became evident. Additionally, the appearance of nucleosomes in this inter-NDR region correlated with a stabilization of silencing until the inter-NDR distance exceeded 193 base pairs. Notably, the protected sequence to the right of NDR-L formed a smaller peak than the same nucleosome seen in **Figure 3.2**, likely reflecting variation in the extent of MNase digestion between different experiments. As the inter-NDR distance expanded beyond 193 base pairs, nucleosome-sized protected fragments were present in the inter-NDR region but appeared to be irregularly positioned in some strains. Generally, inter-NDR distances that were not evenly divisible by nucleosome units exhibited irregularly-positioned nucleosomes and stronger silencing defects. These data suggested that inter-NDR distances that were evenly divisible by nucleosome units facilitated silencing stability by allowing proper nucleosome positioning.

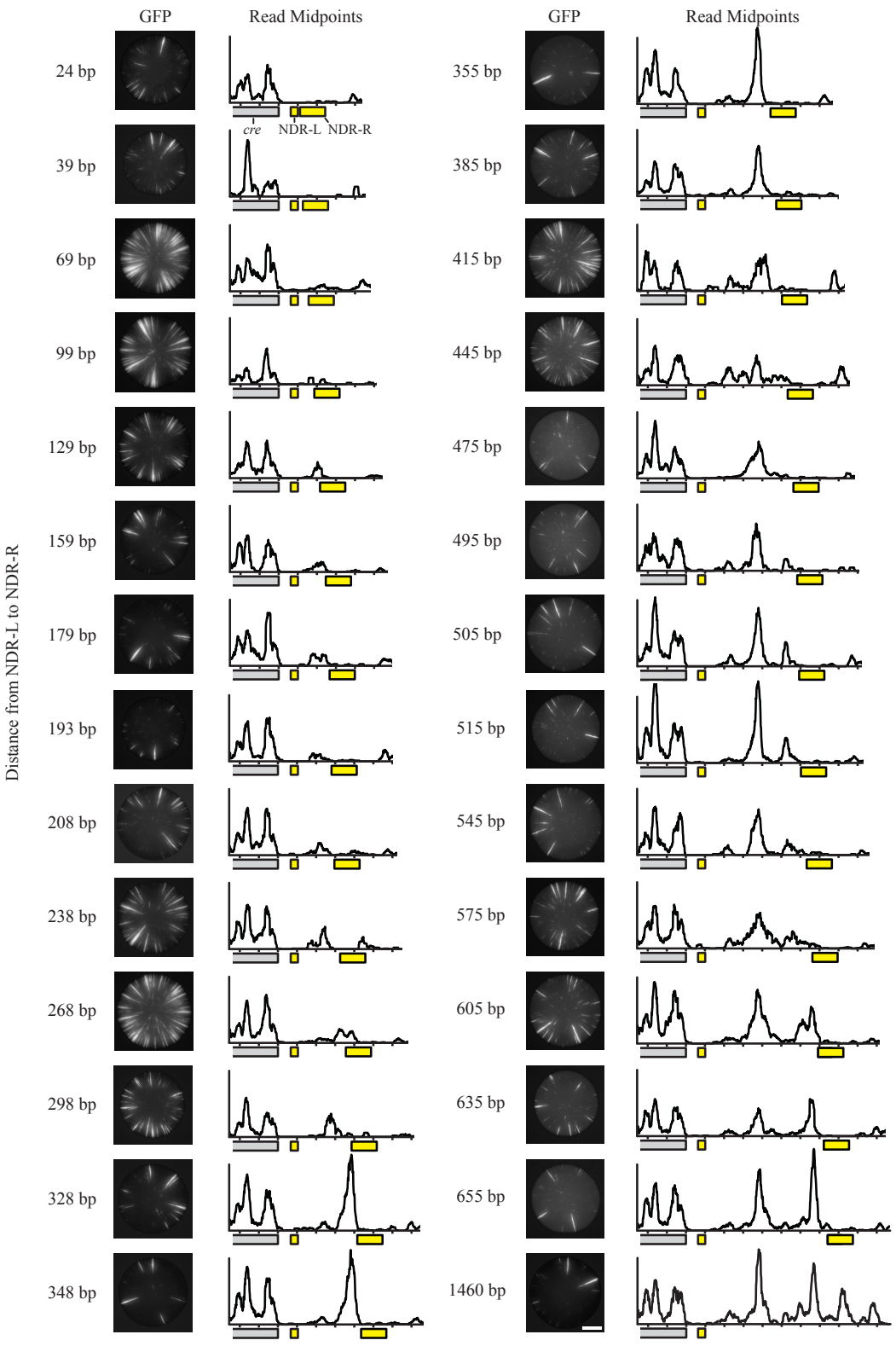

Figure 3.6: Inter-NDR distance affected nucleosome positioning. MNase-Seq was used to identify nucleosome positions in strains with different inter-NDR distances (JRY11259, JRY11280, JRY11281, JRY11296, JRY11297, JRY11317-11327, JRY11330-11342). Midpoints of MNase-protected fragments ranging from 140 base pairs to 180

base pairs in length were plotted and smoothed. The relative positions of *cre* (grey box), NDR-L (leftmost yellow box), and NDR-R (rightmost yellow box) are indicated, with tick marks representing 100 base pair intervals. The distance in base pairs between NDR-L and NDR-R is provided for each strain. Representative CRASH colonies from **Figure 3.1C** and **Figure 3.3** are provided for comparison. The strain with 1460 base pairs between NDR-L and NDR-R contained *HML* lacking any inter-NDR deletions (JRY11259). Scale bar, 2 mm.

3.3.3 NDR-R was Required for Oscillatory Silencing Effects

The deletions made between NDR-L and NDR-R affected both the DNA sequence content in this region and the relative distances between these NDRs. Either or both of these variables could theoretically contribute to nucleosome positioning and therefore be responsible for the oscillatory effects on silencing stability (**Figure 3.1**). To test the contribution of NDRs to the observed silencing effects, we deleted NDR-R in 14 strains with different distances between NDR-L and NDR-R. Deletion of NDR-L was not feasible due to its role in transcription (23). Deletion of NDR-R led to high overall sectoring rates and eliminated the oscillatory silencing effects (**Figure 3.7A**, **Figure 3.8**). Thus, the oscillation in silencing stability reflected the distance between NDR-L and NDR-R rather than some functional properties of the sequences between these NDRs.

Given that NDR-R is a silencer, it was possible that removal of a silencer *per se* could mask the oscillatory silencing effects independently of its ability to act as an NDR. To test this possibility, we also deleted the *HML-E* silencer in strains with different distances between NDR-L and NDR-R. Oscillatory silencing effects were still observed among strains that lacked the *HML-E* silencer (**Figure 3.7B**, **Figure 3.8**). These data further supported the view that the oscillatory silencing effects resulted from changes in distance between NDR-L and NDR-R.

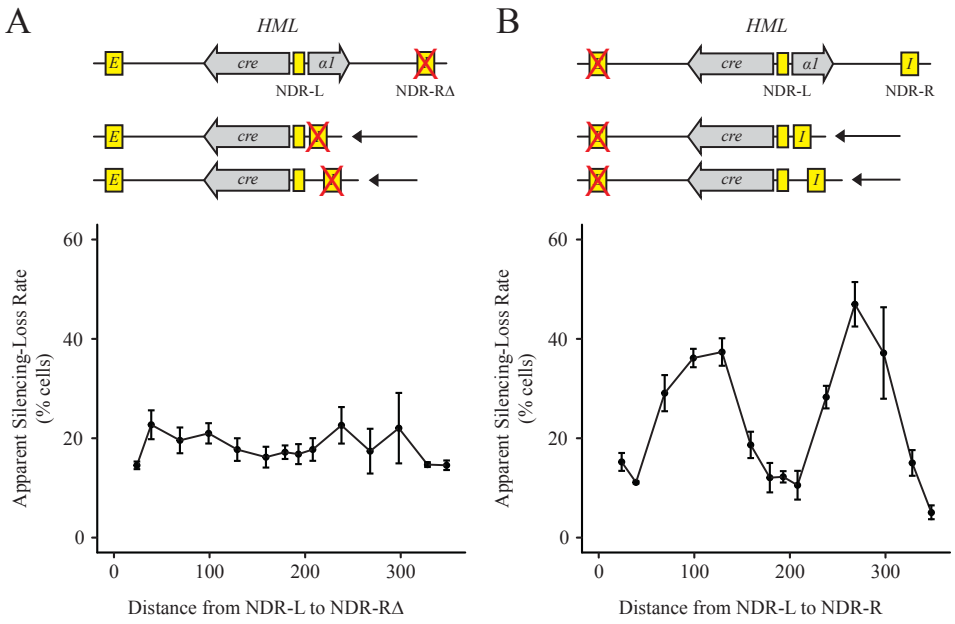

Figure 3.7: NDR-R was necessary for oscillatory silencing effects. A. NDR-R was deleted in strains with different inter-NDR distances (JRY11362-11375). Apparent silencing-loss rates were quantified by flow cytometry. Data are means ± SD (n = 3 independent cultures). B. Quantification of apparent silencing-loss rates in strains with different inter-NDR distances and deletion of the *HML-E* silencer, as calculated by flow cytometry (JRY11377-JRY11390). Data are means ± SD (n = 3 independent cultures). Representative CRASH colonies are shown in **Figure 3.8**

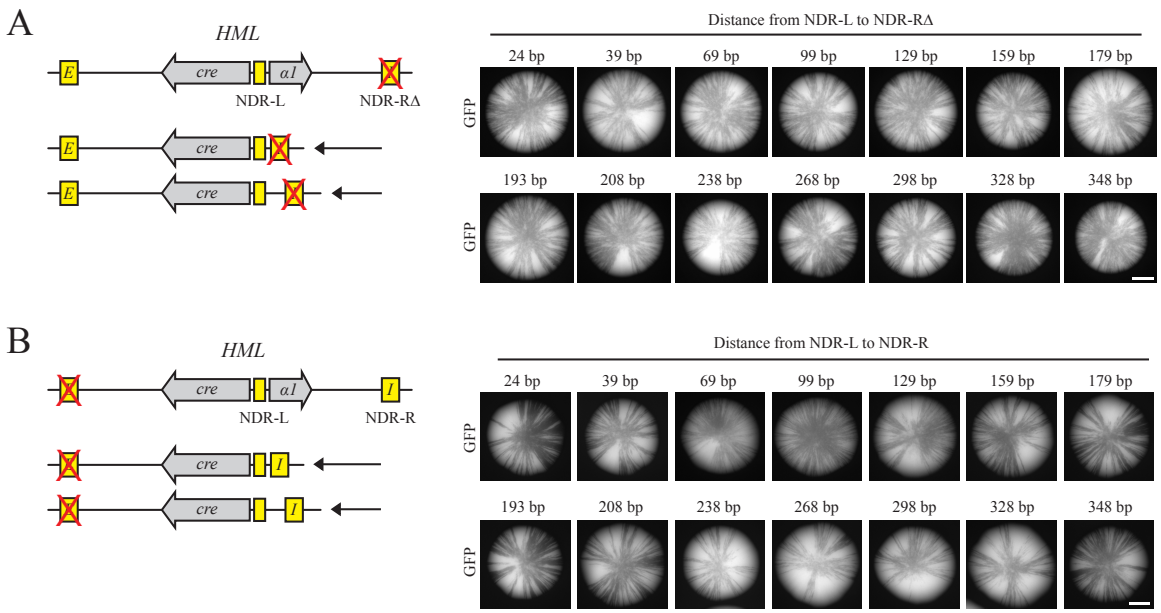

Figure 3.8: Representative CRASH colonies for strains with different inter-NDR distances and deletion of NDR-R (A) (JRY11362-11375) or the *HML-E* silencer (B) (JRY11377-JRY11390). Strains correspond to those analyzed in **Figure 3.7**. Scale bar, 2 mm.

3.3.4 Replacement of NDR-R with Heterologous NDRs

Though the correlation between silencing stability and proper nucleosome positioning suggested a causal relationship between these two variables, it was possible that the observed silencing effects resulted from a separate aspect of NDR repositioning. Previous studies suggest that silencers at *HM* loci can interact with each other and the bidirectional promoter to form loops, and it is possible that such loops facilitate silencing (28, 29). In this case, different distances between NDR-L and NDR-R may be more amenable or refractory to loop formation between these two sites, which could in turn impact silencing stability. To test this possibility, we replaced NDR-R with either of two heterologous NDRs that have no known roles in silencing (**Figure 3.9A**). One of these NDRs consisted of a trio of binding sites for the nucleosome-depleting factor Reb1 (30); these sites were able to efficiently deplete nucleosomes as judged by MNase-qPCR (**Figure 3.10**). The other heterologous NDR consisted of a 100 base pair poly-A sequence, which we utilized based on previous observations that poly-A sequences efficiently deplete nucleosomes *in vivo* (9, 15). We note that our large poly-A sequence was refractory to analysis of nucleosome occupancy by MNase-qPCR and MNase-Seq.

As with the native NDR-R, different inter-NDR distances between NDR-L and either heterologous NDR resulted in oscillatory silencing effects (**Figure 3.9B** and **C**, **Figure 3.11**). Therefore, given that oscillatory effects were still observed when *HML-I* was replaced with either of two heterologous NDRs, we inferred that looping activities involving *HML-I* were not the cause of oscillatory silencing effects. Importantly, both of these heterologous NDRs have transcriptional activation activities (9, 31), and it was possible that a loop with transcriptional activation activity could form between heterologous NDRs and the bidirectional promoter. If this heterologous loop existed and accounted for oscillatory silencing effects, it would also be likely to exhibit oscillatory transcriptional activation effects in unsilenced cells. However, transcription levels of *cre* did not exhibit oscillatory changes in unsilenced cells with different distances

between NDR-L and the trio of Reb1 binding sites (**Figure 3.10**). Therefore, we inferred that any potential looping functions of NDR-R or heterologous NDRs were not responsible for the oscillatory silencing effects. This finding was consistent with the idea that oscillatory silencing effects were caused by changes in nucleosome positioning.

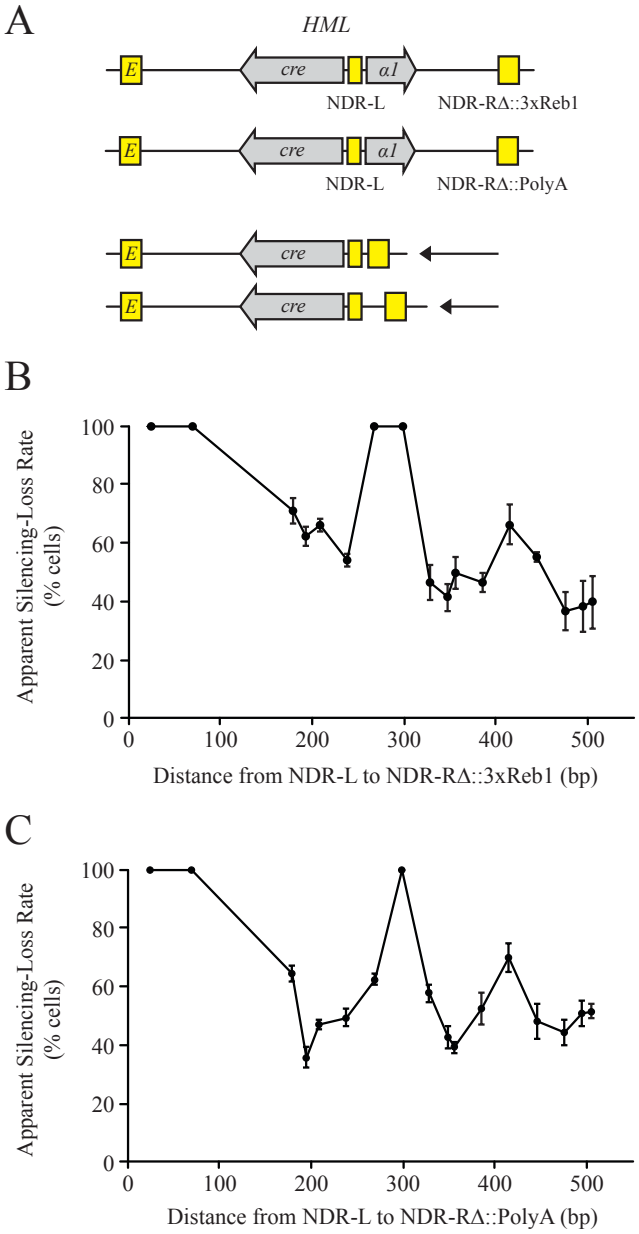

Figure 3.9: Oscillatory silencing effects were observed with heterologous NDRs. A. NDR-R was replaced with either a trio of Reb1 binding sites (JRY12961) or a 100 base pair poly-A sequence (JRY12960), and serial deletions were used to change inter-NDR distance (JRY12969-13002). B. Apparent silencing-loss rates for different inter-NDR distances between NDR-L and NDR-RΔ::3xReb1 (JRY12969-12985), as calculated by flow cytometry. C. Apparent silencing-loss rates for different inter-NDR distances between NDR-L and NDR-RΔ::PolyA (JRY12986-13002), as calculated by flow cytometry. Data are means ± SD (n = 6 independent cultures). Silencing-loss rates labelled as 100% reflect strains in which RFP+ cells were not recoverable during strain generation, as described in Materials and Methods.

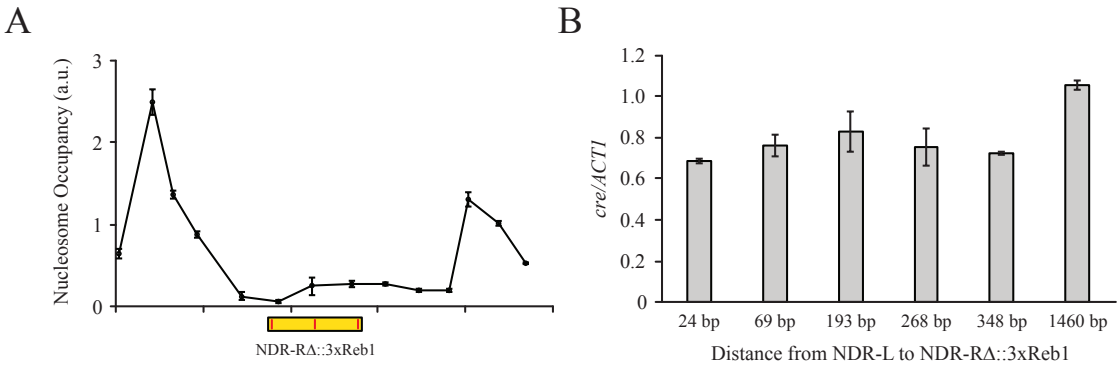

Figure 3.10: A trio of Reb1 binding sites depleted nucleosomes and did not generate oscillations of *cre* transcription in unsilenced cells. A. NDR-RΔ::3xReb1 (JRY12961) exhibited nucleosome depletion as measured by MNase-qPCR (see Materials and Methods). Data are means ± SD (n = 3 technical replicates). Red lines represent Reb1 binding sites, and tick marks are spaced at 100 base pair intervals. B. Different distances between NDR-L and NDR-RΔ::3xReb1 did not exhibit strong differences in transcription of *cre* in unsilenced cells (JRY12969, JRY12970, JRY12972, JRY12975, JRY12978, JRY12961). Cells were grown to log phase in 5mM NAM and transcript levels were quantified with RT-qPCR. Data are means ± SD (n = 3 independent cultures).

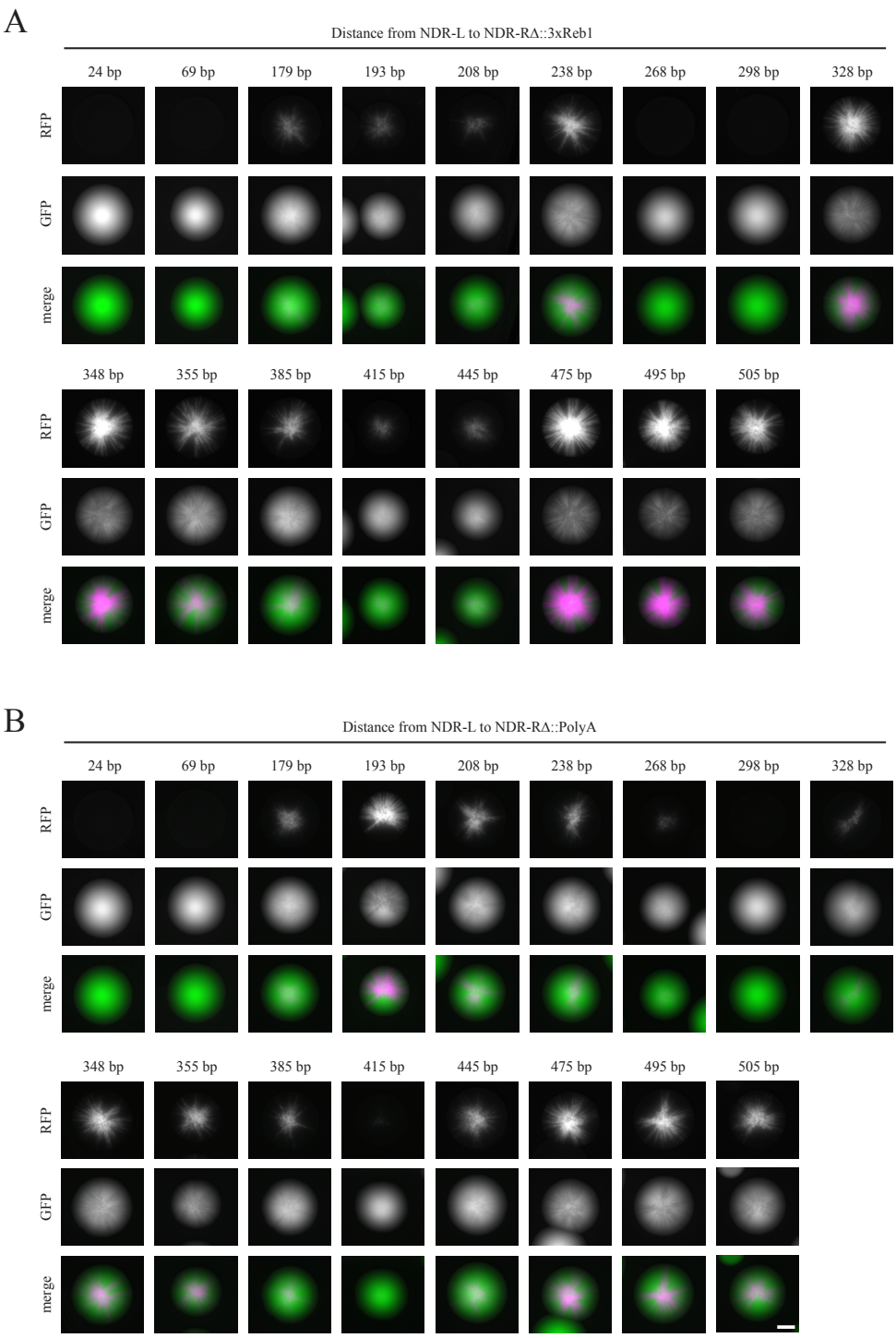

Figure 3.11: Representative CRASH colonies for strains with different distances between NDR-L and either NDR-RΔ::3xReb1 (A) (JRY12969-12985) or NDR-RΔ::PolyA (B) (JRY12986-13002). Colonies that were uniformly RFP- GFP+ reflect strains in which RFP+ cells were not recoverable during strain generation, as described in Materials and Methods. Strains correspond to those analyzed in **Figure 3.9**. Scale bar, 2mm.

3.3.5 Contributions of Inter-NDR DNA Content

In addition to the inter-NDR distance, the DNA sequence between NDR-L and NDR-R might also contribute to the observed oscillatory silencing pattern. For example, it was possible that nucleosome positioning affected binding of a sequence-specific DNA binding protein to its binding site(s) within the inter-NDR region. If this factor affected silencing, then the differential binding of this factor in strains with different inter-NDR distances could conceivably contribute to the oscillatory silencing patterns. The only known motif within the inter-NDR region is the transcription initiation site for the *α1* gene, which resides approximately 50 base pairs to the right of NDR-L. Notably, when the inter-NDR distance was 39 base pairs or less, then the initiation site was absent and silencing was stable (see **Figure 3.1C**). However, when the inter-NDR distance was expanded to 69 base pairs, the initiation site was revealed and silencing was less stable. Therefore, it was possible that the initiation site contributed to the oscillatory silencing effects observed in strains with inter-NDR distances of 69 base pairs or greater.

To test if the initiation site contributed to the oscillatory silencing effects, we deleted the DNA corresponding to the nucleosome that contained the initiation site, and subsequently made serial deletions that changed the distance between NDR-L and NDR-R. The resulting strains exhibited oscillatory silencing effects with different inter-NDR distances (**Figure 3.12**). Thus, the transcription initiation site for the *α1* gene was not necessary for the oscillatory silencing effects.

Given that different DNA sequences have different propensities to form nucleosomes (10), it was possible that the oscillatory silencing effects were influenced by the inter-NDR DNA sequence. To test this possibility, we made serial deletions between NDR-L and NDR-R in which the right side of the deletion, which is adjacent to NDR-R, was varied rather than the left side. This effectively created inter-NDR distances similar to those in **Figures 3.1-3.6**, but changed the DNA sequence between the NDRs. The oscillatory silencing effects were still observed in these strains (**Figure 3.13**). These data suggested that the distance between NDRs, rather than the specific DNA sequence between them, was the central driver of observed silencing effects.

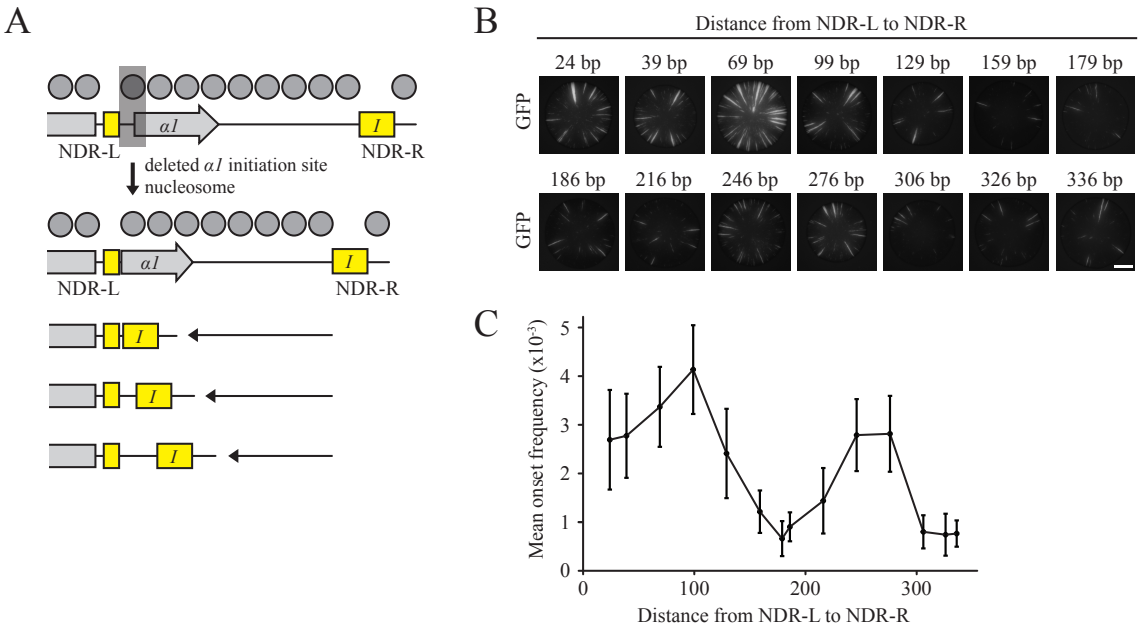

Figure 3.12: The *α1* initiation site was not necessary for oscillatory silencing effects. A. The nucleosome containing the *α1* initiation site was deleted, and additional serial deletions were made to change inter-NDR distance (JRY11259, JRY11452-JRY11464). B. Representative CRASH colonies from strains that lacked the *α1* initiation site nucleosome and had different inter-NDR distances. C. Sectoring rates were quantified using MORPHE software (26). Data are means ± SD (n = 10 colonies per genotype). Scale bar, 2 mm.

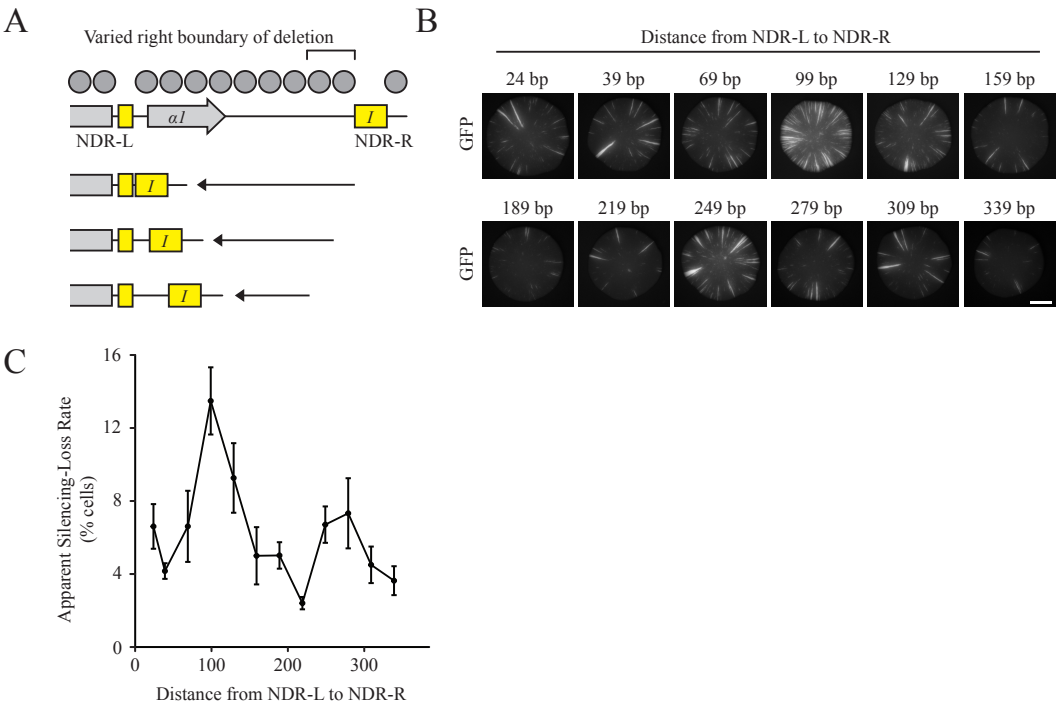

Figure 3.13: Effects of inter-NDR DNA content on oscillatory silencing effects. A. Schematic of deletions made at *HML*. The right boundary of these deletions was varied to alter inter-NDR distance (JRY11259, JRY12720-JRY12730), whereas the left boundary was varied to generate strains shown in **Figures 3.1-3.12**. B. Representative CRASH colonies for strains with different inter-NDR distances, generated by the approach depicted in (A). C. Apparent silencing-loss rates for strains shown in (B), calculated by flow cytometry. Data are means ± SD (n = 3 independent cultures). Scale bar, 2 mm.

3.3.6 Inter-NDR Distance Affected Silencing Stability at *HMRα*

Since all perturbations mentioned thus far were made at *HMLα::cre*, we were curious if nucleosome positioning effects on silencing were specific to *HMLα::cre* or a general feature of heterochromatin. To test this, we employed a variant of the CRASH assay that utilizes a separate heterochromatic domain, *HMRα::cre* (25). Notably, this domain contains the endogenous *HMR* silencers and a fragment from *HMLα::cre* that contains *cre*, the *HML* bidirectional promoter, and the *α1* gene (**Figure 3.14**). A previous study established that the *HML* bidirectional promoter and both *HMR* silencers in *HMRα::cre* are nucleosome depleted, and revealed five well-positioned nucleosomes between the *HML* bidirectional promoter and the *HMR-I* silencer (32). To alter inter-NDR distance, as above, we made a series of 14 deletions between the Rap1 binding site in the *HML* bidirectional promoter, which is termed NDR-L, and the Abf1 binding site in the *HMR-I* silencer, which is termed NDR-R. These mutants exhibited oscillatory silencing effects similar to those seen at *HMLα::cre*, albeit dampened in strains with inter-NDR distances greater than 200 base pairs (**Figure 3.14**). Thus, nucleosome positioning contributed to silencing stability in a second heterochromatic domain.

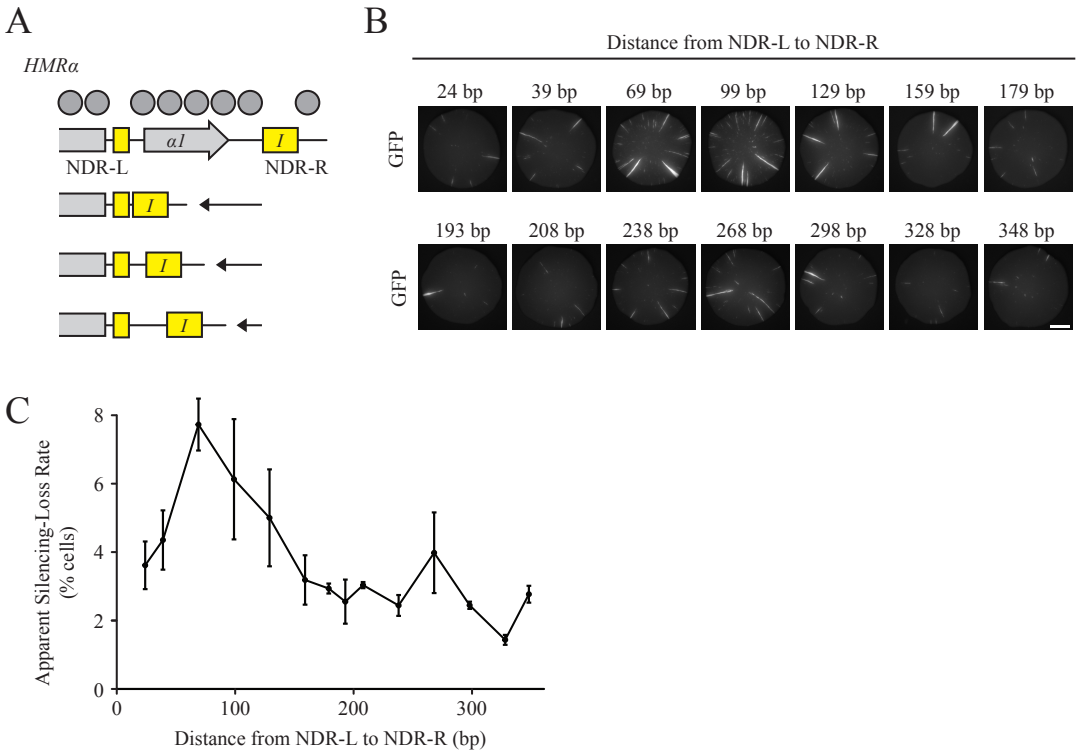

Figure 3.14: Inter-NDR distance affected silencing stability at *HMRα*. A. Schematic of serial deletions used to alter inter-NDR distance at *HMRα*. The *HML* bidirectional promoter is termed NDR-L, and the *HMR-I* silencer is termed NDR-R (yellow boxes). Five well-positioned nucleosomes (grey circles) reside between these NDRs (32). B. Representative CRASH colonies from strains with different inter-NDR distances at *HMRα* (JRY11471, JRY11781-

11794). The distance between NDR-L and NDR-R is indicated for each strain. C. Apparent silencing-loss rates for strains shown in (B), as calculated by flow cytometry. Data are means ± SD (n = 3 independent cultures). Scale bar, 2 mm.

3.3.7 Inter-NDR Distance Influenced Epigenetic Inheritance

It is possible that nucleosome positioning affects both transient loss-of-silencing events, as measured by the CRASH assay, and transmission of epigenetic chromatin states. In the absence of Sir1, genetically identical cells can be either transcriptionally silenced or expressed at individual heterochromatic mating-type loci. These transcriptional states are heritable and switching events between states can be monitored with the FLuorescent Assessment of Metastable Expression (FLAME) assay (32). This assay utilizes *HMLα::RFP* or *HMRα::GFP* in a *sir1*Δ mutant, and fluorescence profiles of cells can be monitored with flow cytometry and microscopy. Since *HMRα::GFP* is silenced more frequently than *HMLα::RFP*, *HMRα::GFP* provides a better dynamic range to measure potential silencing defects.

To test the effects of nucleosome positioning on epigenetic states, we altered the distance between NDR-L and NDR-R in *HMRα::GFP* and calculated the frequency of different epigenetic states by using flow cytometry (**Figure 3.15A** and **B**). Strikingly, the frequency of silenced cells exhibited an oscillatory pattern; strains with inter-NDR distances that were evenly divisible by nucleosome units had more silenced cells, and strains with distances that were not evenly divisible by nucleosome units had more expressed cells (**Figure 3.15C** and **D**). These results suggested that switching rates between states varied in strains with different inter-NDR distances. Indeed, by using time-lapse microscopy to monitor switching events in dividing cells, we found that the rate of silencing loss was higher for inter-NDR distances that were not evenly divisible by nucleosome units (**Figure 3.15E**). Interestingly, these same strains also exhibited a lower rate of silencing establishment (**Figure 3.15F**). These data suggested that proper nucleosome positioning facilitates both establishment and inheritance of the silenced epigenetic state at *HMR*.

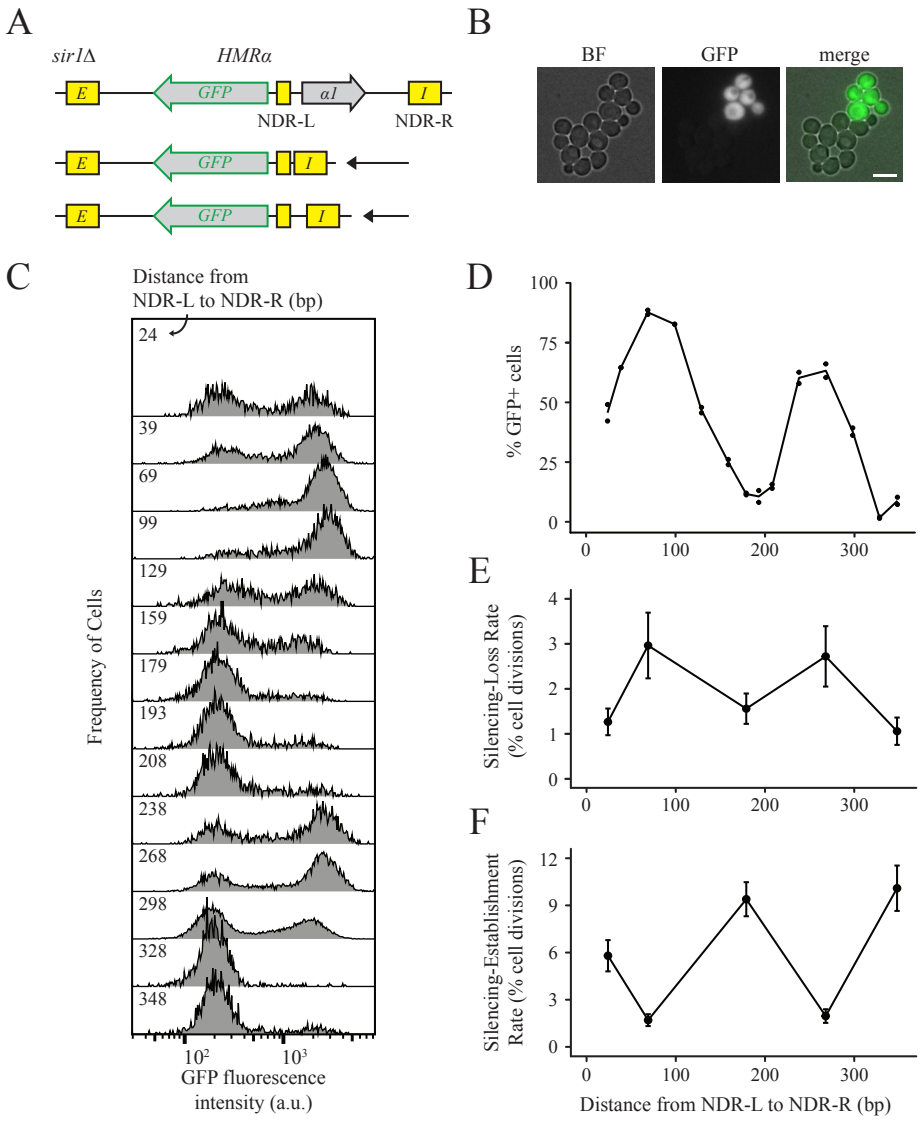

Figure 3.15: Inter-NDR distance influenced transmission of epigenetic states in *sir1*Δ. A. Schematic of the FLuorescent Assessment of Metastable Expression (FLAME) assay (32). In this assay, *GFP* replaces the *α2* gene in *HMRα* in a *sir1*Δ genetic background. NDRs are depicted as yellow boxes, including *HMR-E*, the *HML* bidirectional promoter (NDR-L), and the *HMR-I* silencer (NDR-R). B. Epigenetic states of *HMRα* observed with live-cell microscopy (JRY11478). C. Frequency of silenced and expressed cells in strains with different inter-NDR distances (JRY11543, JRY12306-12318). Serial deletions identical to those made in **Figure 3.14** were used to alter the distance between NDR-L and NDR-R. Cells were grown at log-phase for 48 hours to reach equilibrium, and subsequently analyzed by flow cytometry. D. Quantification of the frequency of expressed cells observed by flow cytometry in (C). Data points represent independent cultures (n = 2 per strain) and the line represents the mean for each strain. E. Quantification of silencing-loss rates observed with time-lapse microscopy (n > 500 cell divisions per genotype) for a subset of strains (JRY11543, JRY12307, JRY12312, JRY12315, JRY12318). F. Quantification of silencing-establishment rates observed with time-lapse microscopy (n > 400 cell divisions per genotype) for the same subset of strains (JRY11543, JRY12307, JRY12312, JRY12315, JRY12318). Error bars represent 95% confidence intervals. Scale bar, 5 μm.

3.4 Discussion

Heterochromatin is a complex structure that usually requires cooperation between modified nucleosome arrays and silencing proteins. Though this cooperative nature suggests that specific configurations of nucleosome arrays may be required for effective silencing, strong evidence for this idea has been lacking. Here, we tested whether nucleosome positioning within heterochromatin affects silencing stability by altering the distance between heterochromatic NDRs. We found that well-localized nucleosomes contribute to silencing stability in two heterochromatic domains and facilitate both the establishment, stability, and heritability of epigenetic silenced states.

3.4.1 Effects of Inter-NDR Distance on Nucleosome Positioning

The barrier model of nucleosome positioning posits that NDRs act as barriers to nucleosome movement, and effectively constrain the positions of adjacent nucleosomes (14). This model has been supported by evidence that nucleosomes are usually well positioned near NDRs and more poorly positioned at locations distant from NDRs (15). Indeed, in contrast to yeast, the much larger human genome has more poorly positioned nucleosomes due to the large amount of space between NDRs at promoters, enhancers, and other regulatory sites (33).

A corollary of the barrier model is that two NDRs in close proximity should constrain the number of nucleosomes that can fit between them. Consistent with this idea, a genome-wide study found that inter-NDR distances that are evenly divisible by nucleosome units have relatively well-positioned nucleosomes in that space, whereas those that are not evenly divisible by nucleosome units correspond to more poorly positioned nucleosomes (16). Our results built on these findings by showing that changes in inter-NDR distance at a specific locus of interest influenced nucleosome array patterns, with the most well-positioned nucleosomes corresponding to inter-NDR distances that are evenly divisible by nucleosome units.

3.4.2 Contributions of Nucleosome Positioning to Heterochromatin Stability

A simple model for the observed oscillatory silencing effects is that poor nucleosome positioning within heterochromatin leads to relatively large gaps between nucleosomes, which in turn causes silencing defects. In this view, inter-NDR distances that are not evenly divisible by nucleosome units would contain the permissible number of nucleosomes, but the inability to make all of the DNA nucleosomal would lead to gaps of unoccupied DNA that destabilize silencing. In support of this idea, the ability of the *HML-I* silencer to silence a nearby reporter gene is blocked by the introduction of a nucleosome-disfavoring DNA sequence between these two sites (34). Similarly, the incorporation of heterologous nucleosomal DNA sequences with long linker regions into *HML* is less permissible to silencing than incorporation of the same DNA sequences with short linker regions (35).

Poorly-positioned nucleosomes and nucleosome-free DNA could destabilize heterochromatin for multiple reasons. Previous work found that disruption of chromatin remodelers can lead to genome-wide defects in nucleosome positioning and increased levels of cryptic transcription (36, 37). Considering that the *HMLα1* initiation site is normally nucleosomal and not leading to active transcription, it was possible that irregular nucleosome positioning over this site led to aberrant transcription and subsequent destabilization of local heterochromatin. However, two independent experiments established that the *HMLα1* initiation site was not necessary for the observed oscillatory silencing effects (**Figure 3.12, Figure 3.13**).

An alternative possibility is that the spreading of silencing factors is limited by gaps of nucleosome-free DNA. Consistent with this idea, nucleosome-disfavoring DNA sequences are able to partially block the spread of Sir proteins from *HML-I* silencer (34). In theory, increased distances between nucleosomes could hinder binding of Sir3, which preferentially binds to di-nucleosomes *in vitro* (4). It is also possible that gaps of nucleosome-free DNA can hinder the iterative rounds of H4K16 deacetylation by Sir2 and histone binding by Sir3 that are thought to promote spreading of the Sir complex (1). Further studies will be needed to identify why altered nucleosome positioning and associated gaps between nucleosomes lead to unstable silencing.

It is important to note that the oscillatory silencing effects diminished with longer inter-NDR distances. This observation may suggest that perturbations to nucleosome positioning, and any resulting effects on silencing, can be mitigated by having larger inter-NDR distances. For example, larger inter-NDR distances facilitate the formation of larger nucleosome arrays, which could mitigate the effects of a fixed amount of non-nucleosomal DNA (such as that generated by an inter-NDR distance that is not evenly divisible by nucleosome units) by distributing it over more spaces between individual nucleosomes. This idea is interesting given that heterochromatic domains are often much larger than the repressed genes within them (38–40), and that NDRs such as silencer elements and the bidirectional promoter in *HML* are located relatively far away from each other. Our findings may suggest that this naturally occuring chromatin architecture acts to buffer silencing against processes that transiently disrupt nucleosome positioning, such as DNA replication and DNA repair (41, 42). Additional studies that test how heterochromatic nucleosome arrays can absorb changes in nucleosome positioning may point to advantages of naturally occurring heterochromatin architectures.

3.4.3 Effects of Nucleosome Positioning on Epigenetic States

A central question in chromatin biology is how genetically identical cells can exhibit different, heritable transcriptional states. This epigenetic phenomenon is frequently observed in heterochromatin, raising the question of how silenced transcriptional states can be generated and inherited. One possibility is that some nucleosome array configurations can favor chromatin structures required for different transcriptional states, such as the silenced and expressed states of *HML* and *HMR* in *sir1*Δ. In support of this idea, removal of the linker histone homolog Hho1 causes *HML* to be silenced more frequently in *sir1*Δ strains (43). Similarly, defects in the chromatin remodeling complex Isw2/yCHRAC cause more cells to be silenced at a reporter gene integrated in a synthetic yeast telomere (44).

We built on these findings by testing the effects of inter-NDR distance on epigenetic states of *HMR* in *sir1*Δ. Interestingly, inter-NDR distances that weren't evenly divisible by nucleosome units led to both higher silencing-loss rates and lower silencing-establishment rates. This result is partially consistent with the earlier discovery that Isw2/yCHRAC contributes only to the silencing-establishment rate at a synthetic yeast telomere (44). Together, these findings argue that poorly-positioned nucleosome arrays provide a poor substrate to establish silencing and can lead to defects in inheritance of silencing in some contexts. Additional studies will improve our understanding of why certain nucleosome array patterns are more permissible to specific epigenetic transcriptional states.

3.4.4 Potential Effects of Inter-NDR Distance in Disease Contexts and Synthetic Biology

These observations that inter-NDR distance affects local nucleosome arrays have additional functional implications. Genome wide, inter-NDR distances that are not evenly

divisible by nucleosome units correspond to higher histone turnover, higher PolII density, and higher transcriptional plasticity (16). These effects may be relevant to diseases that involve trinucleotide repeat expansions, many of which occur in non-coding regions and have unclear molecular consequences (45). As such, repeat expansions that influence inter-NDR distance, and thereby alter nucleosome positioning, may contribute to some pathologies. Additionally, future experiments that utilize synthetic biology to manipulate chromatin architecture may benefit from the knowledge that different inter-NDR distances can affect transcriptional regulation. This may be especially useful for fine-tuning transcriptional outputs in sensitive regulatory circuits. Further research will be needed to address the relevance of NDR positioning in disease contexts such as trinucleotide repeat expansions and in the field of synthetic biology.

3.5 Materials and Methods

Yeast strains

Strains and oligonucleotides used in this study are listed SI Appendix Table S1. All strains were derived from the W303 background. Strains used in the CRASH and FLAME assays were generated as described previously (25, 32).

All deletions were made with CRISPR/Cas9 technology (46). Each deletion required an sgRNA and two oligonucleotides, which are listed in SI Appendix Table S1. The sgRNA was designed to target a site within the region that would be deleted. The two oligonucleotides used for each deletion were partially overlapping and amplified by PCR prior to use. The resulting extended oligonucleotide constituted a repair template that would yield a deletion. Co-transformation of the sgRNA- and Cas9-containing plasmid, as well as the extended oligonucleotide, resulted in transformants with the desired deletion. Deletions were confirmed by junction PCR and sequencing.

To generate strains that replaced the *HML-I* silencer with a trio of Reb1 binding sites or a poly-A sequence, ultramers with the appropriate sequences were amplified and used as repair templates with the appropriate sgRNA- and Cas9-containing plasmid. The ultramer for the trio of Reb1 sites was 5'-
GTTTGACTTCTATGTTAACTTACTTCAACATGAAAGCCCGGTTACCCGGGTTAACAT
GTAGCCCGGCCCTATTAGTACAGCAGTGCCTTGGTTACCCGGAATGACATTCTCATT
ATTAAATTTTCTCTACAGCCAAACGAGTTACCCGGCGCCGGAGGTGCTGGAAATGGC
AAACGAAAATACTATGAC-3' and the ultramer for the poly-A sequence was 5'-
GTTTGACTTCTATGTTAACTTACTTCAACATGAAAGCCCGAAAAAAAAAAAAAAAA
AAAAAAAAAAAAAAAAAAAAAAAAAAAAAAAAAAAAAAAAAAAAAAAAAAAAAAA
AAAAAAAAAAAAAAAAAAAAAAAAAAAAACGCCGGAGGTGCTGGAAATGGCAA
ACGAAAATACTATGAC-3'. The primers and sgRNA sequences are listed in SI Appendix Table S1. The Reb1 consensus sequence GTTACCCGG was used (47) and the three Reb1 sites were each spaced 40 base pairs apart. Insertions were confirmed by junction PCR and sequencing.

When *HML-IΔ::3xReb1* or *HML-IΔ::PolyA* were generated in strains with different inter-NDR distances, a subset of transformations yielded only colonies that were RFP- GFP+. This result suggested that the resulting genotype had such unstable silencing that recovery of RFP+ cells was impossible or extremely difficult. We tested this by confirming the correct genotype of at least ten colonies that had the correct repair event and were RFP- and GFP+. Additionally, a significant number of colonies on control plates without a repair template were RFP+,

demonstrating that RFP+ cells had indeed been used in the transformation and that an immediate switch to GFP+ had probably occurred in correct transformants.

CRASH assay

To generate colonies, cells were plated at a density of ~10 cells/plate (CSM -Trp (Sunrise Science Products, San Diego, CA), 1% agar) and grown into colonies over 3-4 days. Colonies were imaged with a Leica M205 FA fluorescence stereomicroscope (Leica Camera AG, Wetzlar, Germany) equipped with a DFC3000G CCD camera, a Leica PLANAPO 0.63x objective, ET RFP filter (Leica 10450224), ET GFP filter (Leica 10447408), and Leica Application Suite X (LAS X) imaging software. A minimum of ten colonies were imaged per genotype.

Quantification of sectoring rates with MORPHE software was performed as previously described (26). As the onset point of each sector in a colony represented a single silencing-loss event, an average onset frequency for all sectors was calculated for each colony. At least ten colonies were analyzed per genotype.

To quantify apparent silencing-loss rates by flow cytometry, cells were first inoculated in liquid media (CSM -Trp (Sunrise Science Products)) and grown to saturation overnight. These cultures were subsequently back-diluted in CSM -Trp, grown at log-phase for 4 hours, and analyzed with a BD LSR Fortessa cell analyzer (BD Biosciences, San Jose, CA) with a FITC filter and PE-TexasRed filter. Subsequent analysis was performed with FlowJo software. Distinct populations of RFP+ GFP- cells (which had not lost silencing), RFP+ GFP+ cells (which had recently lost silencing), and RFP- GFP+ cells (which had lost silencing less recently) were observed. The apparent silencing-loss rate was calculated by dividing the frequency of RFP+ GFP+ cells by the combined frequencies of RFP+ GFP- and RFP+ GFP+ cells. Apparent silencing-loss rates were calculated for three independent cultures per genotype.

FLAME assay

Two independent cultures for each strain were grown in liquid media (CSM (Sunrise Science Products)) to saturation overnight. These cultures were then grown at log-phase for 48 hours by repeated serial back-dilutions, ultimately allowing each population to reach an equilibrium of silenced and unsilenced cells.

First, samples from each culture were analyzed by flow cytometry. The frequencies of silenced and unsilenced cells were similar between both independent cultures for each strain, therefore representative flow cytometry profiles were shown for only one culture per strain in **Figure 3.9C**. Second, samples from a subset of the cultures were used for time-lapse microscopy as previously described (32). Briefly, cells were sonicated and placed between an agar pad (CSM, Sunrise Science Products) and a glass coverslip. Time-lapse imaging was subsequently performed using a Zeiss Z1 inverted fluorescence microscope (Zeiss, Oberkochen, Germany). Cells were kept at 30°C and images were taken every 10 minutes for 10 hours. In subsequent analysis, cell divisions and switching events between epigenetic states were manually counted and the counter was blind to the genotype (single-blind study).

Expression levels by RT-qPCR

Cells were grown to log phase in liquid media (CSM, Sunrise Science Products) and RNA was extracted with a RNeasy Kit (Qiagen, Hilden, Germany) that included treatment with DNaseI (Qiagen). Reverse transcription was performed using the Invitrogen Superscript III kit (Invitrogen, Carlsbad, CA) and oligo (dT) primers. Quantitative PCR was performed with the

DyNAmo HS SYBR Green kit (Thermo Fischer Scientific, Waltham, MA) on an Mx3000P machine (Stratagene, La Jolla, CA) using two primers for *cre*: 5'-CGTACTGACGGTGGGAGAAT-3' and 5'-CCCGGCAAAACAGGTAGTTA-3'. Primers for *ACT1* were used for a control: 5'-TGTCCTTGTACTCTTCCGGT-3' and 5'-CCGGCCAAATCGATTCTCAA-3'. Samples were analyzed in technical triplicate for three independent RNA preparations per strain.

MNase-Seq and MNase-qPCR

MNase digestion was performed as previously described (32). Briefly, cultures were grown to log-phase in CSM liquid media (Sunrise Science Products) and spheroplasted. Nuclei were subsequently purified and treated with MNase (Worthington Biochemical Corporation, Lakewood, NJ). Mononucleosomes were isolated and nucleosomal DNA was purified. For MNase-Seq, MNase libraries were constructed with a NEBnextUltra II library preparation kit (New England Biolabs) and sequenced on an Illumina HiSeq4000 (Illumina, San Diego, CA) as 100 base pair paired-end reads. Reads were mapped to the *Saccharomyces cerevisiae* S288C genome (GenBank accession number GCA_000146045.2) using Bowtie2 (48). Mapped reads between 140 base pairs and 180 base pairs in length were used to provide mononucleosome resolution. Midpoints were calculated for each read and stacked in a histogram. Finally, a 25 base pair rolling mean was used to smooth the histogram of nucleosome peaks. All sequences and processed data files have been deposited in the NCBI Gene Expression Omnibus archive under accession number GSE144808. For MNase-qPCR, purified nucleosomal DNA was amplified by stacked primer sets that made ~100 base pair amplicons and were spaced ~30 base pairs, as previously described (49). To control for different amplification efficiencies, each primer pair was also used to amplify gDNA. Purified nucleosomal DNA and purified gDNA were each amplified in technical triplicate for each primer pair.

3.6 References

1. L. N. Rusché, A. L. Kirchmaier, J. Rine, Ordered nucleation and spreading of silenced chromatin in Saccharomyces cerevisiae. *Molecular biology of the cell* **13**, 2207–2222 (2002).

2. G. J. Hoppe, *et al.*, Steps in Assembly of Silent Chromatin in Yeast: Sir3-Independent Binding of a Sir2/Sir4 Complex to Silencers and Role for Sir2-Dependent Deacetylation. *Molecular and Cellular Biology* **22**, 4167–4180 (2002).

3. I. M. Hall, *et al.*, Establishment and maintenance of a heterochromatin domain. *Science* **297**, 2232–2237 (2002).

4. R. Behrouzi, C. Lu, M. A. Currie, G. Jih, N. Iglesias, Heterochromatin assembly by interrupted Sir3 bridges across neighboring nucleosomes. *eLife* (2016) https:/doi.org/10.7554/elife.17556.001.

5. S. Machida, *et al.*, Structural Basis of Heterochromatin Formation by Human HP1. *Molecular cell* **69**, 385-397.e8 (2018).

6. S. Poepsel, V. Kasinath, E. Nogales, Cryo-EM structures of PRC2 simultaneously engaged with two functionally distinct nucleosomes. *Nature Publishing Group*, 1–14 (2018).

7. Q. Yu, X. Zhang, X. Bi, Roles of Chromatin Remodeling Factors in the Formation and Maintenance of Heterochromatin Structure. *Journal of Biological Chemistry* **286**, 14659–14669 (2011).

8. K. M. Creamer, *et al.*, The Mi-2 Homolog Mit1 Actively Positions Nucleosomes within Heterochromatin To Suppress Transcription. *Molecular and Cellular Biology* **34**, 2046–2061 (2014).

9. V. Iyer, K. Struhl, Poly(dA:dT), a ubiquitous promoter element that stimulates transcription via its intrinsic DNA structure. *The EMBO journal* **14**, 2570–2579 (1995).

10. E. Segal, *et al.*, A genomic code for nucleosome positioning. *Nature* **442**, 772–778 (2006).

11. N. Kaplan, *et al.*, The DNA-encoded nucleosome organization of a eukaryotic genome. *Nature* **458**, 362–366 (2009).

12. G. Badis, *et al.*, A Library of Yeast Transcription Factor Motifs Reveals a Widespread Function for Rsc3 in Targeting Nucleosome Exclusion at Promoters. *Molecular cell* **32**, 878–887 (2008).

13. T. N. Mavrich, *et al.*, A barrier nucleosome model for statistical positioning of nucleosomes throughout the yeast genome. *Genome research* **18**, 1073–1083 (2008).

14. R. D. Kornberg, L. Stryer, Statistical distributions of nucleosomes: nonrandom locations by a stochastic mechanism. *Nucleic acids research* **16**, 6677–6690 (1988).

15. G.-C. Yuan, *et al.*, Genome-scale identification of nucleosome positions in S. cerevisiae. *Science* **309**, 626–630 (2005).

16. C. Vaillant, *et al.*, A novel strategy of transcription regulation by intragenic nucleosome ordering. *Genome research* **20**, 59–67 (2010).

17. A. R. Buchman, W. J. Kimmerly, J. Rine, Two DNA-binding factors recognize specific sequences at silencers, upstream activating sequences, autonomously replicating sequences, telomeres in *Saccharomyces cerevisiae*. *Molecular and Cellular Biology* **8**, 210-225 (1988).

18. K. Weiss, R. T. Simpson, High-resolution structural analysis of chromatin at specific loci: Saccharomyces cerevisiae silent mating type locus HMLalpha. *Molecular and Cellular Biology* **18**, 5392–5403 (1998).

19. A. Ravindra, K. Weiss, R. T. Simpson, High-resolution structural analysis of chromatin at specific loci: Saccharomyces cerevisiae silent mating-type locus HMRa. *Molecular and Cellular Biology* **19**, 7944–7950 (1999).

20. T. Triolo, R. Sternglanz, Role of interactions between the origin recognition complex and SIR1 in transcriptional silencing. *Nature* (1996).

21. P. Moretti, K. Freeman, L. Coodly, D. Shore, Evidence that a complex of SIR proteins interacts with the silencer and telomere-binding protein RAP1. *Gene Dev* **8**, 2257–2269 (1994).

22. A. A. Carmen, L. Milne, M. Grunstein, Acetylation of the Yeast Histone H4 N Terminus Regulates Its Binding to Heterochromatin Protein SIR3. *Journal of Biological Chemistry* **277**, 4778–4781 (2002).

23. P. G. Siliciano, K. Tatchell, Transcription and regulatory signals at the mating type locus in yeast. *Cell* **37**, 969–978 (1984).

24. T. H. Cheng, M. R. Gartenberg, Yeast heterochromatin is a dynamic structure that requires silencers continuously. *Genes & development* **14**, 452–463 (2000).

25. A. E. Dodson, J. Rine, Heritable capture of heterochromatin dynamics in Saccharomyces cerevisiae. *eLife* **4**, e05007 (2015).

26. T.-Y. Liu, A. E. Dodson, J. Terhorst, Y. S. Song, J. Rine, Riches of phenotype computationally extracted from microbial colonies. *Proceedings of the National Academy of Sciences of the United States of America* **113**, E2822-31 (2016).

27. J. Ocampo, R. V. Chereji, P. R. Eriksson, D. J. Clark, The ISW1 and CHD1 ATP-dependent chromatin remodelers compete to set nucleosome spacing in vivo. *Nucleic acids research* **44**, 4625–4635 (2016).

28. J. F.-X. Hofmann, T. Laroche, A. H. Brand, S. M. Gasser, RAP-1 factor is necessary for DNA loop formation in vitro at the silent mating type locus HML. *Cell* **57**, 725–737 (1989).

29. L. Valenzuela, N. Dhillon, R. N. Dubey, M. R. Gartenberg, R. T. Kamakaka, Long-range communication between the silencers of HMR. *Mol Cell Biol* **28**, 1924–35 (2008).

30. M. J. Fedor, N. F. Lue, R. D. Kornberg, Statistical positioning of nucleosomes by specific protein-binding to an upstream activating sequence in yeast. *J Mol Biol* **204**, 109–127 (1988).

31. D. I. Chasman, *et al.*, A yeast protein that influences the chromatin structure of UASG and functions as a powerful auxiliary gene activator. *Gene Dev* **4**, 503–514 (1990).

32. D. S. Saxton, J. Rine, Epigenetic memory independent of symmetric histone inheritance. *eLife* **8**, 585 (2019).

33. D. E. Schones, *et al.*, Dynamic Regulation of Nucleosome Positioning in the Human Genome. *Cell* **132**, 887–898 (2008).

34. X. Bi, Q. Yu, J. J. Sandmeier, Y. Zou, Formation of Boundaries of Transcriptionally Silent Chromatin by Nucleosome-Excluding Structures. *Molecular and Cellular Biology* **24**, 2118–2131 (2004).

35. S. A. Chakraborty, A. A. Kazi, T. M. Khan, S. G. Genetics, 2014, Nucleosome-positioning sequence repeats impact chromatin silencing in yeast minichromosomes. *Genetics Soc America* **198** (2014).

36. V. Cheung, *et al.*, Chromatin- and Transcription-Related Factors Repress Transcription from within Coding Regions throughout the Saccharomyces cerevisiae Genome. *PLoS Biology* **6**, e277-13 (2008).

37. B. P. Hennig, K. Bendrin, Y. Zhou, T. aacute s Fischer, Chd1 chromatin remodelers maintain nucleosome organization and repress cryptic transcription. *EMBO reports* **13**, 997–1003 (2012).

38. A. Hecht, S. Strahl-Bolsinger, M. Grunstein, Spreading of transcriptional represser SIR3 from telomeric heterochromatin. *Nature* **383**, 92–96 (1996).

39. K. Noma, C. D. Allis, S. I. S. Grewal, Transitions in Distinct Histone H3 Methylation Patterns at the Heterochromatin Domain Boundaries. *Science* **293**, 1150–1155 (2001).

40. Y. B. Schwartz, *et al.*, Genome-wide analysis of Polycomb targets in Drosophila melanogaster. *Nature genetics* **38**, 700–705 (2006).

41. M. J. Smerdon, M. W. Lieberman, Nucleosome rearrangement in human chromatin during UV-induced DNA- reapir synthesis. *Proc National Acad Sci* **75**, 4238–4241 (1978).

42. P. Vasseur, *et al.*, Dynamics of Nucleosome Positioning Maturation following Genomic Replication. *Cell reports* **16**, 2651–2665 (2016).

43. Q. Yu, *et al.*, Saccharomyces cerevisiaeLinker Histone Hho1p Functionally Interacts with Core Histone H4 and Negatively Regulates the Establishment of Transcriptionally Silent Chromatin. *Journal of Biological Chemistry* **284**, 740–750 (2009).

44. T. Iida, H. Araki, Noncompetitive Counteractions of DNA Polymerase and ISW2/yCHRAC for Epigenetic Inheritance of Telomere Position Effect in Saccharomyces cerevisiae. *Molecular and Cellular Biology* **24**, 217–227 (2003).

45. C. T. McMurray, Mechanisms of trinucleotide repeat instability during human development. *Nature reviews. Genetics* **11**, 786–799 (2010).

46. M. E. Lee, W. C. DeLoache, B. Cervantes, J. E. Dueber, A Highly Characterized Yeast Toolkit for Modular, Multipart Assembly. *ACS Synthetic Biology* **4**, 975–986 (2015).

47. C. Yan, H. Chen, L. Bai, Systematic Study of Nucleosome-Displacing Factors in Budding Yeast. *Molecular cell* **71**, 294-305.e4 (2018).

48. B. Langmead, S. L. Salzberg, Fast gapped-read alignment with Bowtie 2. *Nature Methods* **9**, 357–359 (2012).

49. E. A. Sekinger, Z. Moqtaderi, K. Struhl, Intrinsic Histone-DNA Interactions and Low Nucleosome Density Are Important for Preferential Accessibility of Promoter Regions in Yeast. *Molecular cell* **18**, 735–748 (2005).

Chapter 4:
A novel allele of *SIR2* reveals a heritable intermediate state of gene silencing

4.1 Abstract

Genetic information acquires additional meaning through epigenetic regulation, the process by which genetically identical cells can exhibit heritable differences in gene expression and phenotype. Inheritance of epigenetic information is a critical step in maintaining cellular identity and organismal health. In *Saccharomyces cerevisiae*, one form of epigenetic regulation is the transcriptional silencing of two mating-type loci, *HML* and *HMR,* by the SIR-protein complex. To focus on the epigenetic dimension of this gene regulation, we conducted a forward mutagenesis screen to identify mutants exhibiting an epigenetic or metastable silencing defect. We utilized fluorescent reporters at *HML* and *HMR*, and screened yeast colonies for epigenetic silencing defects. We uncovered numerous independent *sir1* alleles, a gene known to be required for stable epigenetic inheritance. More interestingly, we recovered a missense mutation within *SIR2*, which encodes a highly conserved histone deacetylase. In contrast to *sir1*Δ*,* which exhibits states that are either fully silenced or fully expressed, this *sir2* allele exhibited heritable states that were either fully silenced or expressed at an intermediate level. The heritable nature of this unique silencing defect was influenced by, but not completely dependent on, changes in rDNA copy number. Therefore, this study revealed a heritable state of intermediate silencing and linked this state to a central silencing factor, Sir2.

4.2 Introduction

Transcriptional gene silencing is critical for proper cellular function, differentiation, and development. A temporally coordinated program of changing chromatin environments maintains cell fate by altering gene expression. Consequently, aberrant gene silencing and expression can lead to a variety of disease states (reviewed in Lee and Young 2013). A better understanding of how transcriptional silencing is maintained over time and remembered through cellular division is therefore crucial to understanding its misregulation.

One context in which transcriptional silencing has been studied in detail is the single-celled eukaryote *Saccharomyces cerevisiae*. *S. cerevisiae* exhibits stable, epigenetic silencing of transcription through the action of the SIR complex, which produces heterochromatin-like repressive chromatin domains (Kueng *et al.* 2013; Gartenberg and Smith 2016). This budding yeast has two mating types, *a* and *α,* with mating-type-specific information expressed from the two alleles of the *MAT* locus on Chromosome III. Two loci that undergo stable silencing are the silent mating type loci, *HML* and *HMR.* These extra copies of mating-type information are distal to the expressed *MAT* locus and allow for mating-type switches in the subset of strains with the *HO* gene, which encodes a site-specific nuclease that cuts at *MAT* (Kostriken *et al.* 1983).

HML and *HMR* are stably repressed, making mating type solely dependent on the allele of the *MAT* locus. Mutations in *SIR2, SIR3,* or *SIR4*, which collectively encode the SIR complex, result in complete loss of silencing at *HML* and *HMR* (Rine and Herskowitz 1987). The SIR complex is recruited to silencer elements within *HML* and *HMR*, deacetylates histones via the catalytic activity of Sir2, and binds to nucleosomes throughout the locus, resulting in transcriptional repression (Hoppe *et al.* 2002; Rusché *et al.* 2002; Thurtle and Rine 2014). Though Sir2, Sir3 and Sir4 are necessary for *HML* and *HMR* silencing, Sir1 was identified by mutant alleles that produced only partial loss of silencing at these loci (Rine *et al.* 1979). Characterization of the *sir1* phenotype at the single-cell level revealed that the expression states

of *HML* and *HMR* are bistable in the absence of Sir1 (Pillus and Rine 1989). Quantitative RNA FISH studies show that in the silenced fraction of a *sir1*Δ population, *HML* and *HMR* are as fully silenced as in *SIR* cells (Dodson and Rine 2015). Likewise, in the unsilenced fraction, *HML* and *HMR* are as expressed as in *sir2*Δ*, sir3*Δ or *sir4*Δ mutants. These two expression states in *sir1*Δ are also heritable, as the mother cell's expression state can be passed on faithfully to daughter cells for multiple generations, with switches to the opposite expression state occurring at a low rate.

In *sir1*Δ mutants, some cells manage to heritably silence *HML* and *HMR*, while others exhibit derepression of these loci. One possible explanation for the partial loss of silencing would be the existence of another gene with an overlapping function with *SIR1;* the absence of both factors would then be necessary to observe full derepression. Screens for enhancers of the *sir1*Δ silencing defect have largely uncovered more alleles of *SIR2*, *SIR3* and *SIR4* (Stone *et al.* 2000). Screens for multicopy suppressors of the silencing defect of *sir1*Δ mutants recovered *HTZ1*, which encodes a variant of histone H2A, and *ESC2* (Dhillon and Kamakaka 2000). However unlike *sir1*Δ, *htz1* and *esc2* do not exhibit a bistable phenotype. Therefore, mutants that function similarly to *sir1*Δ have eluded previous studies.

A screen to identify bistable silencing mutants has not previously been reported, nor have any reports appeared of heritable intermediate levels of gene silencing. In this study, we carried out a forward mutagenesis screen to identify metastable silencing mutants in *S. cerevisiae.* This screen differed from past screens in the use of fluorescent reporter genes at *HML* and *HMR*, providing the opportunity to observe silencing and heritability quantitatively at both the population and single-cell level.

4.3 Results

4.3.1 Identification of metastable mutants.

To isolate mutants that displayed metastable silencing defects at *HML* and *HMR,* we utilized an assay that reveals the expression state of these two loci individually. The FLuorescent Analysis of Metastable Expression (FLAME) assay utilizes fluorescent reporters integrated at *HML* and *HMR,* termed *hmlα2*Δ*::RFP* and *hmrα2*Δ*::GFP,* respectively (Saxton and Rine 2019, **Figure 4.1A**). In wild-type cells, these loci are stably silenced by the SIR complex (Rine and Herskowitz 1987). Thus, when SIR complex members Sir2, Sir3, or Sir4 are absent, these loci are fully expressed. In the FLAME assay, loss of silencing results in expression of the fluorescence reporters, which can be evaluated at either the single-cell or colony level. The colony phenotype offers additional historical information about the expression state of *HML* and *HMR.* Due to the pattern of cell divisions, ancestors are proximal to their descendants, forming sectors of related cells which radiate to the periphery of the colony. In *sir2, sir3,* or *sir4* mutants, colonies are uniformly fluorescent, whereas in a *sir1*Δ mutant, a sectored fluorescence pattern is observed; this sectoring indicates heritable phenotypic variation within a genetically identical population (**Figure 4.1B**). By screening colonies arising from the mutagenized *SIR* reporter strain, we identified six mutants with metastable silencing of *HML* and *HMR* (**Figure 4.2A**).

As a complement to direct screening of colonies, we adapted Fluorescence Activated Cell Sorting (FACS) to detect and sort fluorescent cells within a mutagenized population. These sorted cells were then interrogated for clonal heritability of expression states at the colony level (see *Materials and Methods*). Using a double-FACS sorting strategy, three additional mutants of interest were found (**Figure 4.2A**).

4.3.2 Genetic analysis identified eight unique *sir1* alleles

The metastable phenotype was recessive in all nine mutants of interest, based on the fluorescence of diploids heterozygous for the new mutations (**Figure 4.1C** and **4.2B**). To test if the metastable phenotype was due to a single mutation, seven of the diploids from the dominance test were sporulated and the phenotype evaluated among the tetrad segregants. The characteristic 2:2 segregation of mutant to wild-type phenotypes was observed for at least ten tetrads from each of the mutants tested, strongly suggesting that a mutation in a single gene caused the metastable phenotype.

A complementation test was used to determine whether these mutants revealed new genes capable of metastable phenotypes or were new alleles of *SIR1*. In this test, *MATα* mutants were mated to an isogenic *MATa sir1Δ* strain. All seven mutants tested failed to complement a *sir1*Δ mutation (**Figure 4.1C** and **4.2C**). Interestingly, in diploids, the silencing phenotype was less severe than in haploids, and far more evident at *HML*. This discrepancy likely reflects previous findings that silencing is stronger in diploids than in haploids (Dodson and Rine 2015), and that haploid *sir1*Δ cells are more frequently silenced at *HMR* than at *HML* (Saxton and Rine 2019).

The *sir1* alleles of each mutant strain were sequenced, revealing mutations within the coding region of *SIR1* (**Figure 4.1D**). Two independent rounds of mutagenesis produced identical nonsense mutations, resulting in identical *sir1-W251** alleles. As expected from EMS mutagenesis, all of the *sir1* alleles contained a single point mutation resulting from GC to AT transitions, with five of the eight unique point mutations resulting in a nonsense mutation (**Figure 4.2D**). These point mutations were engineered into the parent strain using molecular cloning techniques, where they recapitulated the phenotypes observed in the original mutants, showing that the *sir1* alleles were necessary and sufficient to produce the metastable phenotype observed (**Figure 4.1E**).

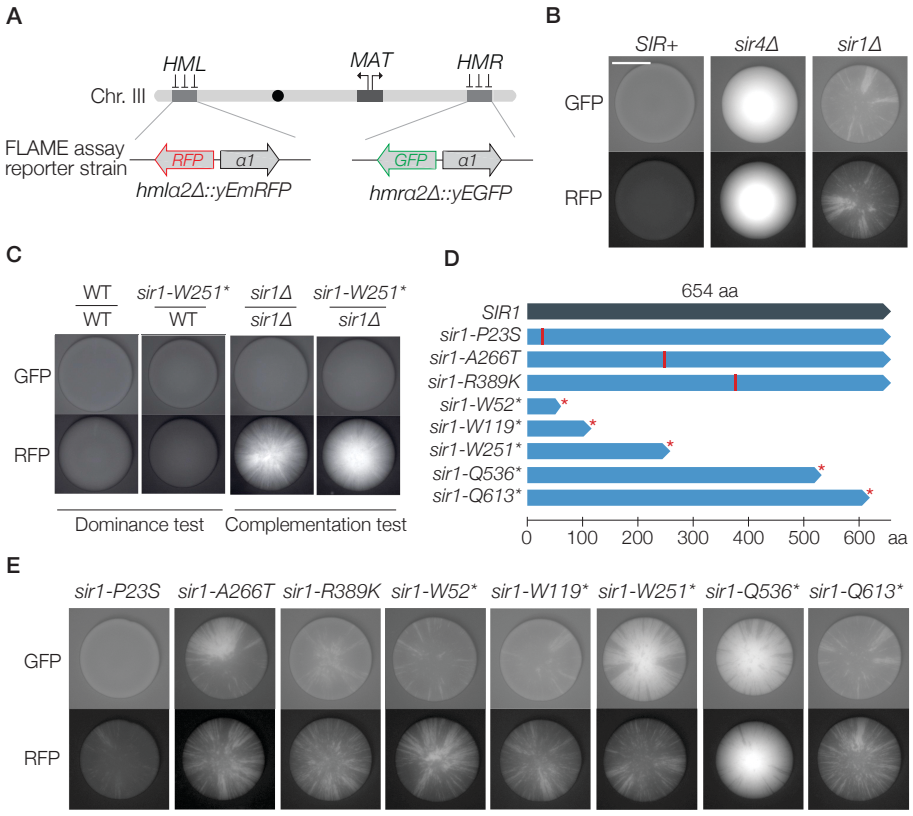

Figure 4.1: A screen for metastable silencing mutants revealed eight unique alleles of *sir1*. A. Schematic of the FLuorescent Analysis of Metastable Expression "FLAME" reporter strain (JRY12860) used in this study: fluorescent reporters *yEGFP* and *yEmRFP* replaced *α2* at *HMRα* and *HMLα,* respectively. B. Colony phenotypes of control strains (JRY12860 - JRY12862) in both the GFP and RFP channel. Colonies were grown on YPD and imaged at identical exposures (Scale bar, 4 mm). C. Representative colony images of diploid strains for the dominance and complementation tests. For dominance testing, a *MATa* wild-type FLAME strain was mated with *MATα* mutant strain (JRY11955, JRY11915); for complementation testing, a *MATa sir1Δ* strain was mated with a *MATα* mutant strain (JRY11957, JRY11950). D. A schematic of the *sir1* alleles identified. The *SIR1* encodes a 654 amino acid protein (top bar in dark blue). Mutant alleles contained either a missense mutation or a nonsense mutation. Premature stop codons are indicated with an asterisk, i.e. *sir1-W52**. E. Colony images of the engineered single point mutation *sir1* alleles, imaged on YPD in both the GFP and RFP channel. Differences in fluorescence profiles between colonies mostly reflect the high degree of variability between colonies of a given genotype, rather than differences between genotypes.

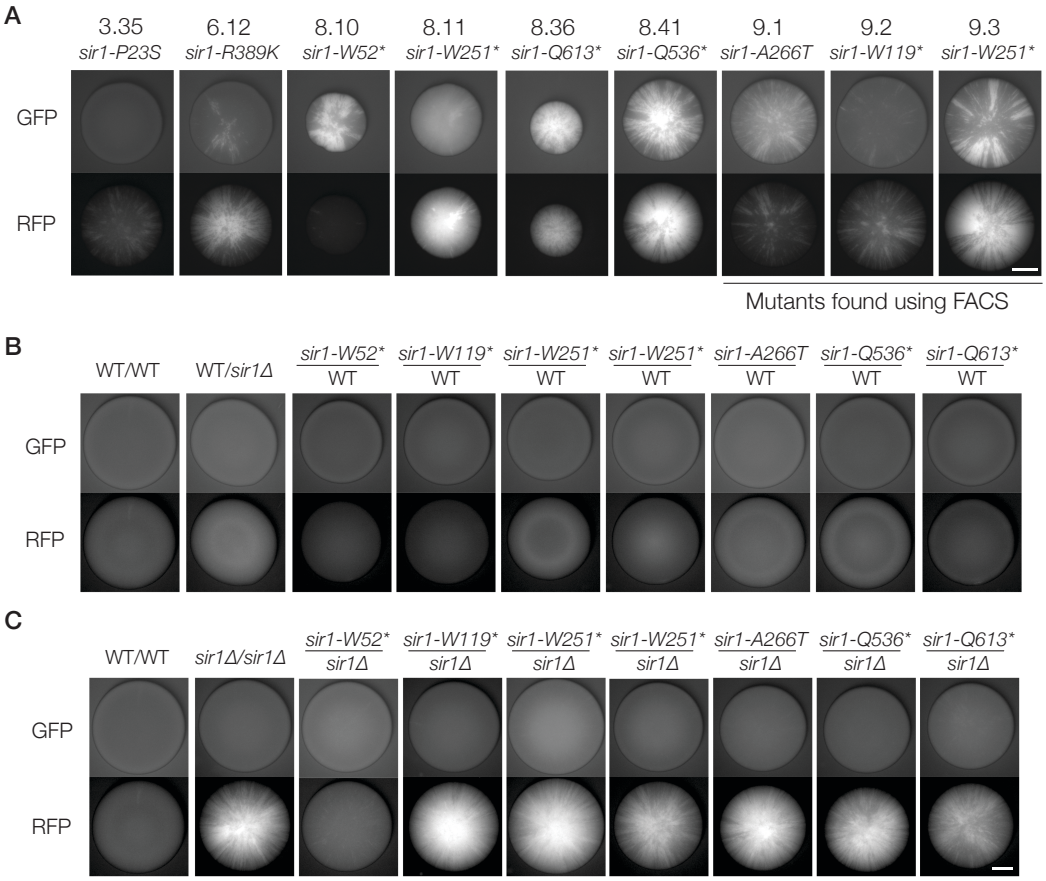

D

Mutant ID	*sir1* allele	Nucleotide position mutated	Base pair change
3.35	*sir1-P23S*	67	CCA to TCA
8.10	*sir1-W52**	155	TGG to TAG
9.2	*sir1-W119**	356	TGG to TAG
8.11	*sir1-W251**	752	TGG to TAG
9.3	*sir1-W251**	752	TGG to TAG
9.1	*sir1-A266T*	796	GCA to ACA
6.12	*sir1-R389K*	1166	AGG to AAG
8.41	*sir1-Q536**	1606	CAA to TAA
8.36	*sir1-Q613**	1837	CAA to TAA

Figure 4.2: Additional FLAME phenotypes and characterization of the *sir1* mutants identified. A. Colony phenotypes of the mutants identified (JRY11896, JRY11897, JRY11901, JRY11902, JRY11904, JRY11905, JRY11918-11920). Colonies were labeled with both the initial mutant ID and its associated *sir1* allele; an asterisk indicates a premature stop codon. Each mutant found during FACS sorting was from an independent mutagenized culture. B. Colony images of the dominance test diploid strains (*MATa* FLAME strain crossed with a *MATα* mutant FLAME strain) (JRY11908, JRY11909, JRY11914-11917, JRY11922-11924, JRY11955), in both the GFP and RFP channel, plated on YPD. Some variable autofluorescence was seen in the RFP channel at the colony level, however variable autofluorescence in the RFP channel was also seen in colonies without an endogenous source of RFP (data not shown). C. Colony images of the *sir1*Δ complementation test diploid strains (*MATa sir1*Δ FLAME strain crossed with a *MATα* mutant FLAME strain) (JRY11946-11957), in both the GFP and RFP channel, plated on YPD. Mutant *sir1-W52** displayed a much weaker phenotype than other colonies, yet some small sectors are seen in the RFP channel. D. Table indicating the initial mutant ID, the associated *sir1* allele, the location of the nucleotide mutation, and the resulting base pair change. Mutants 8.11 and 9.3 were isolated from independent rounds of mutagenesis and had identical *sir1* alleles, *sir-W251**. Scale bars, 2 mm.

4.3.3 A metastable phenotype from a mutation in *SIR2*

Having identified eight independent and unique *SIR1* alleles, we revised the screening strategy to reduce the likelihood of finding more *sir1* mutants. We reasoned that if two *SIR1* alleles were present in our haploid reporter strain, the probability of random mutagenesis disrupting both in the same cell would be reduced. Therefore, an additional copy of *SIR1* was maintained on a plasmid in the parental strain of the screen (JRY12860 containing pJR909). After mutagenesis, a single-FACS enrichment step was employed (see *Materials and Methods*). With this additional extrachromosomal copy of *SIR1*, very few mutants with a metastable phenotype were produced. After mutagenizing and sorting twelve independent cultures with FACS, no further *sir1* alleles were found. One colony of interest was identified, which exhibited a mild but noticeable silencing defect (**Figure 4.3A**). The phenotype was unlike any other observed during both iterations of mutagenesis and unique from all other mutant phenotypes studied using the FLAME assay. In this mutant, the entire colony exhibited expression of *HML* and *HMR*, but the strength of expression was less than that observed in *sir2*Δ. Moreover, close examination of the colony revealed streaks of greater or lesser fluorescence intensity, suggesting the possibility of heritable intermediate defects in silencing, a phenotype not previously described. The mutant phenotype was recessive, complemented a *sir1*Δ mutation, and produced a 2 wild-type: 2 mutant segregation pattern after diploid sporulation and tetrad analysis (**Figure 4.4**).

To identify the causative gene resulting in the mutant phenotype, we first assayed the ability of *SIR2, SIR3,* or *SIR4* to rescue the silencing defect. Transformation of a *SIR2* plasmid into the parent strain restored wild-type silencing, whereas *SIR3* and *SIR4* plasmids had no effect on the silencing phenotype. Sir2 is a highly conserved histone deacetylase and is the sole catalytic component of the SIR complex (Landry *et al.* 2000; Imai *et al.* 2000). Sequencing of *SIR2* from the mutant strain revealed a single point mutation at residue 436, changing the encoded amino acid from a glycine to an aspartic acid (*sir2-G436D*). Using molecular cloning techniques, the *sir2-G436D* point mutation was introduced into the parental strain (JRY12564); this mutant recapitulated the intermediate silencing phenotype (**Figure 4.3A**). Thus, the missense *sir2-G436D* allele was sufficient to produce the intermediate silencing defect. Colony imaging at longer exposures highlighted the unique fluorescence pattern of this mutant, with streaks of brighter fluorescence superimposed on a low-fluorescence colony (**Figure 4.3B**). Interestingly, these streaks of brighter fluorescence overlapped in the RFP and GFP channels, suggesting that *hmlα2*Δ*::RFP* and *hmrα2*Δ*::GFP* were coordinately impacted by *sir2-G436D*. The similarity between RFP and GFP channels was not caused by bleedthrough, as streaks were still visualized when only one of the two fluorophores was present (**Figure 4.4**). Importantly, this concordance between RFP and GFP in *sir2-G436D* contrasted with the colony phenotype of *sir1*Δ, in which *hmlα2*Δ*::RFP* and *hmrα2*Δ*::GFP* are silenced or expressed independently of each other (**Figure 4.3A**, Xu *et al.* 2006).

4.3.4 A unique silencing defect in *sir2-G436D*

To further characterize this mutant phenotype, flow cytometry was used to quantify the *hmlα2*Δ*::RFP* and *hmrα2*Δ*::GFP* fluorescence intensities in log-phase cells. The *SIR* reporter strain existed as a homogenous population lacking both GFP and RFP fluorescence, whereas the *sir2*Δ strain strongly expressed both GFP and RFP (**Figure 4.3C**). Using the *SIR*+ and *sir2*Δ control strains, gates were established to create four quadrants representative of the four possible FLAME expression states. As expected, *sir1*Δ cells existed in all four quadrants and therefore

exhibited all possible combinations of expression states for *HML* and *HMR*. The *sir2-G436D* mutant strain exhibited a distinct pattern of expression, with a broad spread in fluorescence intensities for *hmrα2Δ::GFP* and *hmlα2Δ::RFP*. The distribution of fluorescence intensities appeared bimodal for *hmrα2Δ::GFP*, and distinctly less so for *hmlα2Δ::RFP*, which was more uniformly expressed. Interestingly, GFP^+ cells and RFP^+ cells appeared less fluorescent in *sir2-G436D* than in *sir1Δ* or *sir2Δ*. Therefore, flow cytometry indicated that *sir2-G436D* cells exhibited either a fully silenced state or intermediate silenced state at both *hmrα2Δ::GFP* and *hmlα2Δ::RFP*.

To evaluate this intermediate silencing phenotype further, the *sir2-G436D* allele was introduced into a strain with wild-type *HML* and *HMR*. Using these strains, silencing of *HML* and *HMR* was measured by a patch mating assay and a single-cell α-factor confrontation assay. In both assays, expression of *HML* or *HMR* causes cells to behave as pseudo *a*/*α* diploids that don't mate or respond to *α* factor. In the patch mating test, *sir2-G436D* silenced *HML* and *HMR* inefficiently relative to wild type (**Figure 4.3D**). An *α*-factor confrontation assay (Pillus and Rine 1989) revealed that approximately 7% of *MATa sir2-G436D* cells were able to sufficiently silence *HML* and thus avoid the the α-factor resistance of pseudo *a*/*α* diploids (**Figure 4.3E**). Compared to *sir1,* which by α-factor confrontation was previously shown to effectively repress *HML* in 20% of cells, *sir2-G436D* showed a more pronounced silencing defect. Thus, as confirmed by three independent assays, the *sir2-G436D* mutation resulted in partially defective silencing.

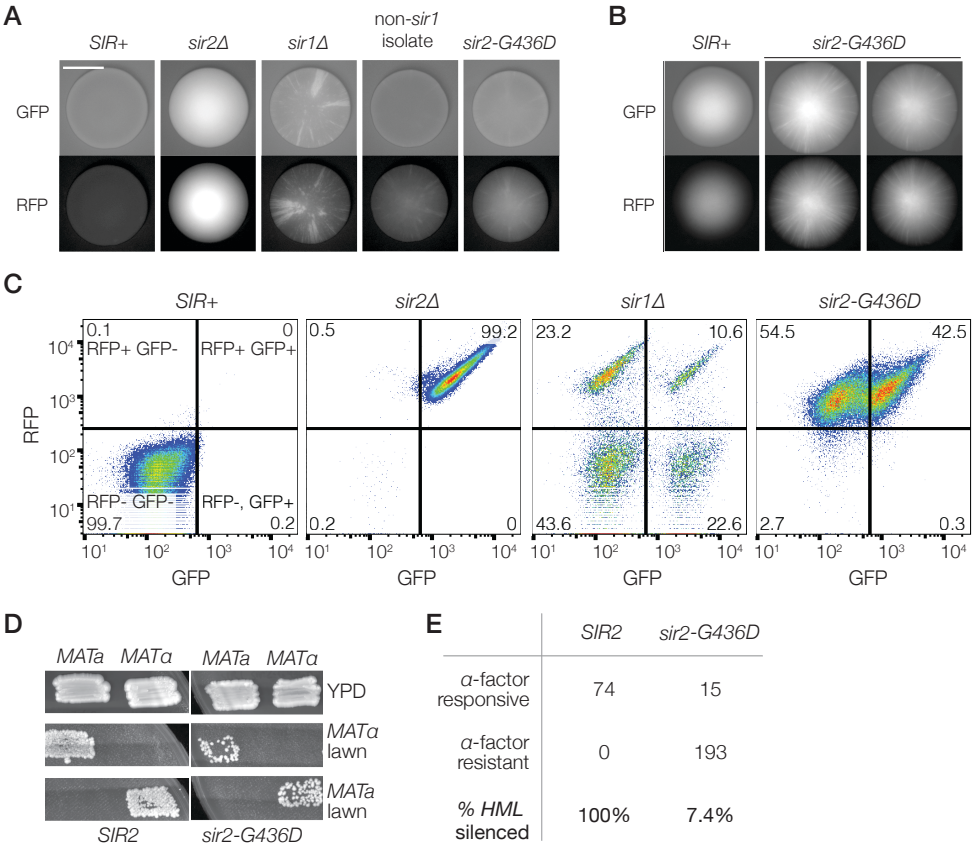

Figure 4.3: Characterization of mutant *sir2-G436D.* A. Representative colony images of FLAME control strains, the mutant of interest, and *sir2-G436D* in both the GFP and RFP channel (JRY12860, JRY12259, JRY12861, JRY12466, JRY12564), grown on YPD. B. Colony images of FLAME strain *SIR+* colonies and two biological replicates of the engineered single point mutation strain (JRY12860, JRY12564). Colonies were grown on CSM and imaged at approximately 10-fold longer exposure than (A) (Scale bar, 4 mm). C. Flow cytometry plots of the fluorescence profiles for both *hmlα2Δ::RFP* (PE-Texas Red) and *hmrα2Δ::GFP* (FITC). Cells were grown in CSM liquid media for 24 hours, fixed, and analyzed. Quadrants were established using *SIR+* and *sir2Δ* strains (JRY12860, JRY12466), and the resulting percentage of the population per quadrant was labeled in the corresponding corner. *sir1Δ* cells (JRY12861) exhibited distinct populations in all four quadrants, while *sir2-G436D* (JRY12564) cells exhibited fully silenced states and intermediate silenced states. D. Patch mating assays of *SIR2* and *sir2-G436D* in *MATa* (JRY4012, JRY12667) and *MATα* (JRY4013, JRY12669) cells. The extent of growth on the YM minimal media reflected the strength of silencing. A complete loss of silencing, such as that seen in *sir2Δ*, would yield no mating and therefore no growth. E. Results of the α-factor confrontation assay (JRY4012, JRY12667). *HML* silencing was calculated by dividing the number of α-factor responsive cells by the total number of cells assayed. A complete loss of silencing, such as that seen in *sir2Δ*, would cause all cells to be α-factor resistant.

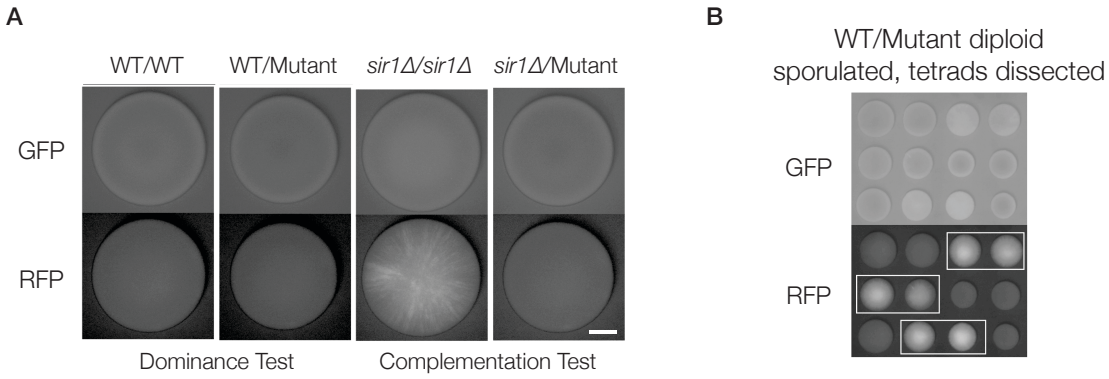

Figure 4.4: Genetic analysis of the mutant isolated from the second mutagenesis screen. A. Representative colony images of the diploid strains (JRY11957, JRY12476, JRY11952, JRY12477), grown on CSM. These strains were generated by mating the mutant isolated from the second mutagenesis screen (JRY12466) to *SIR+* and *sir1Δ* strains (JRY12863 and JRY12864, respectively). Scale bar, 2 mm. B. The wild-type/mutant diploid (JRY12476) was sporulated and tetrads were dissected on YPD.

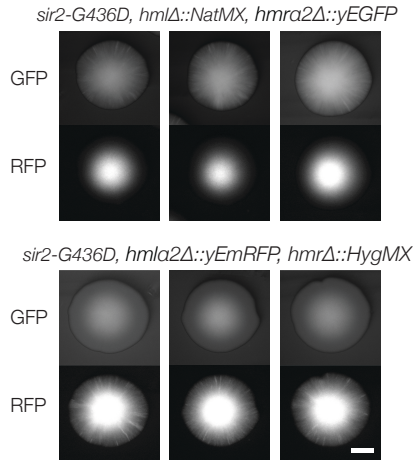

Figure 4.5: Overlap in GFP and RFP channels in *sir2-G436D* was not due to spectral bleedthrough. Representative colony images of *sir2-G436D, hmlΔ::NatMX, hmrα2Δ::GFP* (JRY13197) and *sir2-G436D, hmlα2Δ::RFP, hmrΔ::HygMX* (JRY13198), grown on CSM. Scale bar, 2mm.

4.3.5 *sir2-G436D* produced intermediate, heritable expression

To monitor the different silencing states of *sir1*Δ and *sir2-G436D* over time, we first tested whether these states were evident by live-cell microscopy. To simplify the analysis by microscopy, we first focused on the expression states of *hmrα2Δ::GFP.* As previously established by RNA FISH (Dodson and Rine 2015), *sir1*Δ cells exhibited either full silencing or full expression of *HMR* (**Figure 4.6A**). In partial contrast, *sir2-G436D* cells exhibited full silencing or partial silencing of *HMR* (**Figure 4.6A**). To quantify fluorescence levels, cell segmentation and quantification were performed. Using bright-field images, individual cells were segmented with Yeast Spotter (Lu *et al.* 2019). Once segmented, single-cell data were extracted and displayed as a histogram (**Figure 4.6B** and **C**). As anticipated, cell size was approximately normally distributed, with no meaningful difference between the genotypes (**Figure 4.6B**); however, the GFP fluorescence profiles per genotype were distinct. *sir1*Δ cells were either fully silenced or fully expressed, similar to the flow cytometry data, whereas *sir2-G436D* cells were either fully silenced or partially silenced (**Figure 4.6C**). Using fluorescence intensities of *sir1*Δ cells*,* threshold values were established to demarcate three fluorescence states: "*HMR* off", "*HMR* intermediate", and "*HMR* on". Using these thresholds, approximately 40% of the *sir2-G436D* cells measured exhibited intermediate fluorescence ("*HMR* intermediate")*,* while only 4% of *sir1*Δ cells displayed intermediate expression.

For a transcriptional state to be classified as epigenetic, it must be heritable through cell divisions. Therefore, we assessed the ability of the *sir1*Δ and *sir2-G436D* mutants to reliably transmit the observed silencing states over multiple generations. Time-lapse movies of dividing cells qualitatively suggested that the observed states were heritable. To quantitatively assess this heritability, we monitored the fluorescence of individual mother cells over the course of four division events, or approximately six hours. In both *sir1*Δ and *sir2-G436D*, the fluorescence states of individual cells could be maintained over this entire period or switch to a different state (**Figure 4.6D** and **E**). Additionally, the frequency at which a *sir2-G436D* mother-daughter pair exhibited the same fluorescence state was significantly higher than the frequency at which two randomly chosen cells exhibited the same state (**Figure 4.6F**).

To calculate approximate switching rates, unbudded cells and the resulting progeny of two generations were manually tracked, and each cell assigned an *HMR* expression state according to the threshold values in **Figure 4.6C**. A pedigree was designated as "heritable" if all cells within the pedigree exhibited the same expression state of *HMR* at all three time points (**Figure 4.6G**). In contrast, the pedigree was designated as a "switch" if any of the cells within the pedigree switched to a different *HMR* expression state. Two generations were analyzed to increase our confidence that the *HMR* expression states were heritable and did not simply reflect variation in fluorescent properties of individual cells. Using this method, 250 pedigrees per genotype were analyzed (**Figure 4.6H**).

Recent studies using microscopy and flow cytometry show that approximately 10% of *sir1*Δ cell divisions give rise to a switch in *HMR* expression state (Saxton and Rine 2019). Consistent with this finding, approximately 10% of *sir1*Δ pedigrees analyzed resulted in a switch

in *HMR* silencing, while the other 90% of pedigrees displayed heritability (**Figure 4.6H**). The occurrence of switching in *sir2-G436D* was higher than in *sir1*Δ. However, a majority of pedigrees, approximately 62%, displayed heritability of the *HMR* expression state. Though the majority of these heritable pedigrees displayed "*HMR* off" silencing, 28% of the *sir2-G436D* pedigrees analyzed showed stable transmission of the "*HMR* intermediate" state. This live-cell imaging analysis further supported that *sir2-G436D* exhibited an intermediate silenced state and showed that this state was inherited through cellular division.

To further test if *sir2-G436D* yields heritable states of intermediate silencing, we also analyzed expression of *hmlα2*Δ*::RFP* by microscopy. Consistent with flow cytometry, *sir1*Δ exhibited a mix of cells that were either fully silenced or fully expressed at *HML*, and *sir2-G436D* cells were mostly in the intermediate silenced state, though some were fully silenced (**Figure 4.7A-C**). The same single-cell analyses that were performed on *HMR* in **Figure 4.6** were also applied to *HML*, and strongly suggested that the different expression states of *HML* were heritable in both *sir1*Δ and *sir2-G436D* (**Figure 4.7D-F**). Additionally, an analysis of concordance between the expression states of *HML* and *HMR* suggested that the states at each locus were at least partly independent (**Figure 4.7G**). Therefore, a heritable intermediate silenced state was observed at *HML* in some *sir2-G436D* cells, similar to *HMR*.

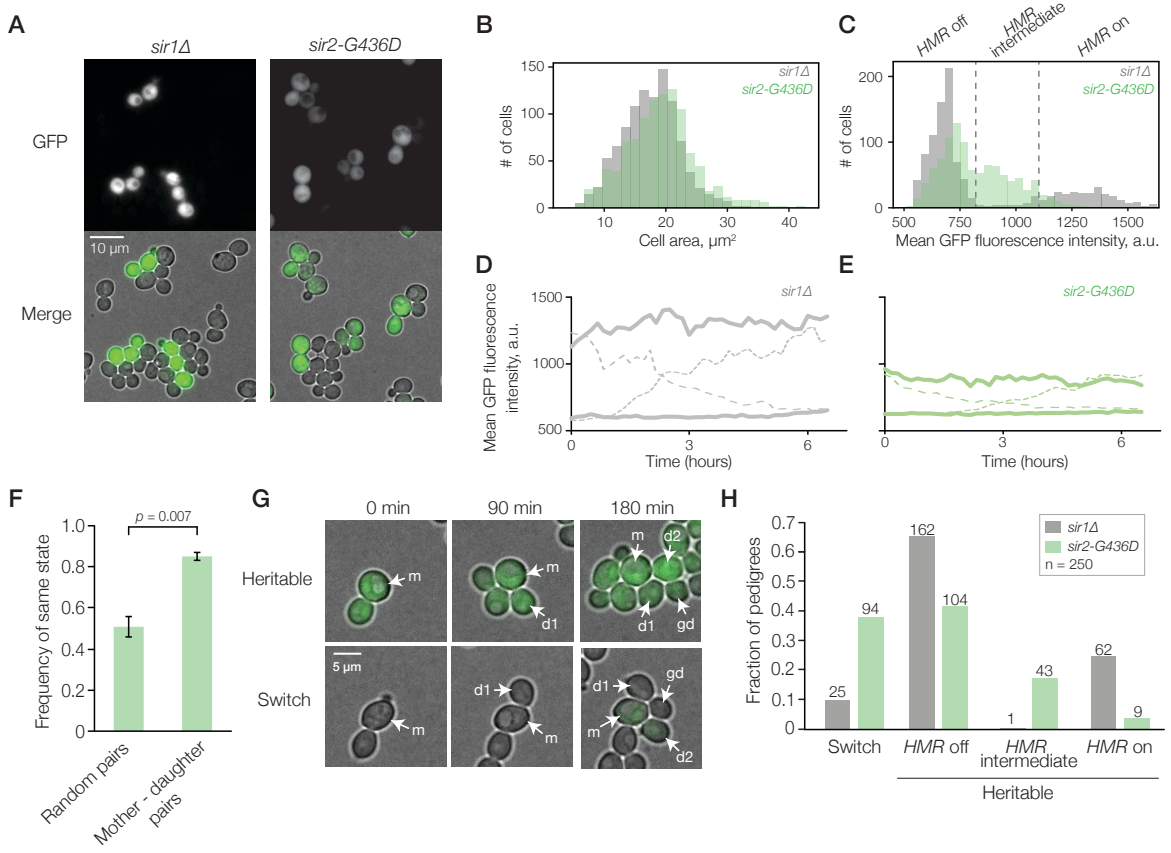

Figure 4.6: Live-cell imaging revealed the intermediate and heritable *sir2-G436D* expression state. A. GFP and merged (bright-field and GFP) fluorescence microscopy images of *sir1*Δ and *sir2-G436D* cells (JRY12861, JRY12564), imaged with identical exposures. B. Distribution of the cell size for both *sir1*Δ and *sir2-G436D,* with number of cells on the y-axis and cell area in μm^2 on the x-axis. C. Distribution of the GFP mean fluorescence

intensity (arbitrary units, a.u.) per cell for both *sir1*Δ and *sir2-G436D.* Dashed lines demarcate the boundaries of the three fluorescence states: *HMR* off, *HMR* intermediate, and *HMR* on. Details on how thresholds were assigned are in *Materials and Methods*. D. GFP mean fluorescence intensity for individual *sir1*Δ cells over 6.5 hours. 12 individual cells were monitored, and 4 representative fluorescence trajectories are displayed. Each solid line represents a single cell that maintained a similar fluorescence level over the timecourse, whereas each dashed line represents a single cell that experienced a change in fluorescence. E. Same as (D), but for 4 individual *sir2-G436D* cells. F. Frequency at which either mother – daughter pairs or random pairs of cells exhibited the same expression state, as determined by threshold values in (C). Five different fields of view were analyzed (n > 50 random pairs and n > 50 mother – daughter pairs per field of view). Data are means ± SD. A two-tailed t-test was used for statistical analysis. G. An example of the pattern of divisions and pedigrees designated as "heritable" versus a "switch" in *sir2-G436D* cells. A single mother cell (m, t = 0 min) budded twice, producing daughter 1 (d1, t = 90 minutes) and daughter 2 (d2, t = 180 minutes). Budding of daughter 1 gave rise to a grand-daughter (gd, t = 180 minutes) cell. In the "heritable" example, all cells at all time points displayed a fluorescence level falling within the "*HMR* intermediate" range; in the "switch" example, a loss of silencing occured during the second division, giving rise to cells with fluorescence classified as "*HMR* intermediate". H. Bar chart showing the fraction of pedigrees designated as a "switch" or "heritable". 250 pedigrees were observed per genotype, with the number of pedigrees per category above each bar.

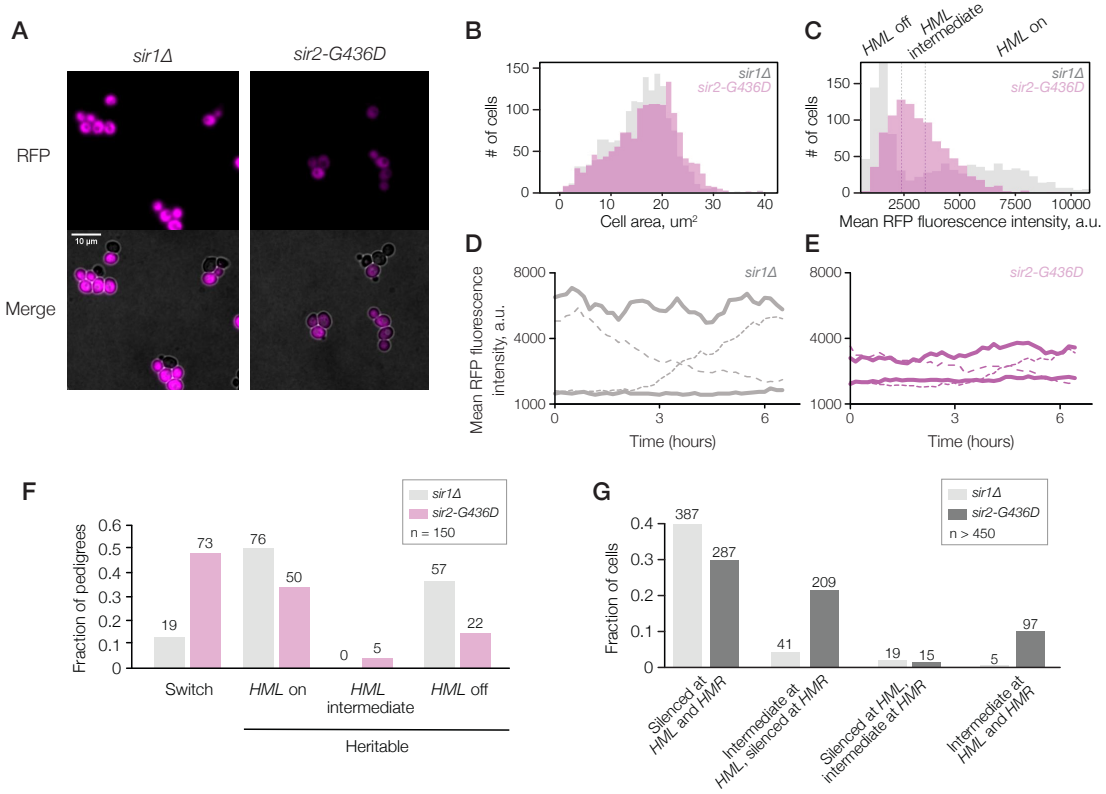

Figure 4.7: Live-cell imaging of *hmlα2*Δ*::RFP* in *sir2-G436D*. A. RFP and merged (bright-field and RFP) fluorescence microscopy images of *sir1*Δ and *sir2-G436D* cells (JRY12861, JRY12564), imaged with identical exposures. B. Distribution of the cell size for both *sir1*Δ and *sir2-G436D,* with number of cells on the y-axis and cell area in μm^2 on the x-axis. C. Distribution of the RFP mean fluorescence intensity (arbitrary units, a.u.) per cell for both *sir1*Δ and *sir2-G436D.* Dashed lines demarcate the boundaries of the three fluorescence states: *HML* off, *HML* intermediate, and *HML* on. Details on how thresholds were assigned are in *Materials and Methods*. D. RFP mean fluorescence intensity for individual *sir1*Δ cells over 6.5 hours. 12 individual cells were monitored, and 4 representative fluorescence trajectories are displayed. Each solid line represents a single cell that maintained a similar fluorescence level over the timecourse, whereas each dashed line represents a single cell that experienced a change in fluorescence. E. Same as (D), but for 4 individual *sir2-G436D* cells. F. Bar chart showing the frequency

of pedigrees designated as a "switch" or "heritable", as described in **Figure 4.6G**. 150 pedigrees were observed per genotype, with the number of pedigrees per category above each bar. G. Frequency of cells exhibiting the silenced or intermediate states at *HML* and *HMR*. At least 450 cells were analyzed per genotype, with the number of cells in each category above each bar.

4.3.6 *sir2-G436D* silencing defects were partially due to reduced levels of Sir2

Based on the crystal structure of the Sir2 protein (Hall and Ellenberger 2008; Hsu *et al.* 2013), codon 436 falls within the highly conserved C-terminal catalytic domain. However, residue 436 is distinct from the site of catalysis and is in close proximity to the zinc ion within the zinc-finger domain (**Figure 4.8A**). A previous study found that disruption of the zinc-finger domain by mutation of the coordinating cysteine residues results in full silencing loss (Sherman *et al.* 1999). Strikingly, the aspartic acid introduced by the *sir2-G436D* mutation is predicted to encroach on the zinc-coordinating site, which may disrupt the protein stability and silencing capacity of Sir2-G436D (**Figure 4.8A**).

To test whether this mutation affected the stability of Sir2, the wild-type and mutant Sir2 proteins were tagged with the V5 epitope and protein levels were evaluated by immuno-blot. Mutant Sir2-G436D levels were roughly 40% of the wild-type Sir2 levels (**Figure 4.8B**, **Figure 4.9**). If this reduced expression was responsible for the observed silencing defects, we would expect that higher expression of *sir2-G436D* would ameliorate these defects. Indeed, expression of *sir2-G436D* from a high copy number plasmid reduced the amount of variegation in the *sir2-G436D* mutant strain, as compared with a vector-only control (**Figure 4.8C**, **Figure 4.10A**). These data suggested that the *sir2-G436D* silencing defect was partially due to reduced levels of Sir2-G436D. Surprisingly, the effects of this *sir2-G436D* plasmid were not observed by flow cytometry (**Figure 4.8D** and **E**, **Figure 4.10B**). This discrepancy provided an early indication that the variegation observed in *sir2-G436D* colonies is a relatively small part of the heritability observed at the single-cell level. This idea is explored further in the subsequent section.

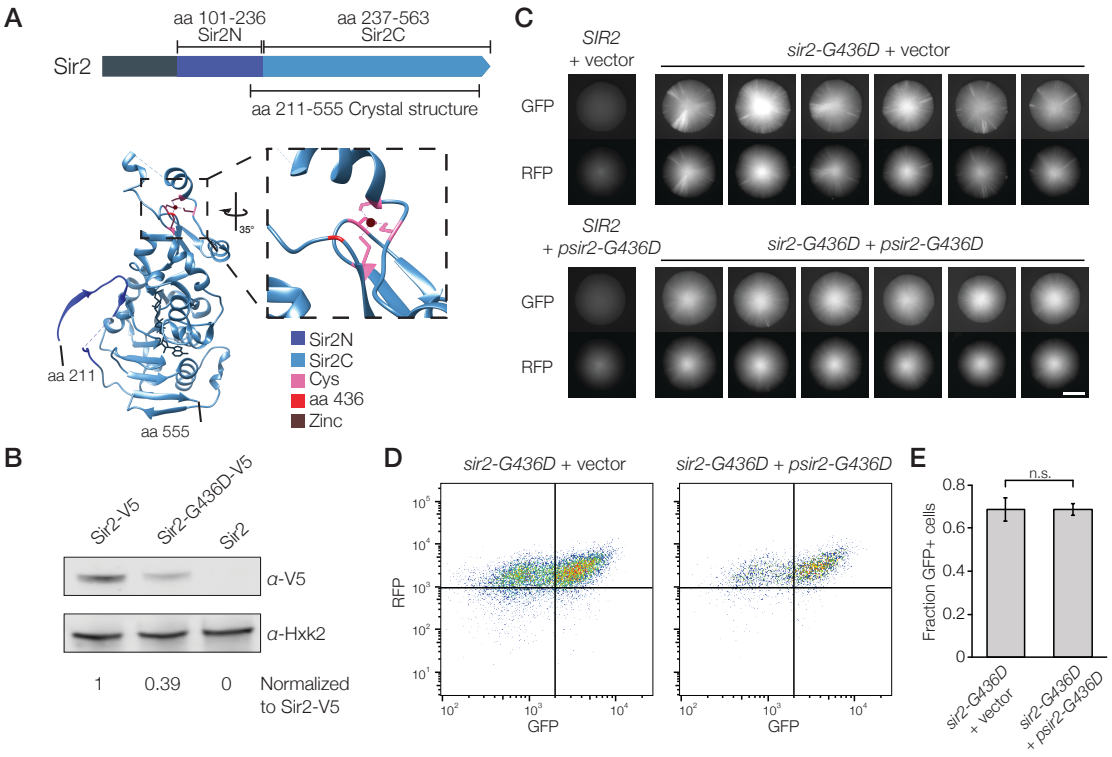

Figure 4.8: Sir2-G436D levels were partially responsible for variegated silencing. A. A schematic of the Sir2 protein and its crystal structure (Hall and Ellenberger 2008, Hsu *et al.* 2013). The N-terminal helical domain (dark blue) and C-terminal catalytic domain (light blue) are indicated. The crystal structure spans from amino acid 211-555 and contains a zinc ion (brown), zinc-coordinating cysteines (pink), and the site of the Sir2-G436D point mutation (red). The inset shows the zinc-coordinating site in Sir2. B. Immunoblot to detect Sir2-V5, Sir2-G436D-V5, and an internal loading control Hxk2 (JRY12589, JRY12590). Protein levels were quantified, normalized to the loading control, and compared to wild-type Sir2-V5 levels. A biological replicate was performed and is presented in **Figure 4.9**. C. Representative colony images of *SIR2* (JRY12860) or *sir2-G436D* (JRY12564) plus a 2 micron plasmid vector (pRS426) or a 2 micron plasmid containing *sir2-G436D* (pJR3525). Six colonies are shown for each *sir2-G436D* strain. Colonies were grown on CSM -Ura to select for plasmids. Scale bar, 3 mm. D. Representative flow cytometry profiles of same strains shown in (C). Independent cultures (n = 3 per genotype) were grown at log phase for 24 hours in CSM -Ura liquid media, fixed, and analyzed. Representative flow cytometry profiles for each strain are shown. Quadrants were established by using the fluorescence profiles of *SIR2* and *sir2*Δ cells (**Figure 4.10**). E. Fraction of GFP$^+$ cells in independent cultures grown in (D). Data are means ± SD (n = 3 independent cultures per genotype). A two-tailed t-test was used for statistical analysis.

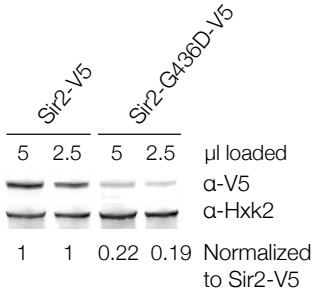

Figure 4.9: Sir2-G436D was present at lower levels than Sir2. Immunoblot to detect Sir2-V5, Sir2-G436D-V5, and an internal loading control Hxk2 (JRY12589, JRY12590). Protein levels were quantified, normalized to the loading control, and compared to wild-type Sir2-V5 levels.

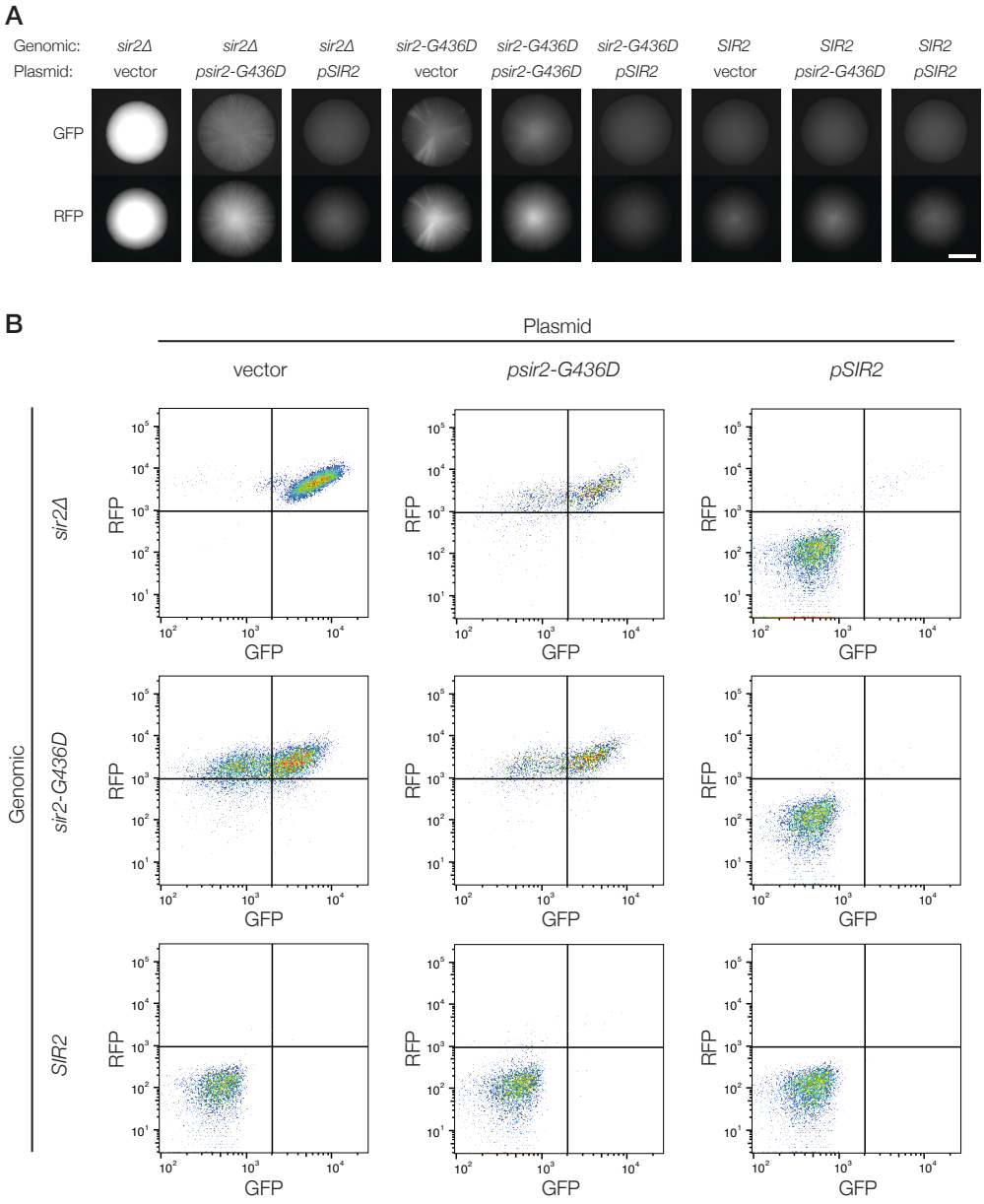

Figure 4.10: Effects of *SIR2* and *sir2-G436D* overexpression. A. Representative colony images of *sir2*Δ (JRY12259), *sir2-G436D* (JRY12564), and *SIR2* (JRY12860) strains with a 2 micron vector (pRS426), a 2 micron vector containing *sir2-G436D* (*psir2-G436D*) (pJR3525), or a 2 micron vector containing *SIR2* (*pSIR2*) (pJR3524). Colonies were grown on CSM -Ura to select for plasmids. Scale bar, 3 mm. B. Flow cytometry profiles of strains shown in (A). Independent cultures (n = 3 per genotype) were grown at log phase for 24 hours in CSM -Ura liquid media, fixed, and analyzed. Representative flow cytometry profiles for each strain are shown. Quadrants were established by using the fluorescence profiles of *SIR2* and *sir2*Δ cells.

4.3.7 rDNA recombination accounted for variegated silencing in *sir2-G436D* colonies

In addition to its role in silencing at *HML*, *HMR*, and telomeres, Sir2 is also part of the RENT complex, which binds to rDNA and suppresses recombination between rDNA repeats (Gottlieb and Esposito 1989; Straight *et al.* 1999; Kobayashi *et al.* 2004). Though this activity stabilizes the rDNA copy number, the copy number can still expand and contract in *SIR2* cells. A previous study found that cells with low rDNA copy numbers exhibit stronger heterochromatic silencing at an artificial telomere and destabilized version of *HMR*, suggesting that the SIR complex competes with the RENT complex for a limiting amount of Sir2 (Michel *et al.* 2005). By extension, this study suggests that different rDNA copy numbers require different amounts of the RENT complex, which changes the amount of Sir2 that is available for heterochromatic silencing. Therefore, heritable differences in rDNA copy number may lead to the heritable differences in silencing efficiency in *sir2-G436D*.

Fob1 is a nucleolar protein that functions to create replication fork barriers in the rDNA, which prevent collisions between DNA polymerase and RNA polymerase I (Kobayashi and Horiuchi 1996; Kobayashi *et al.* 1998). Additionally, replication fork barriers generate recombinogenic replication intermediates that drive the expansion and contraction of rDNA repeats. Thus, in the absence of *FOB1*, recombination in the rDNA is greatly reduced. To test if changes in rDNA copy number contributed to changes in silencing states of *HML* and *HMR*, we generated a *sir2-G436D, fob1*Δ double mutant. In comparison to *sir2-G436D*, the *sir2-G436D*, *fob1*Δ double mutant exhibited substantially less variegation of *HML* and *HMR* expression at the colony level (**Figure 4.11A**, **Figure 4.12A**). These data suggested that rDNA recombination plays a role in the *sir2-G436D* silencing defect.

Though the variegation at the colony level was strongly reduced in the *sir2-G436D*, *fob1*Δ double mutant, these colonies still exhibited a uniform hazy fluorescence. Therefore, we tested whether *fob1*Δ altered the fluorescence profiles of single cells. Similar to the *sir2-G436D* single mutant, *sir2-G436D*, *fob1*Δ double mutant cells were either fully silenced or silenced to an intermediate level and exhibited switching events between these two states (**Figure 4.11B-E**), Supplemental Movie 3). Additionally, the *sir2-G436D*, *fob1*Δ double mutant exhibited fewer cells in the intermediate silenced state (**Figure 4.11B and C**). This may suggest a difference in switching rates between states in *sir2-G436D* and *sir2-G436D*, *fob1*Δ, though a calculation of these switching rates by timelapse microscopy did not reveal significant differences (**Figure 4.11D and E**). Together, these data suggested that the heritability of silencing at the single-cell level was partially independent of rDNA copy number. In this framework, our data indicated that *sir2-G436D* silencing defects reflected an admixture of two phenomena: (1) switching events that occured with a high frequency at the single-cell level, which manifested as intermediate, hazy fluorescence at the colony level and was not heavily influenced by rDNA copy number, and (2) switching events that were difficult to observe in single cells, but were readily observed at the macroscopic level of a colony, and due to changes in rDNA copy number.

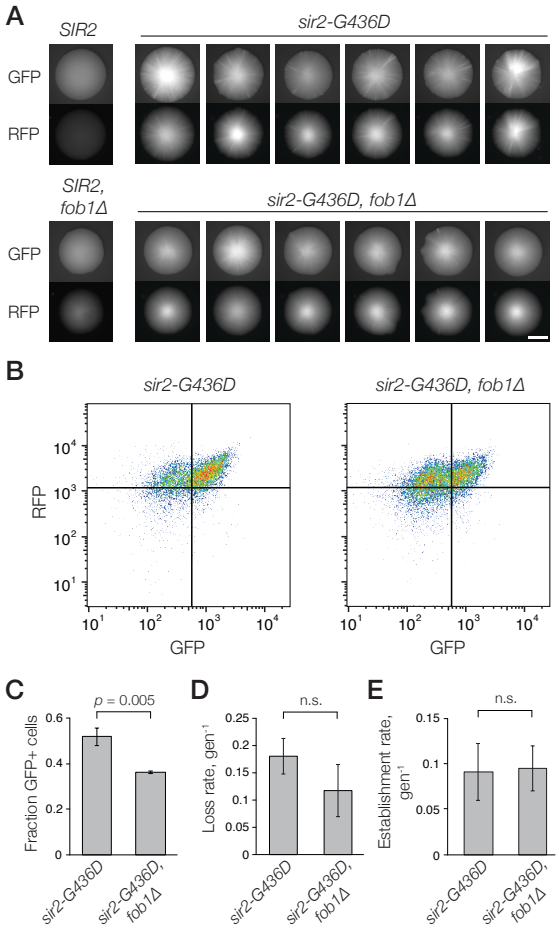

Figure 4.11: Changes in rDNA copy number were partially responsible for silencing variegation in *sir2-G436D*. A. Representative colony images of *SIR2* (JRY12860), *SIR2, fob1*Δ (JRY12899), *sir2-G436D* (JRY12564), *sir2-G436D, fob1*Δ (JRY12901). Six colonies are shown for each strain with *sir2-G436D*. Colonies were grown on CSM. Scale bar, 3 mm. B. Flow cytometry profiles of same strains shown in (A). Independent cultures (n = 3 per genotype) were grown at log phase for 24 hours in CSM liquid media, fixed, and analyzed. A representative flow cytometry flow profile for each strain is shown. C. Fraction of GFP^+ cells in independent cultures grown in (B). Data are means ± SD (n = 3 independent cultures per genotype). A two-tailed t-test was used for statistical analysis. D. The rate of silencing loss per generation, which represented the frequency at which a GFP^- cell switched to GFP^+ per cell division, as calculated by monitoring cell divisions by live-cell microscopy (n > 500 cell divisions per genotype). Error bars represent 95% confidence intervals, and statistical analysis was performed by using a Yates chi-square test. E. The rate of silencing establishment per generation, which represented the frequency at which a GFP^+ cell switched to GFP^- per cell division, as calculated by monitoring cell divisions by live-cell microscopy (n > 400 cell divisions per genotype). Error bars represent 95% confidence intervals, and statistical analysis was performed by using a Yates chi-square test.

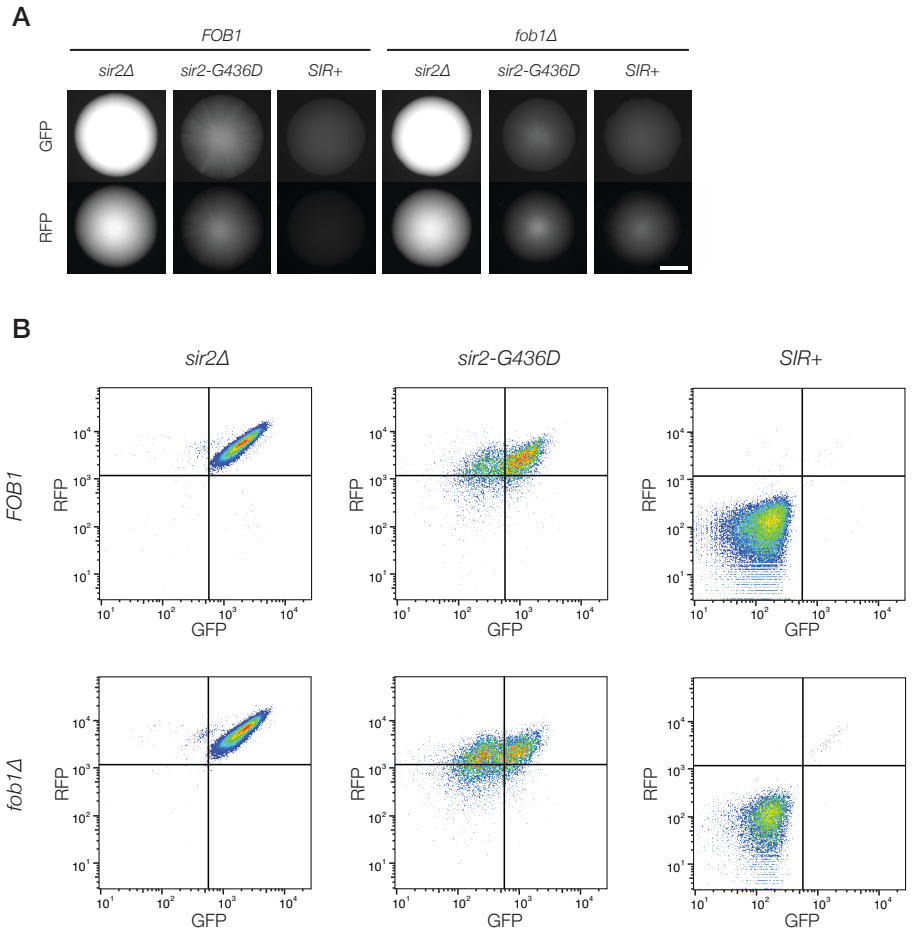

Figure 4.12: Effects of rDNA recombination on *sir2-G436D*. A. Representative colony images of *sir2*Δ, *sir2-G436D*, and *SIR2* with or without *FOB1* (JRY12259, JRY12564, JRY12860, JRY12900-12902), grown on CSM. Scale bar, 3 mm. B. Flow cytometry profiles of strains shown in (A). Independent cultures (n = 3 per genotype) were grown at log phase in CSM liquid media for 24 hours, fixed, and analyzed. Representative flow cytometry profiles are shown for each strain. Quadrants were established by using the fluorescence profiles of *SIR2* and *sir2*Δ cells.

4.3.8 *sir2-G436D* affects rDNA recombination rates

Given that rDNA recombination strongly contributed to the the variegated silencing observed in *sir2-G436D* colonies, we tested whether *sir2-G436D* influences rates of rDNA recombination *per se*. Previous studies utilize reporter genes that are inserted at a single location in the rDNA and use the rate of reporter gene loss as a proxy for the rate of rDNA recombination (Merker and Klein 2002; Kobayashi *et al.* 2004). To this end, we inserted *GFP* into rDNA and monitored the rate of *GFP* loss in different strain backgrounds. Importantly, these strains did not contain *GFP* at any other genomic location, such as *HML* or *HMR.* To assess the rate of *GFP* loss, we plated and analyzed colonies of each strain. The frequency of GFP- sectors in an otherwise GFP+ colony provides a qualitative measure of the loss rate. Additionally, rare colonies that exhibit half sectors (i.e. one half of the colony is completely GFP-) reflect colonies in which the first cell division yielded a single loss event; therefore, the frequency of half-sectors reflects the *GFP* loss rate per cell division.

To test the role of *sir2-G436D* in rDNA recombination, we examined *sir2-G436D* alongside other mutations that affect rDNA recombination rates. Consistent with previous studies, *sir2*Δ increased the rate of rDNA recombination, and *fob1*Δ strongly reduced the rate of rDNA recombination (**Figure 4.13A** and **B**). Surprisingly, *sir2-G436D* increased the rate of rDNA recombination to similar levels as *sir2*Δ, indicating that this mutation abolishes the role of Sir2 in suppressing rDNA recombination. A previous study found that the *fob1*Δ*, sir2*Δ double mutant exhibits a similar rDNA recombination rate as *fob1*Δ, indicating that *fob1*Δ is epistatic to *sir2*Δ (Kobayashi *et al.* 2004). Similarly, we found that *fob1*Δ was epistatic to *sir2-G436D* by this criterion. These data strongly suggested that the *sir2-G436D* mutation affected the role of Sir2 at rDNA, in addition to the role of Sir2 at silenced loci.

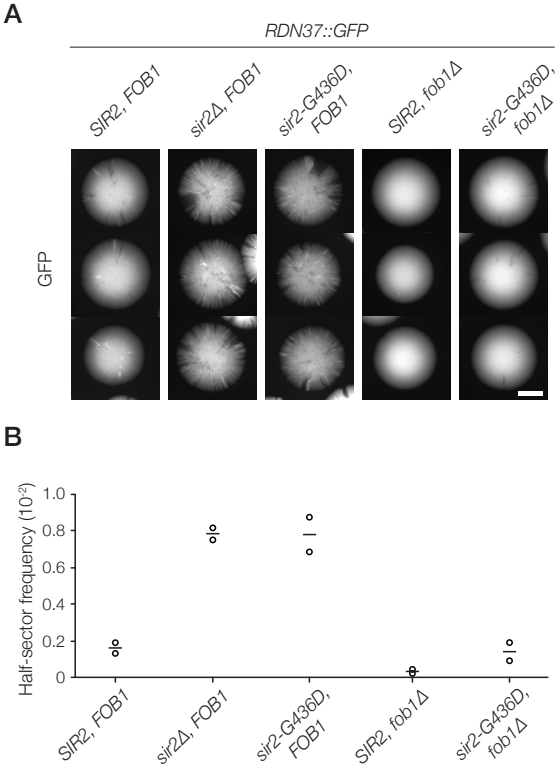

Figure 4.13: *sir2-G436D* lacks the ability to repress rDNA recombination. A. Representative colony images of strains containing *RDN37::GFP* (JRY13204-13208), grown on CSM. Three colonies are shown for each genotype. GFP$^-$ sectors represent events in which rDNA recombination yielded a loss of *GFP*, and sectors with stronger GFP signal represent events in which rDNA recombination likely yielded a duplication of *GFP*. Scale bar, 2mm. B. Quantification of half-sector frequency for strains containing *RDN37::GFP* (JRY13204-13208), as described in *Materials and Methods*. Each circle represents the frequency of half-sector colonies in an independent experiment, and lines represent the means of both experiments. At least 7000 GFP$^+$ colonies were analyzed per genotype.

4.4 Discussion

The ability of cells to "remember" a silenced state has historically been uncovered by mutations that generate variegated expression. Despite the value of these mutations, such as *sir1*Δ, previous studies have not systematically screened for variegated silencing phenotypes in *S. cerevisiae*. Here, we performed a metastability screen that uncovered multiple new alleles of

SIR1, but also identified a novel allele of *SIR2* that exhibited a heritable, intermediate silenced state. Further characterization of *sir2-G436D* revealed that the heritability of this state was not based on rDNA copy number, though changes in rDNA copy number influenced the silencing profile at the colony level. Additionally, this mutation affected the role of Sir2 at rDNA.

4.4.1 Sir1 was the main factor preventing metastable silencing of *HML* and *HMR*

Using a forward genetic screen and an assay for metastable silencing defects, we identified nine independent mutant alleles of *sir1*, of which eight were unique. Thus, to a first approximation, the screen had been saturated. It was therefore unlikely that variable penetrance of the *sir1*Δ silencing phenotype was due to a second non-essential gene with overlapping function. Once an additional copy of *SIR1* was introduced for screening purposes, no further *sir1* alleles were found, and very few mutants displayed a metastable phenotype. These results strongly suggested that Sir1 was the most important protein in converting silencing of *HML* and *HMR* from a metastable to fully silenced regime. This idea is consistent with a previous study in which metastable silencing at a telomeric reporter was strengthened by ectopic recruitment of Sir1 (Chien *et al.* 1993).

4.4.2 The unique phenotype of *sir2-G436D*

A novel mutation, *sir2-G436D*, was identified with two striking qualities: 1) The mutation created an intermediate level of silencing, which was heritable through cell divisions as documented by single cell analysis. 2) At the colony level, this intermediate level of silencing was accompanied by radial streaks of cells with different expression states of the fluorescent reporters. Before discussing the phenotype of this mutant in detail, it is useful to consider the growth dynamics of a yeast colony. Any cell in a colony is a descendant from its more centrally located ancestors. When there is a heritable change in the expression state of a fluorescent reporter gene, that expression state is propagated outward, resulting in a wedge-shaped sector of cells that all exhibit the same state. Thus, a fluorescent sector represents a historical record of a transcriptional switching event that occurred at the apex of the sector, and that was inherited during subsequent colony growth.

The colony-level phenotype of *sir2-G436D* differed from that of *sir1*Δ in multiple ways. First, fluorescent sectors were less fluorescent in *sir2-G436D*, suggesting that the cells in these streaks also had an intermediate level of silencing. Second, the fluorescent sectors were more frequent in *sir2-G436D*, indicating that the switching rate between expression states differed from that seen in *sir1*Δ. Finally, *sir2-G436D* exhibited high concordance between the GFP and RFP channel (**Figure 4.3B**), implying that *HML* and *HMR* were coordinately impacted during the majority of the colony growth. This observation strongly suggested that the process responsible for radial streaks of fluorescence acted in *trans*. In contrast, the expression states of *HML* and *HMR* behave independently of each other in *sir1*Δ (Xu *et al.* 2006, **Figure 4.1B**), demonstrating *cis*-transmission of expression states in this context. Together, these data suggested that the variegated expression seen in *sir2-G436D* and *sir1*Δ colonies were driven by fundamentally different mechanisms.

4.4.3 rDNA copy number contributed to variegated expression in *sir2-G436D*

Given that deletion of *SIR2* causes full loss of silencing, it was likely that *sir2-G436D* was a hypomorphic allele. The G436D mutation was predicted to affect the zinc finger domain by generating a large polar side chain that disrupted the zinc finger domain (**Figure 4.11**). A

previous study found that mutation of the four cysteine residues that coordinate with the zinc ion does not affect Sir2 levels but abolishes the silencing capacity of this protein (Sherman *et al.* 1999). In contrast, Sir2-G436D protein levels were reduced by 40% compared to wild-type Sir2 and exhibited a partial silencing defect. This dichotomy suggested that the Sir2-G436D may have partially disrupted the function of the zinc-coordinating domain and destabilized the mutant protein. Thus, altered levels of Sir2-G436D may be responsible for the silencing defects observed in this mutant. Consistent with this idea, overexpression of *sir2-G436D* from a high copy number plasmid strongly reduced silencing variegation observed at the colony level (**Figure 4.11**).

Sir2 is a protein that has multiple functions at different genomic locations. At silenced loci, Sir2 is part of the Sir2/3/4 complex and functions to deacetylate H4K16, which is necessary for silencing (Moazed and Johnson 1996; Landry *et al.* 2000; Imai *et al.* 2000). Separately, Sir2 is part of the RENT complex at rDNA repeats, where it stabilizes rDNA copy number by repressing transcription and regulating cohesin dynamics (Gottlieb and Esposito 1989; Straight *et al.* 1999; Kobayashi and Ganley 2005). Previous studies demonstrate that lower rDNA copy numbers enhance Sir2/3/4-dependent silencing at telomeres, suggesting that the RENT complex and Sir2/3/4 complex compete for a limited amount of Sir2 (Michel *et al.* 2005). We hypothesized that this competition for Sir2 was the underlying mechanism for the variegation observed in *sir2-G436D*. In this model, variation in rDNA copy number would change the amount of rDNA-bound RENT complex, which would then change the amount of Sir2 available for silencing at loci such as *HML* and *HMR*. This model would be consistent with coregulation of *HML* and *HMR* observed at the colony level in *sir2-G436D*, as altered levels of free Sir2 would influence *HML* and *HMR* equally in *trans*.

This model predicted that cells with a reduced ability to change rDNA copy number would exhibit reduced variegation of silencing in *sir2-G436D*. Indeed, removal of *FOB1*, which is necessary for rDNA recombination, strongly reduced the silencing variegation of *HML* and *HMR* in this context. These data strongly suggested that the heritability of expression states observed in *sir2-G436D* was due to rDNA copy number. In light of this finding, we speculated that under normal conditions, Sir2 levels were high enough that Sir2/3/4 and RENT complexes were not in conflict over Sir2. In contrast, *sir2-G436D* reduced Sir2-G436D levels such that it could not simultaneously meet the requirements of both the Sir2/3/4 and RENT complexes.

Though heterochromatic silencing is often framed as an epigenetic mechanism, our data suggested that genetically heritable differences in rDNA copy number is an additional mechanism that can lead to variable yet heritable expression states of heterochromatin. The genetic heritability of different rDNA copy numbers is broadly conserved (Lyckegaard and Clark 1989; Zhang *et al.* 1990; Gibbons *et al.* 2015), and it is interesting to speculate how cells either utilize or mitigate the effects of this variation. In yeast, different rDNA copy numbers are linked to differences in gene silencing, the monitoring of replication initiation, and replicative lifespan (Kaeberlein *et al.* 1999; Michel *et al.* 2005; Ganley *et al.* 2009). Whether these differences provide adaptive benefits or simply reflect the competition of different cellular processes over limiting factors, such as Sir2, will certainly be a motivating question for future studies.

4.4.4 The impact of *sir2-G436D* on rDNA recombination

Previous studies show that Sir2 represses recombination between rDNA repeats (Kobayashi *et al.* 2004). Specifically, *sir2*Δ increases the rate of rDNA recombination in a *FOB1*-dependent manner. We found that *sir2-G436D* increased rDNA recombination rates to the

same degree as *sir2*Δ, and that this effect was also dependent on *FOB1.* These data suggested that *sir2-G436D* lacked a central function of Sir2 at rDNA.

The effect of *sir2-G436D* at rDNA was interesting in light of variegated silencing defects observed at the colony level. If variegated silencing at the colony level was the result of fluctuating ratios of Sir2-G436D bound at rDNA versus silenced loci, yet Sir2-G436D cannot suppress rDNA recombination, then Sir2-G436D would be recruited rDNA but exist in an inactive conformation or be catalytically inefficient.

A recent study demonstrated that rDNA copy number influences the transcriptional activation of *SIR2*, providing a feedback mechanism for proper maintenance of rDNA copy number (Iida and Kobayashi 2019). In light of our findings, this feedback mechanism suggests that the *sir2-G436D* mutant may have an interesting array of cause-effect relationships between (1) transcriptional silencing of *HML* and *HMR*, (2) the rate of rDNA recombination, and (3) expression levels of *sir2-G436D*. Though *fob1*Δ is able to simplify this network of factors by substantially reducing rDNA recombination, future studies that focus on complex circuitries may benefit from alleles such as *sir2-G436D*.

4.4.5 The existence of an intermediate silenced state

Single-cell analysis is useful to study heritable expression states in a cell population; this concept has been illustrated by multiple studies that uncovered and characterized the epigenetic states seen in *sir1*Δ (Pillus and Rine 1989; Xu *et al.* 2006). One important aspect of silencing in *sir1*Δ is that silenced cells are silenced to the same degree as *SIR+* cells, and expressed cells are expressed to the same degree as *sir2*Δ cells (**Figure 4.3**). In contrast, *sir2-G436D* exhibited a mix of silenced cells and cells that exhibited intermediate expression, as measured by flow cytometry and microscopy. Remarkably, these intermediate states were heritable through multiple cell divisions.

Curiously, overexpression of *sir2-G436D* did not influence the frequency of different expression states seen in *sir2-G436D* by flow cytometry, and *fob1*Δ had relatively small effects on this frequency. This result contrasted with the ability of *sir2-G436D* overexpression to partially reduce, and of *fob1*Δ to strongly reduce, variegation of silencing at the colony level. Together, these results suggested that the majority of switching events at the single cell level were independent of changes in rDNA copy number and the associated colony-level variegation. In this model, a relatively high switching rate between silencing states of *sir2-G436D* manifested as uniform, intermediate fluorescence at the colony level in *fob1*Δ. Then, the added layer of rDNA copy number changes in *FOB1* altered heritability of these silencing states in a manner that was relatively small or absent at the single-cell level, but readily observed as radial streaks at the macroscopic level of a colony. Therefore, the intermediate expression state observed in *sir2-G436D* was mostly independent of changes in rDNA copy number and may have derived from a unique behavior of the Sir2-G436D protein at silenced loci.

A recent study found that Sir-based silencing establishment at both *HML* and *HMR* occurs through an intermediate silenced state, rather than an abrupt switch from the fully expressed to fully silenced state (Goodnight and Rine 2020). Furthermore, this intermediate state could be generated and stably maintained when certain histone modifying enzymes were absent in G1-arrested cells. Ultimately, that study concluded that silencing establishment occurs through a shift in the landscape of histone modifications at *HML* and *HMR*, and that cells that do not fully experience this shift can maintain a partially silenced state. In this view, the intermediate silencing state observed in *sir2-G436D* may reflect a partial deficiency in its ability to

deacetylate H4K16. It is interesting to note that deletion of *SAS2*, which is responsible for acetylation of H4K16, also exhibits intermediate silencing states at *HML* and *HMR* at the single-cell level (Xu *et al.* 2006). Notably, the intermediate silencing state in *sas2*Δ is not a bona fide epigenetic state, as it is present in all cells of that genotype. Taken together, these results strongly suggest that defects in different histone modifying enzymes can exhibit similar phenotypes of intermediate silencing. This trend points to the existence of silencing intermediates that can be uncovered by modulating a complex landscape of histone modifications. The concept that histone modifications can tune trancription is broadly relevant, and the subject of studies like the modENCODE project, which classifies different chromatin landscapes and transcription profiles in *Drosophila melanogaster* and *C. elegans* (Gerstein *et al.* 2010; Kharchenko *et al.* 2011). Additional studies on *sir2-G436D*, *sas2*Δ, and other mutants will clarify how histone modifying complexes can shift the strength of silencing and, in some cases, reveal heritable properties of heterochromatin.

4.5 Materials and Methods

Strains and Culture methods

All strains were derived from W303 and are listed in the Supplemental Material, Table S1. Plasmids used in the study are listed in Table S2. All oligonucleotides, used for cloning, PCR, and sequencing, are listed in Table S3. Strains were grown in Yeast Peptone Dextrose (YPD), or Complete Supplement Mixture (CSM) with or without individual amino acids left out (Sunrise Science Products), as indicated. The FLuorescent Analysis of Metastable Expression (FLAME) reporter strain was initially published in (Saxton and Rine 2019). Throughout this study, there were subtle differences between the silencing levels of *HML* versus *HMR*; however, the expression phenotypes of both remained similar. Elucidating any differences between the two loci was not pursued further. Mutagenesis was induced with Ethyl Methane Sulfonate (EMS). Diploid strains were created by genetic crosses and phenotypes were confirmed following sporulation by tetrad analysis. The point mutations within *SIR1* and *SIR2* were identified by PCR amplification and sequencing. Each mutant generated by mutagenesis was expected to contain multiple base-pair substitutions. Strains with single point mutations in the genes of interest were engineered using Cas9 technology, as previously described (Lee *et al.* 2015; Brothers and Rine 2019). Single guide RNAs (sgRNAs) targeting *SIR2* and a unique linker region in *sir1*Δ*::LEU2* (JRY12861) are listed in Table S3. To generate *sir1* alleles in an unmutagenized parent strain, PCR-amplified repair templates of sequence-confirmed *sir1* alleles replaced the *sir1*Δ*::LEU2* allele in JRY12861. To create *sir2-G436D* in an unmutagenized parent strain, *sir2-G436D* was PCR amplified from JRY12466 and provided as a repair template to replace the *SIR2* allele in JRY12860. Both *sir1* and *sir2-G436D* mutant allele integration replaced the Cas9-directed cut site. All single point mutations were sequence confirmed. The Sir2-3xV5 fusion protein used for immunoblotting was created as described (Longtine *et al.* 1998). Strains were transformed with an amplified fragment of pJR3190 (Bähler *et al.* 1998), which allowed for homologous recombination and integration of the *KanMX* cassette and the 3x-V5 tag to the carboxyl terminus of the *SIR2* open reading frame. *SIR2* and *sir2-G436D* were amplified from JRY12860 and JRY12564, respectively, with 300 base pairs of 5' promoter sequence and 200 base pairs of 3' terminator sequence. These fragments were integrated into the 2 micron plasmid vector pRS426 to generate pJR3523 and pJR3524. *fob1*Δ*::KanMX* was generated by amplification of *KanMX* from pJR3190 and subsequent transformation. To test rDNA recombination rates, *yEGFP::K.lac.URA3* was integrated into *RDN37*.

EMS mutagenesis

The EMS protocol was adapted from previously reported protocols (Winston 2008; Liu and Hu 2010) and optimized for our reporter strain (JRY12860) and reagents to yield ~50-60% lethality. Cells were plated at a low density (~150-200 colonies) on YPD for screening. Twelve independent rounds of mutagenesis were conducted. Approximately 11,000 mutagenized colonies were screened using fluorescence microscopy in the first eight rounds, and six mutants of interest were recovered. The final four rounds were initially screened in parallel via Fluorescent Activated Cell Sorting (FACS), as described below, and three mutants of interest were isolated (each mutant was selected from an independent culture). Mutants of interest were assigned a unique identifier during screening and identification (**Figure 4.2**), but throughout the text are referenced by the associated mutant allele, i.e. *sir1-P23S* or *sir2-G436D.*

FACS Single Sort

Following EMS mutagenesis, independent mutagenized cultures were grown in liquid medium prior to parallel FACS sorting. Specifically, after the final resuspension in 500 uL YPD ($\sim 2 \times 10^8$ cells), for each independent culture, 50 mLs of YPD were inoculated with the mutagenized cells and grown to saturation overnight. The following day, saturated cultures were back diluted to 0.1 OD in YPD and grown to log phase (~0.6-1.0 OD). 2 mL of each log-phase culture was harvested, washed, and resuspended in 2 mL 1X sterile PBS. Samples were strained through a 5 μm sterile mesh cap into a 5 mL polypropylene tube (Falcon), and kept on ice until sorting. *SIR*+ and *sir4*Δ control strains (JRY12860, JRY12862) were used to determine fluorescence threshold levels, as all *SIR* cells were nonfluorescent, and all *sir4*Δ cells were fluorescent. One large gate for fluorescent cells (only GFP^+, only RFP^+, and GFP^+ and RFP^+) was created, and fluorescent cells (approximately 10,000 per culture) were sorted, grown at 30°C overnight, and then plated for screening. Plates were incubated at 30°C until colonies formed and were large enough for screening (2-4 days). Only a single mutant of interest was followed from each independent mutagenized culture.

FACS Double sort

Double FACS sorting was performed for one round of mutagenesis. Strain JRY11906 was mutagenized. The first part of the double sort strategy was identical to the single sort strategy. Sorted fluorescent cells were then grown at 30°C in liquid culture overnight. Fresh YPD was inoculated with the daughters of the sorted cells to a density of 0.1 OD, and maintained near log-phase growth through continuous back dilution for two days, providing ample time for some fluorescent cells to switch into a silenced state. After these two days of growth, samples were prepared for sorting as above, but this time a gate for GFP^- and RFP^- cells was created, and these sorted cells were grown at 30°C in YPD overnight and prepared for colony screening as indicated above. Again, a single mutant of interest was followed per independent mutagenized culture.

Colony Imaging

Cells were plated at a low density (20-35 cells/plate) on solid medium as indicated in individual figures. Single cells were then grown into colonies for 3-5 days at 30°C and imaged using a Leica M205 FA fluorescence stereo microscope and a Leica DFC3000 G microscope

camera equipped with LAS X software (Leica). For all colony images within a given experiment, all conditions (growth, media, magnification, and exposure) were identical.

Flow cytometry

Cells were inoculated into 150 uL of CSM in 96-well plates (Corning). Three biological replicates per strain were grown overnight. Saturated cultures were back diluted to ~0.1 OD in fresh CSM, and continuously back diluted to maintain log-phase growth for 24 hours; this growth period allowed the distribution of cells with silenced or non-silenced *HML* and *HMR* to reach equilibrium. After 24 hours of log-phase growth, cells were harvested by centrifugation, resuspended in 100 µL of 4% paraformaldehyde and incubated at room temperature for 15 minutes. Samples were pelleted and the fixed cells were resuspended in 100-150 uL of a 1X PBS solution. These fixed samples were stored at 4°C and analyzed by flow cytometry within 5 hours of fixation. Flow cytometry was performed using a BD LSRFortessa (BD Biosciences) with a FITC filter (for GFP) and a PE-TexasRed filter (for RFP), and at least 10,000 cells were analyzed per sample. Flow cytometry data was analyzed and visualized using FlowJo (BD Biosciences). All flow cytometry data were gated identically, omitting aggregates and cellular debris from analysis.

Immunoblotting

Protein isolation, immunoblotting, and quantification were carried out as previously described (Brothers and Rine 2019). The membranes were blocked in Odyssey Blocking Buffer (LI-COR Biosciences), and the following primary antibodies and dilutions were used for detection: mouse anti-V5 (Invitrogen R960-25, 1:5,000) and rabbit anti-Hxk2 (Rockland #100-4159, 1:10,000). The secondary antibodies used were goat anti-rabbit (Li-Cor #C60531-05 1:20,000) and goat anti-mouse (Li-Cor #C81106-03 1:20,000). The immunoblot was imaged using a Li-Cor infrared fluorescent scanner.

Patch mating assay

Strains to be assayed were patched onto solid YPD and grown at 30°C. After 1 day, these YPD plates were replica plated onto a mating-type tester lawn with complementary auxotrophic markers (*MATa* JRY2726, and *MATα* JRY2728, plated on YPD), and grown at 30°C for 1 day. Lawns were then replicated onto minimal YM medium, grown at 30°C for 2 days, and imaged.

α-factor Confrontation Assay

This assay was carried out as previously described (Pillus and Rine 1989). Single, unbudded cells were micromanipulated approximately ½ field of view at 200X magnification away from the streak of *MATα* cells which served as a source of α-factor. The plates were incubated at 30°C for approximately 3 hours and the morphology of single cells was observed.

Live-cell imaging

Strains JRY12861, JRY12564, and 12901 were grown as described above for flow cytometry, but in 5 mL cultures of CSM. After 24 hours of log-phase growth, a 500 µL aliquot of cell suspension at approximately 0.6-1.0 OD was harvested and resuspended in 500 uL sterile water. This cellular suspension was then sonicated for 5 seconds at 20% amplitude (Branson Ultrasonics Digital Sonifier 100-132-888R with Sonicator Tip 101-135-066R) to disrupt aggregates. A 5 µL aliquot of sonicated cells was spotted onto a CSM 2% agar pad. Once dry,

the agar pads were inverted onto a 35 mm glass bottom dish (Thermo Scientific) and imaged using a Zeiss Z1 inverted fluorescence microscope with a Prime 95B sCMOS camera (Teledyne Photometrics), Plan-Apochromat 63x/1.40 oil immersion objective (Zeiss) filters, MS-2000 XYZ automated stage (Applied Scientific Instrumentation), and Micro-Manager imaging software (Open Imaging). Samples were incubated at 30°C and imaged every 10 minutes or 15 minutes for a total of 10 hours in bright-field, GFP, and RFP. Time-lapse movies were prepared and analyzed using FIJI software (Schindelin *et al.* 2012).

Single-cell segmentation and fluorescence quantification

Bright-field microscopy images from live-cell imaging were segmented using the online tool Yeast Spotter (Lu *et al.* 2019) or manually for individual cells over long time courses, such as those shown in **Figure 4.6B** and **C**. Individual cells were parsed and labeled using the "analyze particles" tool in FIJI, and measurements taken, including area and GFP mean fluorescence intensity.

Individual cells were assigned a silencing state of *hmrα2Δ::GFP* ("*HMR* off", "*HMR* intermediate", "*HMR* on"), using threshold values determined from the *sir1*Δ (JRY12861) single-cell analysis data. The *sir1*Δ cell data was split into two populations (*"sir1*Δ off" and "*sir1*Δ on"), with each population assumed to be normally distributed, and the threshold values designated to include 90% of the respective *sir1* population. The "*HMR* off" to "*HMR* intermediate" boundary was defined as the 90th percentile rank GFP fluorescence intensity value for the "*sir1*Δ off" population (798 GFP mean fluorescence intensity). The "*HMR* intermediate" to "*HMR* on" boundary was defined as the 5th percentile rank GFP fluorescence intensity value for the "*sir1*Δ on" population (1103 GFP mean fluorescence intensity). For **Figure 4.7**, this approach to quantitatively establish thresholds did not yield thresholds that could accurately demarcate the local minimum between the *sir1*Δ "*HML* on" and "*HML* off" populations. Therefore, the thresholds for **Figure 4.7** were determined qualitatively from the *sir1*Δ fluorescence analysis, and subsequently applied to *sir2-G436D*.

Pedigree analysis for measuring heritability

Time-lapse microscopy movies (described above) were analyzed to measure the heritability of a fluorescence state. For each pedigree analyzed, a single cell (mother) and the resulting three progeny (daughter 1, daughter 2, grand-daughter (daughter of daughter 1)) were manually segmented and the fluorescence state was measured using FIJI software. At each time point (t = 0 minutes, t = 90 minutes, t = 180 minutes), all cells were measured and assigned a fluorescence state, using the threshold values established above. If all progeny at all time points displayed the same expression state as the mother cell had at t = 0 minutes, the pedigree was labeled "heritable" reflecting the heritability of that expression state. If any of the cells in the pedigree switched state designations, the pedigree was labeled as a "switch", reflecting the absence of heritability of that expression state in that pedigree.

rDNA recombination assay

To measure rDNA recombination in *RDN37::yEGFP* strains, cells were grown overnight, back diluted, and plated on YPD at a concentration of 30 cells/plate for sector analysis, or 500 cells/plate for half-sector quantification. To quantify half-sectors, parallel lines were drawn along the plate to demarcate regions of interest, and the viewer manually scanned these regions of

interest with a Leica M205 FA fluorescence stereo microscope and manually counted colonies that exhibited GFP+ signal and either had half-sectors or not.

4.6 References

Bähler J., J. Wu, M. S. Longtine, N. G. Shah, A. M. III, *et al.*, 1998 Heterologous modules for efficient and versatile PCR-based gene targeting in *Schizosaccharomyces pombe*. *Yeast* **14**: 943–951. https://doi.org/10.1002/(sici)1097-0061(199807)14:10<943::aid-yea292>3.0.co;2-y

Brothers M., and J. Rine, 2019 Mutations in the PCNA DNA Polymerase Clamp of *Saccharomyces cerevisiae* Reveal Complexities of the Cell Cycle and Ploidy on Heterochromatin Assembly. *Genetics* **213**: 449–463. https://doi.org/10.1534/genetics.119.302452

Chien C. T., S. Buck, R. Sternglanz, and D. Shore, 1993 Targeting of SIR1 protein establishes transcriptional silencing at HM loci and telomeres in yeast. *Cell* **75**: 531–541.

Dhillon N., and R. T. Kamakaka, 2000 A Histone Variant, Htz1p, and a Sir1p-like Protein, Esc2p, Mediate Silencing at HMR. *Mol. Cell.* **6**: 769–780. https://doi.org/10.1016/s1097-2765(00)00076-9

Dodson A. E., and J. Rine, 2015 Heritable capture of heterochromatin dynamics in *Saccharomyces cerevisiae*. *eLife* **4**: e05007. https://doi.org/10.7554/elife.05007

Ganley A. R. D., S. Ide, K. Saka, and T. Kobayashi, 2009 The Effect of Replication Initiation on Gene Amplification in the rDNA and Its Relationship to Aging. *Mol. Cell.* **35**: 683–693. https://doi.org/10.1016/j.molcel.2009.07.012

Gartenberg M. R., and J. S. Smith, 2016 The Nuts and Bolts of Transcriptionally Silent Chromatin in *Saccharomyces cerevisiae*. *Genetics*. https://doi.org/10.1534/genetics.112.145243/-/dc1

Gerstein M. B., Z. J. Lu, E. L. V. Nostrand, C. Cheng, B. I. Arshinoff, *et al.*, 2010 Integrative Analysis of the *Caenorhabditis elegans* Genome by the modENCODE Project. *Science* **330**: 1775–1787. https://doi.org/10.1126/science.1196914

Gibbons J. G., A. T. Branco, S. A. Godinho, S. Yu, and B. Lemos, 2015 Concerted copy number variation balances ribosomal DNA dosage in human and mouse genomes. *Proc. National Acad. Sci.* **112**: 2485–2490. https://doi.org/10.1073/pnas.1416878112

Goodnight D., and J. Rine, 2020 S-phase-independent silencing establishment in *Saccharomyces cerevisiae*. *eLife* **9**: e58910. https://doi.org/10.7554/elife.58910

Gottlieb S., and R. E. Esposito, 1989 A new role for a yeast transcriptional silencer gene, SIR2, in regulation of recombination in ribosomal DNA. *Cell* **56**: 771–776. https://doi.org/10.1016/0092-8674(89)90681-8

Hall, B. E., and T. E. Ellenberger, 2008 Crystal Structure of the Sir2 deacetylase, PBD ID: 2HJH doi: 10.2210/pdb2HJH/pdb

Hoppe G. J., J. C. Tanny, A. D. Rudner, S. A. Gerber, S. Danaie, *et al.*, 2002 Steps in Assembly of Silent Chromatin in Yeast: Sir3-Independent Binding of a Sir2/Sir4 Complex to Silencers and Role for Sir2-Dependent Deacetylation. *Molecular and Cellular Biology* **22**: 4167–4180. https://doi.org/10.1128/mcb.22.12.4167-4180.2002

Hsu H.-C., C.-L. Wang, M. Wang, N. Yang, Z. Chen, *et al.*, 2013 Structural basis for allosteric stimulation of Sir2 activity by Sir4 binding. *Gene. Dev.* **27**: 64–73. https://doi.org/10.1101/gad.208140.112

Iida T., and T. Kobayashi, 2019 RNA Polymerase I Activators Count and Adjust Ribosomal RNA Gene Copy Number. *Mol. Cell.* **73**: 645-654.e13. https://doi.org/10.1016/j.molcel.2018.11.029

Imai S., C. M. Armstrong, M. Kaeberlein, and L. Guarente, 2000 Transcriptional silencing and longevity protein Sir2 is an NAD-dependent histone deacetylase. *Nature* **403**: 795–800. https://doi.org/10.1038/35001622

Kaeberlein M., M. McVey, and L. Guarente, 1999 The SIR2/3/4 complex and SIR2 alone promote longevity in *Saccharomyces cerevisiae* by two different mechanisms. *Gene. Dev.* **13**: 2570–2580. https://doi.org/10.1101/gad.13.19.2570

Kharchenko P. V., A. A. Alekseyenko, Y. B. Schwartz, A. Minoda, N. C. Riddle, *et al.*, 2011 Comprehensive analysis of the chromatin landscape in *Drosophila melanogaster*. *Nature* **471**: 480–485. https://doi.org/10.1038/nature09725

Kobayashi T., and T. Horiuchi, 1996 A yeast gene product, Fob1 protein, required for both replication fork blocking and recombinational hotspot activities. *Genes Cells* **1**: 465–474. https://doi.org/10.1046/j.1365-2443.1996.d01-256.x

Kobayashi T., D. J. Heck, M. Nomura, and T. Horiuchi, 1998 Expansion and contraction of ribosomal DNA repeats in *Saccharomyces cerevisiae*: requirement of replication fork blocking (Fob1) protein and the role of RNA polymerase I. *Gene. Dev.* **12**: 3821–3830. https://doi.org/10.1101/gad.12.24.3821

Kobayashi T., T. Horiuchi, P. Tongaonkar, L. Vu, and M. Nomura, 2004 SIR2 Regulates Recombination between Different rDNA Repeats, but Not Recombination within Individual rRNA Genes in Yeast. *Cell* **117**: 441–453. https://doi.org/10.1016/s0092-8674(04)00414-3

Kobayashi T., and A. R. D. Ganley, 2005 Recombination Regulation by Transcription-Induced Cohesin Dissociation in rDNA Repeats. *Science* **309**: 1581–1584. https://doi.org/10.1126/science.1116102

Kostriken R., J. N. Strathern, A. J. S. Klar, J. B. Hicks, and F. Heffron, 1983 A site-specific endonuclease essential for mating-type switching in *Saccharomyces cerevisiae*. *Cell* **35**: 167–174. https://doi.org/10.1016/0092-8674(83)90219-2

Kueng S., M. Oppikofer, and S. M. Gasser, 2013 SIR Proteins and the Assembly of Silent Chromatin in Budding Yeast. *Annu. Rev. Genet*. **47**: 275–306. https://doi.org/10.1146/annurev-genet-021313-173730

Landry J., A. Sutton, S. T. Tafrov, R. C. Heller, J. Stebbins, *et al.*, 2000 The silencing protein SIR2 and its homologs are NAD-dependent protein deacetylases. *Proc. National Acad. Sci.* **97**: 5807–5811. https://doi.org/10.1073/pnas.110148297

Lee T. I., and R. A. Young, 2013 Transcriptional Regulation and Its Misregulation in Disease. *Cell* **152**: 1237–1251. https://doi.org/10.1016/j.cell.2013.02.014

Lee M. E., W. C. DeLoache, B. Cervantes, and J. E. Dueber, 2015 A Highly Characterized Yeast Toolkit for Modular, Multipart Assembly. *ACS Synthetic Biology* **4**: 975–986. https://doi.org/10.1021/sb500366v

Liu E., and Y. Hu, 2010 Construction of a xylose-fermenting *Saccharomyces cerevisiae* strain by combined approaches of genetic engineering, chemical mutagenesis and evolutionary adaptation. *Biochem. Eng. J*. **48**: 204–210. https://doi.org/10.1016/j.bej.2009.10.011

Longtine M. S., A. M. III, D. J. Demarini, N. G. Shah, A. Wach, *et al.*, 1998 Additional modules for versatile and economical PCR-based gene deletion and modification in *Saccharomyces cerevisiae*. *Yeast* **14**: 953–961. https://doi.org/10.1002/(sici)1097-0061(199807)14:10<953::aid-yea293>3.0.co;2-u

Lu A. X., T. Zarin, I. S. Hsu, and A. M. Moses, 2019 YeastSpotter: Accurate and parameter-free web segmentation for microscopy images of yeast cells. *Bioinformatics* **35**: 4525–4527. https://doi.org/10.1093/bioinformatics/btz402

Lyckegaard E. M., and A. G. Clark, 1989 Ribosomal DNA and Stellate gene copy number variation on the Y chromosome of *Drosophila melanogaster*. *Proc. National Acad. Sci.* **86**: 1944–1948. https://doi.org/10.1073/pnas.86.6.1944

Merker R. J., and H. L. Klein, 2002 *hpr1Δ* Affects Ribosomal DNA Recombination and Cell Life Span in *Saccharomyces cerevisiae*. *Mol. Cell Biol.* **22**: 421–429. https://doi.org/10.1128/mcb.22.2.421-429.2002

Michel A. H., B. Kornmann, K. Dubrana, and D. Shore, 2005 Spontaneous rDNA copy number variation modulates Sir2 levels and epigenetic gene silencing. *Gene. Dev.* **19**: 1199–1210. https://doi.org/10.1101/gad.340205

Moazed D., and A. D. Johnson, 1996 A Deubiquitinating Enzyme Interacts with SIR4 and Regulates Silencing in *S. cerevisiae*. *Cell* **86**: 667–677. https://doi.org/10.1016/s0092-8674(00)80139-7

Pillus L., and J. Rine, 1989 Epigenetic inheritance of transcriptional states in *S. cerevisiae*. *Cell* **59**: 637–647.

Rine J., J. N. Strathern, J. B. Hicks, and I. Herskowitz, 1979 A suppressor of mating-type locus mutations in *Saccharomyces cerevisiae*: evidence for and identification of cryptic mating-type loci. *Genetics* **93**: 877–901.

Rine J., and I. Herskowitz, 1987 Four genes responsible for a position effect on expression from *HML* and *HMR* in *Saccharomyces cerevisiae*. *Genetics* **116**: 9–22.

Rusché L. N., A. L. Kirchmaier, and J. Rine, 2002 Ordered nucleation and spreading of silenced chromatin in *Saccharomyces cerevisiae*. *Molecular Biology of the Cell* **13**: 2207–2222. https://doi.org/10.1091/mbc.e02-03-0175

Saxton D. S., and J. Rine, 2019 Epigenetic memory independent of symmetric histone inheritance. *eLife* **8**: 585. https://doi.org/10.7554/elife.51421

Schindelin J., I. Arganda-Carreras, E. Frise, V. Kaynig, M. Longair, *et al.*, 2012 Fiji: an open-source platform for biological-image analysis. *Nat. Methods.* **9**: 676–682. https://doi.org/10.1038/nmeth.2019

Sherman J. M., E. M. Stone, L. L. Freeman-Cook, C. B. Brachmann, J. D. Boeke, *et al.*, 1999 The Conserved Core of a Human SIR2 Homologue Functions in Yeast Silencing. *Mol. Biol. Cell* **10**: 3045–3059. https://doi.org/10.1091/mbc.10.9.3045

Stone E. M., C. Reifsnyder, M. McVey, B. Gazo, and L. Pillus, 2000 Two classes of *sir3* mutants enhance the *sir1* mutant mating defect and abolish telomeric silencing in *Saccharomyces cerevisiae*. *Genetics* **155**: 509–522.

Straight A. F., W. Shou, G. J. Dowd, C. W. Turck, R. J. Deshaies, *et al.*, 1999 Net1, a Sir2-Associated Nucleolar Protein Required for rDNA Silencing and Nucleolar Integrity. *Cell* **97**: 245–256. https://doi.org/10.1016/s0092-8674(00)80734-5

Thurtle D. M., and J. Rine, 2014 The molecular topography of silenced chromatin in *Saccharomyces cerevisiae*. *Gene. Dev.* **28**: 245–58. https://doi.org/10.1101/gad.230532.113

Winston F., 2008 EMS and UV Mutagenesis in Yeast. *Curr. Protoc. Mol. Biology* **82**: 13.3B.1-13.3B.5. https://doi.org/10.1002/0471142727.mb1303bs82

Xu E. Y., K. A. Zawadzki, and J. R. Broach, 2006 Single-Cell Observations Reveal Intermediate Transcriptional Silencing States. *Molecular Cell* **23**: 219–229. https://doi.org/10.1016/j.molcel.2006.05.035

Zhang Q. F., M. A. S. Maroof, and R. W. Allard, 1990 Effects on adaptedness of variations in ribosomal DNA copy number in populations of wild barley (*Hordeum vulgare ssp. spontaneum*). *Proc. National Acad. Sci.* **87**: 8741–8745. https://doi.org/10.1073/pnas.87.22.8741